Multifaceted roles of the lysosome in the establishment and expansion of tuberculous infection

Steven Levitte

A dissertation
submitted in partial fulfilment of the
requirements of the degree of

Doctor of Philosophy

University of Washington
2016

Reading Committee:
Lalita Ramakrishnan, Chair
David R. Sherman
Kevin B. Urdahl

Program Authorized to Offer Degree:
Molecular and Cellular Biology

University of Washington

Abstract

Multifaceted roles of the lysosome in the establishment and expansion of tuberculous infection

Steven Levitte

Chair of the Supervisory Committee:
Lalita Ramakrishnan
Department of Medicine
Department of Immunology
Department of Microbiology

Infection with *Mycobacterium tuberculosis*, the causative agent of TB, begins with the deposition of bacteria into the lung alveolus where they establish infection in host macrophages. *M. tuberculosis* dwells within host macrophages for much of its life cycle, until it again becomes extracellular prior to transmission into a new host. *M. tuberculosis'* use of the macrophage as an expansion niche is surprising because these immune cells are normally tasked with the elimination of invading bacteria by trafficking them to degradative lysosomal compartments. Using the optically transparent and genetically tractable zebrafish model of mycobacterial infection with *M. marinum*, I have evaluated the diverse roles played by the macrophage lysosome at two stages of infection: first, during the initial interaction between infecting mycobacteria and first-responder macrophages; and second, during the stage of infection when bacteria are released from the macrophage and grow extracellularly. When newly infecting bacteria are phagocytosed by macrophages, their survival within these broadly microbicidal cells is thought to depend upon their ability to block phagosome-lysosome fusion and subsequent acidification. This notion persists despite multiple studies in cultured macrophages, spanning several decades, reporting a substantial proportion of viable mycobacteria in phagolysosomes. This work shows that while lysosomal trafficking in the macrophage can slow bacterial replication, it does not kill the pathogen. For its part, the mycobacterium survives within the macrophage lysosome through the action of a highly conserved virulence factor that mediates acid tolerance in vitro. A concurrent forward genetic screen identified a zebrafish mutant that is hypersusceptible to *M. marinum* infection and manifests hallmarks of human lysosomal storage diseases. The mutant is deficient in the lysosomal hydrolases Cathepsin B and L, although its

hypersusceptibility does not stem from defective intramacrophage restriction of mycobacterial growth. Rather the mutant's hypersusceptibility is attributed to defective macrophage migration owing to accumulated undegraded cell products that accumulate through normal homeostatic macrophage function. Similarly, macrophage migration defects underlie hypersusceptibility to mycobacterial infection following disruption of the zebrafish orthologs of genes implicated in human lysosomal storage disorders. All of these migration defects share a common mechanism in disrupted endocytic recycling caused by the lysosomal accumulation of undigestible cargo. Macrophage immotility resulting from lysosomal storage defects causes hypersusceptibility by compromising migration to dying infected cells in the granuloma, resulting in its breakdown with extracellular release of bacteria. Lysosomal storage defects also disrupt macrophage participation in the earliest stage of infection when resident macrophages migrate to and phagocytose newly arriving mycobacteria. The alveolar (lung resident) macrophages of human smokers display lysosomal accumulations of tobacco smoke and fail to migrate to *M. tuberculosis*. This may explain the increased susceptibility of human smokers to TB. This work defines the limited protection afforded to the host by lysosomal trafficking in the restriction of intramacrophage mycobacterial replication, and elucidates the consequences of lysosomal dysfunction, which results in host susceptibility through a completely distinct mechanism of macrophage incapacitation following the lysosomal accumulation of indigestible cargo.

Acknowledgements and Dedication

This work would not have been possible without the contributions of a great number of people. I would like to extend my deepest gratitude to past and present members of the Ramakrishnan lab for their support and collaboration. Specifically, I would like to thank Russell Berg and Antonio Pagán for their tireless support and mentorship; my thesis committee members for their guidance, scientific and otherwise; CJ Cambier, Christine Cosma, Kevin Takaki, and James Cameron for technical know-how; Kevin Takaki for making figures; and my collaborators Kristin Adams, Kevin Urdahl, Mary O'Sullivan, Seonadh O'Leary, and Joseph Keane for their work on the mouse and human experiments. Finally, I want to thank Lalita Ramakrishnan for her unwavering support and dedication to my training.

This work is dedicated to my wife Rebecca who, without pause, left everything behind and moved 4,750 miles so that I could continue my scientific pursuits.

Table of Contents

Abstract 3

Acknowledgements and Dedication 5

Chapter 1: The early pathogenesis of tuberculosis 7

Chapter 2: Mycobacterial Acid Tolerance in Vivo Underlies the Establishment of Tuberculous Infection 13

- Summary 13
- Introduction 14
- Results 16
- Discussion 25
- Experimental Procedures 27
- Chapter 2 Figures and Tables 34

Chapter 3: Lysosomal Disorders Drive Susceptibility to Tuberculosis by Compromising Macrophage Migration 49

- Summary 49
- Introduction 50
- Results 52
- Discussion 65
- Experimental Procedures 70
- Chapter 3 Figures and Tables 80

Chapter 4: Multifaceted roles of the macrophage lysosome during early tuberculous infection 105

- Chapter 4 Figures 113

Concluding Thoughts 114

References 115

Chapter 1: The early pathogenesis of tuberculosis

Between the 17th and 19th centuries, tuberculosis (TB) was a leading cause of human morbidity and mortality worldwide (Holmberg, 1990). Even today, the WHO estimates that more than 1 million people die annually from TB, and upwards of 9 million become infected with *Mycobacterium tuberculosis*, the causative agent of TB. These numbers are startling considering the discovery of compounds capable of killing *M. tuberculosis* occurred well over 50 years ago (Hinshaw et al., 1946). Treatment of TB requires at least 6 months of antimicrobial therapy and the problem of drug resistance is expanding, with nearly half a million new cases of multidrug-resistant TB in 2013 (Zumla et al., 2013). While the BCG vaccine is partially effective in preventing military TB in children, it has no protective effect against adult pulmonary TB, the most common form of disease, and efforts to design an effective vaccine for adult pulmonary TB have so far not shown success, hampering public health interventions aimed at limiting transmission (Tameris et al., 2013). The development of new TB therapies has been stymied by limitations in our understanding of the pathogenesis of *M. tuberculosis* infection in humans. Specifically, little is known about the earliest events of infection, when epidemiological evidence suggests that a large proportion of humans (up to 30-50%) can clear the infection (Morrison et al., 2008; Verrall et al., 2014).

The following is a brief introduction to the early stages of tuberculosis pathogenesis which highlights the points at which infection can be cleared or limited by host immune cells or effectors.

Step 1: Bacteria pass through the entire pulmonary system to arrive at the alveolus

The anatomy of the host respiratory system provides opportunities for clearance at multiple steps during early infection. To arrive in the alveolus, the bacteria must avoid landing in the nasopharynx and bronchial system, where they can be killed by highly activated resident macrophages (Cambier et al., 2014a; Cambier et al., 2014b). In fact, 1-3 bacteria in small aerosol form are more infectious to rabbits than 10,000 bacteria in large aerosolized particles, which become lodged in the trachea and are subsequently destroyed (Ratcliffe and Wells, 1948). If the bacterium passes this barrier and lands in the alveolus, it must then contend with two further challenges. First, the alveolar airspace is nutrient-poor (in contrast to blood, which is nutrient-rich) and is separated from the blood by an epithelial barrier that is not easily crossed. Second, the alveoli are home to alveolar macrophages, first-responding phagocytes that rapidly phagocytose and destroy a wide array of pathogens that arrive in the alveoli (Green and Kass, 1964; Hocking and Golde, 1979a).

Step 2: Bacteria first encounter host resident macrophages

How the fate of newly infecting *M. tuberculosis* is determined within the alveolar macrophage following phagocytosis has been a matter of some debate for decades. Several studies have demonstrated that a substantial proportion of people clear the infection at this initial stage, even despite repeated or prolonged exposure. For example, up to 50% of individuals living in high-incidence areas do not show evidence of an adaptive response to *M. tuberculosis*, meaning that many of these individuals likely cleared infection before it had a chance to spread beyond the initial responding macrophages (Morrison et al., 2008). In 1965, a submariner was discovered to have had active TB while on a 6-month assignment. A detailed study of the submarine crew including sleeping arrangements, social and working interactions yielded several

insights into the epidemiology of TB (Houk et al., 1968). Almost 50% of the crew became infected due to the failure to identify a single case of active TB. Yet in the compartment with the highest number of active infections (6 of 66 individuals with active disease and 52 whose skin antigen test demonstrated conversion indicating evidence of infection with adaptive involvement) there were 13 individuals who had been on board a substantial time yet did not have skin test conversion 6 months later (Houk et al., 1968). The fact that some of these individuals were sleeping adjacent to those with active TB is strong evidence for early clearance (Houk, 1980).

Despite evidence for early clearance, *M. tuberculosis* frequently succeeds in establishing an intramacrophage growth niche as evidenced by the WHO's estimate that more than 9 million people became sick with TB in 2014. The mechanism by which *M. tuberculosis* survives this first interaction has been an area of study for decades. After ingestion of particulate material, macrophages traffic it to intracellular compartments (phagosomes), which undergo stepwise maturation. This maturation consists of compartment acidification mediated by the F0/F1 vacuolar ATPase (V-ATPase) and a series of fusion and fission events that eventually leads to fusion with lysosomes, or the creation of phagolysosomes (Desjardins, 1995). The lysosome is home to a variety of factors lethal to pathogens, including degradative enzymes, antimicrobial chemicals such as reactive nitrogen and oxygen species, and acid. The pH of a mature lysosome can fall well below 5, which is sufficient to kill a variety of common bacteria (Cotter and Hill, 2003; Mindell, 2012). Early studies of the intracellular localization of pathogenic mycobacteria found the majority of bacteria in nonacidified phagosomes but some were located in compartments that had fused with lysosomes (Armstrong and Hart, 1971). This was further complicated when a follow-up study coaxed mycobacteria into lysosomes by coating them with

antibodies so that they were taken up by Fc receptors and delivered to phagolysosomes but found that the bacteria were not killed and in fact still replicated in these compartments (Armstrong and Hart, 1975). An in vitro forward genetic screen identified a *M. tuberculosis* virulence factor that was required for survival in acidic environments (Vandal et al., 2008) though the gene's pleiotropic functions confounded a complete understanding of its role in mediating survival within the macrophage phagolysosome (MacMicking, 2008). In vitro studies after the initial findings by Armstrong and Hart mostly found anywhere between 10 and 30% of mycobacteria in lysosomal compartments, with the rest in nonacidified phagosomes (Barker et al., 1997; Clemens and Horwitz, 1995; Harris et al., 2008; Pethe et al., 2004). If the macrophages were pre-treated with gamma-interferon prior to infection, however, they were able to deliver more of the bacteria to lysosomes and kill them (Schaible et al., 1998; Via et al., 1998). Gamma-interferon is predominantly produced by T-lymphocytes, which are not seen until the onset of adaptive immunity (Flynn and Chan, 2001). Thus, it was proposed that *M. tuberculosis* survives within the alveolar macrophage by blocking phagosomal maturation early, but then endures in lysosomes later during the adaptive immune response when gamma-interferon forces the bacteria into these hostile compartments (MacMicking, 2008). These two models of mycobacterial avoidance and tolerance of phagosomal acidification hint at the potential for a tiered strategy in which an infecting bacterium first attempts to avoid trafficking to the macrophage phagolysosome, but then must tolerate its effects if the macrophage successfully consigns it to the lysosome. But previous studies have left unanswered the question of the relative contribution of avoidance and tolerance strategies to the establishment of in vivo infection, and whether clearance of initial infection is dependent upon quickly delivering *M. tuberculosis* to the macrophage phagolysosome.

Step 3: Infection expands through the recruitment of additional macrophages from afar

If the bacillus survives its encounter with the alveolar macrophage, it is carried by this cell across the alveolar epithelial barrier and meanwhile continues to replicate within the intracellular niche. In mouse models of aerosol tuberculosis infection, the bacteria are found almost exclusively within alveolar macrophages for the first week of infection (Srivastava et al., 2014; Urdahl, 2014). After this timepoint, the infection spreads to other cell types (e.g. dendritic cells and monocytes recruited from peripheral tissues). During this stage, the bacteria manipulate their host macrophage in order to secure a more favourable intracellular growth niche since these recruited cells are less microbicidal than the first-responding alveolar macrophages (CJ Cambier, unpublished results) (Aston et al., 1998).

Eventually the bacteria are transported deeper into the lung and here newly recruited myeloid and other immune cells aggregate around the infected cells to form organized granulomas (Cambier et al., 2014a). The granuloma expands through the apoptotic death of infected macrophages followed by their phagocytosis by additional uninfected macrophages arriving from afar (Davis and Ramakrishnan, 2009). Here the bacteria promote the expansion of infection through their spread into these newly arriving macrophages. The host finds itself in a lose-lose situation; if the supply of uninfected macrophages arriving to the granuloma becomes limiting for any reason, the apoptotic infected cells in the granuloma undergo secondary necrosis, releasing the bacteria into the nutrient-rich extracellular space which accelerates their replication (Pagan et al., 2015).

This work seeks to determine the role of the macrophage lysosome during the establishment and expansion of tuberculous infection in vivo. Previous work supports the idea

that mycobacteria employ both tolerance and avoidance strategies with regard to macrophage lysosomal trafficking. This work aims to deepen our understanding by determining the relative contribution of these strategies to the establishment of infection in the first macrophage that encounters newly infecting mycobacteria, and in the expansion of infection within the macrophages that constitute the forming granuloma. Concomitantly, the study of a separately identified zebrafish mutant that is hypersusceptible to infection and is deficient in two lysosomal hydrolases has identified an intriguing and completely distinct function of the macrophage lysosome in permitting cell migration both to newly infecting bacteria and also to dying infected macrophages within the forming granuloma. The intersection of these two projects has yielded insight into the multifaceted roles of the lysosome during early tuberculous infection, which elucidates the strategies employed by mycobacteria to establish infection in the host, and identifies potential mechanisms by which host cellular defects underlie susceptibility to infection.

Chapter 2: Mycobacterial Acid Tolerance in Vivo Underlies the Establishment of Tuberculous Infection

Summary

The blockade of phagolysosomal fusion is considered a critical mycobacterial strategy to survive in macrophages. This notion persists despite studies in cultured macrophages reporting viable mycobacteria in phagolysosomes and the identification of the mycobacterial virulence determinant MarP, which mediates acid resistance in vitro. Here we show, using mice and zebrafish, that innate macrophages overcome mycobacterial lysosomal avoidance strategies to rapidly deliver a substantial proportion of infecting bacteria to phagolysosomes. We exploit the optical transparency of the zebrafish to track the fates of individual mycobacteria delivered to phagosomes versus phagolysosomes. We find that bacteria survive and grow in phagolysosomes, though growth is slower than in nonacidified phagosomes. MarP is required specifically for phagolysosomal survival making it an important determinant of the ability of mycobacteria to establish infection in their hosts. Our work elucidates the tiered strategy employed by pathogenic mycobacteria wherein they tolerate lysosomal trafficking if they fail to prevent it.

Introduction

As first line immune defense cells, macrophages phagocytose invading microbes, delivering them to the lysosomal compartment for degradation (Huynh and Grinstein, 2007). Therefore, to survive intracellularly, pathogens must avoid phagosomal fusion with lysosomes, escape out of the phagosome to reside in the cytosol, or survive within lysosomal compartments (Asrat et al., 2014). According to the prevailing dogma, active avoidance of phagosome-lysosome fusion is a key mycobacterial survival strategy particularly during the innate immune phase of infection (Asrat et al., 2014; Behar and Baehrecke, 2015; Kasper et al., 2015; MacMicking, 2008; Tan and Russell, 2015). The persistence of this dogma is puzzling given: 1) Multiple studies reporting a substantial proportion of infecting *M. tuberculosis* in phagolysosomes soon after infection of cultured macrophages: 10-25% and 15-36% at 2-3 hours and 24 hours, respectively (Table S1); 2) the demonstration that *M. tuberculosis* coaxed into lysosomes, either through Fc receptor-mediated phagocytosis or co-infection with the lysosomal pathogen *Coxiella,* survives and even replicates in these compartments (Armstrong and Hart, 1975; Gomes et al., 1999); 3) the discovery of a *M. tuberculosis* virulence factor - the membrane serine protease Rv3671c (MarP) - that also mediates acid tolerance in vitro (Small et al., 2013; Vandal et al., 2009; Vandal et al., 2008). Nevertheless, the idea that phagosomal blockade is integral to *Mycobacterium*'s intracellular survival and growth has been perpetuated by studies showing that pretreatment of macrophages with gamma-interferon (IFNγ), a cytokine produced predominantly during the adaptive immune response, increases phagolysosomal fusion and decreases bacterial survival. This led to the conclusion that IFNγ increases macrophage microbicidal capacity by enhancing mycobacterial trafficking to lysosomes (Table S1) (Flynn and Chan, 2001; Harris et al., 2008; Schaible et al., 1998; Via et al., 1998). However, IFNγ can

enhance macrophage killing through multiple mechanisms (Nunes-Alves et al., 2014) and dead mycobacteria are trafficked to macrophage lysosomes independently of IFNγ (Armstrong and Hart, 1975; Barker et al., 1997). Therefore, the enhanced killing mediated by IFNγ might be the cause of increased lysosomal trafficking rather than the effect. Despite this alternative possibility, the lysosomal avoidance model predominates (Asrat et al., 2014; Behar and Baehrecke, 2015; Kasper et al., 2015; MacMicking, 2008; Tan and Russell, 2015).

We directly address the prevalence and consequences of lysosomal trafficking in vivo using the optically transparent zebrafish larva, which allows for real-time tracking of infection with *M. marinum,* a close genetic relative of *M. tuberculosis* and a natural agent of tuberculosis in ectotherms (Ramakrishnan, 2013). We find that innate macrophages in the absence of IFNγ stimulation deliver a substantial proportion of infecting mycobacteria to lysosomes. We find that lysosomal trafficking does represent a host-beneficial strategy; however, it is effectively counteracted by mycobacterial MarP, which enables bacterial survival and growth within lysosomes.

Results

M. tuberculosis resides in macrophage phagosomes and phagolysosomes after aerosol infection of mice

Macrophages derived from a variety of hosts rapidly traffic a proportion of infecting mycobacteria to lysosomes in vitro (Table S2.1). We asked whether this was also the case in vivo during the first macrophage-mycobacterium interaction, which in humans and mice is thought to occur within lung-resident macrophages (Verrall et al., 2014). We infected mice with ~ 200 fluorescent *M. tuberculosis* by aerosolization and assessed lysosomal trafficking as judged by bacterial co-localization with LysoTracker, an acidophilic dye that labels lysosomes. We chose 13 days and 19 days post-infection, timepoints that flank the 14-15 day time point when IFNγ-producing T cells begin to arrive in the lung after aerosol *M. tuberculosis* infection (Khader et al., 2007). (Analysis before 13 days was precluded by the rarity of *M. tuberculosis*-infected cells.) *M. tuberculosis* in lysosomal compartments was readily observed in all animals (two at 13 days and three at 19 days) (Figure 2.1 and Figure S2.1) though the relative rarity of infected cells even at these timepoints precluded quantification of the extent of lysosomal trafficking. Because lung-resident macrophages are the predominant infected cell type at the earlier time point after aerosolized *M. tuberculosis* infection (Wolf et al., 2007), our findings suggest that these first-responding cells can traffic *M. tuberculosis* to lysosomes in the sole context of innate immunity. Our findings are supported by observations of *M. tuberculosis* in lysosomal compartments of infected macrophages in the liver 3 days following intravenous infection (Jayachandran et al., 2007); the infected cells are likely liver-resident macrophages or Kupffer cells that rapidly phagocytose blood-borne mycobacteria (Egen et al., 2008). A human study of HIV-positive

tuberculosis patients also found ~ 30% of *M. tuberculosis* in phagolysosomes of alveolar macrophages obtained by bronchoalveolar lavage, although the duration of infection was unknown in this case (Table S2.1) (Mwandumba et al., 2004).

A proportion of *M. marinum* is rapidly trafficked to lysosomes after infection of larval zebrafish

To probe lysosomal trafficking of mycobacteria and its consequences in vivo in real-time, we turned to zebrafish larvae infected with *M. marinum*. In cultured macrophages, a similar proportion of *M. marinum* (21% at 4 hours post-infection) as *M. tuberculosis* is rapidly trafficked to lysosomes (Table S2.1) (Barker et al., 1997). We infected zebrafish larvae with fluorescent *M. marinum* in the hindbrain ventricle (HBV), a cavity to which resident macrophages from the brain rapidly migrate to phagocytose the bacteria (Cambier et al., 2014b) (C.J. Cambier and L.R., unpublished results) (Figure 2.2A). Using LysoTracker, which has been shown to label lysosomes in larval zebrafish (Peri and Nüsslein-Volhard, 2008), we found that a substantial proportion of the bacteria was in acidified compartments within 24 hours post-infection (hpi) (Figure 2.2B and 2.2C). To see if phagolysosomal fusion was also a feature of mycobacteria infecting monocytes (cells that are more likely than resident macrophages to harbor bacteria later in infection), we repeated the analysis after injecting bacteria into the caudal vein (CV), which traverses the hematopoietic tissue, the site of intermediate myelopoiesis giving rise to circulating monocytes (Clements and Traver, 2013) (Figure 2.2A). Again we found that mycobacteria were rapidly and progressively delivered to acidified compartments within 3–24 hpi (Figure 2.2D). Because the mycobacterial phagosome has been reported to be acidified in vitro with a pH of 6.2 (Tan and Russell, 2015), we asked whether the bacteria colocalizing with LysoTracker were in

slightly acidified phagosomes or in bona fide lysosomal compartments, which are characterized by a pH < 5 and contain hydrolytic enzymes. We directly assessed the pH at the bacterial surface by labeling *M. marinum* prior to infection with pHrodo, a pH-sensitive dye. Incubation of pHrodo-stained *M. marinum* in phosphate-citrate buffer at a range of pH values showed that fluorescence was greatly increased in bacteria experiencing a pH of ≤ 5.0 (Figure S2.2A). We used a fluorescence intensity cutoff for imaging pHrodo-stained bacteria in the zebrafish so as to exclude those experiencing pH> 5.0 (Figure S2.2A). pHrodo-stained bacteria were detected soon after both HBV and CV infection (Figure 2.2E and 2.2F), and co-staining with LysoTracker and pHrodo showed strong overlap (Figure S2.2B and S2.2C). Staining with MR-Cathepsin and DQ-BSA, fluorogenic protease substrates that fluoresce only upon hydrolysis and label macrophage lysosomes in zebrafish (Peri and Nüsslein-Volhard, 2008), revealed a similar proportion of phagolysosome-localized bacteria as did pHrodo staining (Figure 2.2G and 2.2H). Thus, during in vivo infection, macrophages rapidly deliver a proportion of mycobacteria to bona fide lysosomal compartments characterized by hydrolase activity and pH < 5. The faster kinetics of lysosomal trafficking in infected resident macrophages (HBV) versus monocytes (CV) (Figure 2.2F-H) is consistent with the observed increased phagolysosomal fusion activity of primary human lung-resident alveolar macrophages versus blood monocytes upon infection with *M. tuberculosis* (O'Leary et al., 2011).

In the context of cultured macrophages, the observed distribution of *M. tuberculosis* and *M. marinum* in phagosomes versus phagolysosomes is the result of counteracting macrophage and bacterial strategies. While the macrophage can consign a significant proportion to the lysosome, the majority of bacteria actively avoid this fate, as evidenced by the finding that killed bacteria are rapidly trafficked to lysosomes (Armstrong and Hart, 1971; Barker et al., 1997).

Multiple determinants have been implicated in *M. tuberculosis'* avoidance of lysosomes, e.g. the tyrosine phosphatase PtpA (Bach et al., 2008), and the specialized secretion system ESX-1 (MacGurn and Cox, 2007). To further validate our findings in zebrafish macrophages, we first asked if *M. marinum* actively avoids lysosomal trafficking by comparing pHrodo-stained live and heat-killed bacteria (Figure 2.2I). We observed increased lysosomal localization of killed *M. marinum*. Moreover, both a *M. marinum ptpA* (*mmar_3309*) transposon insertion mutant and an ESX-1-deficient mutant displayed increased lysosomal localization albeit less than heat-killed bacteria (Figure 2.2I and 2.2J), suggesting the presence of additional mycobacterial factors that mediate phagolysosomal blockade, as has been reported for *M. tuberculosis* (Asrat et al., 2014).

In sum, our findings suggest that *M. marinum* actively blocks phagosome-lysosome fusion during zebrafish infection through mechanisms similar to those used by *M. tuberculosis* in cultured macrophages. But similarly to observations in cultured macrophages, this blockade is only partially successful. Conversely, macrophages, regardless of lineage or species, are robustly equipped to consign a substantial proportion of infecting mycobacteria to lysosomal compartments.

Trafficking of mycobacteria to lysosomes does not require IFNγ

Our observed proportions of phagolysosomal bacteria at 24 hpi (45% in CV and 52% in HBV) were a little higher than the 15-36% reported for *M. tuberculosis* and *M. marinum* in cultured macrophages (Figure 2.2C and 2.2D and Table S2.1). Since IFNγ stimulates phagosome-lysosome fusion in cultured macrophages (Schaible et al., 1998; Via et al., 1998), we asked if it could be responsible for the small increase in lysosomal trafficking observed in vivo. In mammals, IFNγ is predominantly produced by T-lymphocytes, which have not yet developed

in the zebrafish larvae (Trede et al., 2001); however there are also innate sources of IFNγ (e.g. natural killer cells) (Renshaw and Trede, 2012). There are two zebrafish IFNγ orthologues--*ifng1-1* and *ifng1-2*. Both were induced largely in a RAG-dependent fashion at 6 weeks post-infection in adult zebrafish similar to mouse *M. tuberculosis* infection where adaptive immune cells are the predominant source of IFNγ (Baldridge et al., 2010; Flynn and Chan, 2001) (Figure S2.3A and S2.3B). Similar trends were observed by two weeks post-infection in adults (Figure S2.3C and S2.3D). To look for innate sources of IFNγ with a more sensitive assay, we tested *ifng1-2* expression in response to the potent IFNγ inducer, the TLR3 agonist poly(I:C) (Aggad et al., 2010) (Figure S2.3E). We confirmed its rapid induction (4 hours post-administration) in adult animals from both innate and adaptive immune sources, but predominantly the latter (Figure S2.3E). In the larva also, we observed poly(I:C)-mediated induction of IFNγ starting at 4 days postfertilization but failed to detect induction of either homolog earlier in development (Figure S2.3F). This pattern held up for *M. marinum* infection: neither *ifng1-1* nor *ifng1-2* induction was detected before four days post-fertilization (two days post-infection) (Figure S2.3G). In sum, our data suggest that zebrafish induce IFNγ in response to *M. marinum* similarly to mice responding to *M. tuberculosis*. While some IFNγ can be made by innate sources, these innate cells have yet to mature during the window used in our studies on phagolysosomal fusion. While we failed to observe induction of IFNγ at early timepoints, this does not exclude small amounts being present from early during development. We addressed this possibility by assessing infection in larvae injected with *ifng1-1* and *ifng1-2* morpholinos, *crfb17* morpholino (part of the signaling machinery for both IFNγ1 and IFNγ2), and a mutant in *crfb17* (Aggad et al., 2010; Sieger et al., 2009). We did not observe hypersusceptibility to infection in any of these conditions (Figure

S2.3H-J). Thus, this early phagolysosomal fusion likely represents the intrinsic ability of the macrophage to deliver infecting bacteria to lysosomal compartments.

The host-protective effect of lysosomal trafficking is limited through the action of the mycobacterial serine protease MarP

Studies in cultured macrophages have come to different conclusions about the consequences of mycobacterial phagolysosomal trafficking depending on the stimulus used to achieve it. Mycobacteria delivered into phagolysosomes by opsonization or by co-infection with the lysosomally-localized bacterium *Coxiella burnetti* survived and even replicated in lysosomes whereas bacteria reaching lysosomes following IFNγ stimulation of the macrophages were killed (Armstrong and Hart, 1975; Cosma et al., 2003; Gomes et al., 1999). To test macrophage-intrinsic phagosomal maturation as a microbicidal effector mechanism in vivo, we disrupted phagosomal maturation by treating larvae with the vATPase inhibitor Bafilomycin (Peri and Nüsslein-Volhard, 2008), or used a translation-blocking morpholino targeting *atp6v1a*, a subunit required for vATPase function in the zebrafish (Horng et al., 2007). LysoTracker and pHrodo staining each confirmed disruption of lysosomal localization in the context of infection (Figure S4A-C). Bafilomycin treatment and *atp6v1a* knockdown both increased bacterial burdens within 24 hours (Figure 2.3A and 2.3B). This increase in bacterial burdens was reflected in increased bacterial replication within individual larval macrophages (Figure 2.3C), similar to the reduced microbicidal capacity of TNF-deficient macrophages (Figure 2.3C) (Clay et al., 2008; Takaki et al., 2013). Thus, phagosomal maturation restricts the progression of infection by decreasing intramacrophage replication of *M. marinum*.

The fact that *M. marinum* infection progresses overall despite growth restriction mediated by the lysosome suggested one of two explanations: either that the expansion of overall infection is driven exclusively by the bacterial population avoiding lysosomes, or that bacteria can replicate in both phagosomes and lysosomes. To distinguish between these possibilities, we used two mutants - a transposon mutant in the ortholog (*mmar_5159*) of the *M. tuberculosis* membrane serine protease MarP, which is required for acid tolerance in vitro and virulence in mice (Vandal et al., 2008); and *ptpA*::Tn which displays increased lysosomal trafficking (Figure 2I). We confirmed that *marP*::Tn was acid-sensitive and hypersusceptible to lipophilic antibiotics in vitro, and attenuated in vivo (Figure S2.5A-D and Figure 2.3D), consistent with the phenotypes of its *M. tuberculosis* counterpart (Vandal et al., 2008). Because of MarP's multiple in vitro phenotypes (increased susceptibility to acid, hydrophobic antibiotics and detergents, reactive oxygen species and nitric oxide), it has not been clear which of these is responsible for its attenuation in vivo (Ehrt et al., 2015; Stallings and Glickman, 2010). We reasoned that if defective lysosomal tolerance contributes to *marP*::Tn attenuation, then Bafilomycin should enhance *marP*::Tn growth more than wildtype. It did (2.0±0.15 fold increase in burden for *marP*::Tn versus 1.5±0.06 for wildtype, $p = 0.01$) (Figure 2.3E and 2.3F). Furthermore, *marP*::Tn was ~ 25 times more attenuated than *ptpA*::Tn during a 5-day infection (Figure 2.3F and 2.3G), suggesting that, in vivo, tolerance of the acidic lysosomal environment is a more significant determinant of mycobacterial growth than avoidance of phagosome-lysosome fusion. This is consistent with findings in the mouse-*M. tuberculosis* aerosol infection model where the MarP mutant is severely attenuated but the PtpA mutant is not (Grundner et al., 2008; Vandal et al., 2008). In sum, lysosomal trafficking is a host-beneficial strategy that limits intramacrophage mycobacterial growth and thereby expansion of infection in the granuloma. The effectiveness of

this strategy is substantially offset, however, by MarP-mediated tolerance of lysosomal trafficking.

Mycobacteria delivered to phagolysosomes can successfully establish infection in a MarP-dependent fashion

Next, we probed the basis of lysosomal trafficking as a host-protective mechanism (bactericidal, bacteriostatic or simply slowing bacterial growth), and conversely how mycobacterial MarP counters this strategy. The optical transparency of the zebrafish allowed us to map the fate of individual mycobacteria following initial distribution into phagosomes versus phagolysosomes. We injected single pHrodo-labeled bacteria into the HBV (Figure 2.4A), sorted the animals based on whether the bacteria colocalized with pHrodo at 12 hpi, and then tracked bacterial fates for 48 hours to determine if the host was still infected based on the presence of fluorescent *M. marinum* in the HBV (Figure 2.4A). The fraction of infected larvae at 60hpi was not significantly different between the phagosomal and phagolysosomal groups (Figure 2.4B). We confirmed that the bacteria were alive and metabolically active by photobleaching them and assessing for recovery of fluorescence (Figure 2.4C and 2.4D). In infected animals, we assessed the extent of bacterial growth in phagosomes versus phagolysosomes by enumerating the number of bacteria at 60 hpi. *M. marinum* replicated within the phagolysosome, though at a slower rate than in the non-acidified phagosome (Figure 2.4E).

Consistent with a primary role of MarP in tolerating the lysosomal environment, *marP*::Tn was cleared more than wildtype only when it was trafficked to the phagolysosome (Figure 2.4F). Individual mutant bacteria that were in nonacidified phagosomes survived similarly to wildtype (compare Figures 2.4F and 2.4D). In contrast, *ptpA*::Tn and ΔESX-1,

which are preferentially trafficked to the phagolysosome but are not sensitive to acid in vitro, survived in either compartment similarly to wildtype (Figure 2.4G and 2.4H).

In sum, these experiments suggest that lysosomal residence is fully conducive to mycobacterial survival and also supports growth, albeit at a slower rate than nonacidified phagosomes. Mycobacterial MarP mediates this lysosomal survival.

Discussion

Our works suggests that pathogenic mycobacteria encounter and counter macrophage phagolysosomal fusion from the earliest stage of infection. Our findings elucidate the tiered strategy employed by newly arriving mycobacteria to successfully establish infection in first-responder macrophages. In the face of frequently successful phagosome-lysosome fusion by these macrophages, mycobacteria must fall back on their ability to contend with microbicidal arsenal of the lysosome (Vandal et al., 2009).

The increased lysosomal localization (40-50%) we observe in vivo over cultured macrophages (15-36%) may reflect the enhancement of intrinsic macrophage phagolysosomal fusion capacity by cues in vivo - cues that must derive from innate immunity since they are independent of both IFNγ and Fc receptor (i.e. antibodies).

In terms of the consequences of phagolysosomal fusion, we find that it does not enhance the macrophage's ability to kill bacteria nor does it induce bacteriostasis. Mycobacteria continue to grow in both compartments albeit more slowly in phagolysosomes. These in vivo findings differ from those in cultured macrophages where lysosomal fusion was induced by Fc receptor-dependent phagocytosis and where decreased growth of the lysosomal bacteria was not observed (Armstrong and Hart, 1975). The ability of in vivo macrophage phagolysosomes to limit mycobacterial growth to some extent may reflect the presence of lysosomally-activated immune determinants such as nitric oxide (Vandal et al., 2009). This in turn suggests that ultimately lysosomal trafficking may serve as a host-protective mechanism. However, its efficacy may be limited later in infection as well, as supported by previous work showing that morphologically intact *M. marinum* were present in frog granuloma macrophage lysosomes in

unchanging and substantial numbers throughout the 17-52 week observation period infection when overall infection burdens were increasing (Bouley et al., 2001).

This work firmly links the acid tolerance conferred by mycobacterial MarP to its function as a virulence determinant during the early stages of infection. Importantly, we show that MarP specifically enables mycobacteria consigned to lysosomes to establish infection. This likely represents a critical determinant of the evolutionary survival of *M. tuberculosis* as human TB is thought to begin with the deposition of 1-3 bacteria into the lung alveolus (Bates et al., 1965; Ratcliffe and Wells, 1948), and the initial interaction between these bacteria and the first-responder, tissue-resident host macrophage is thought to determine whether the infection is cleared or progresses (Verrall et al., 2014). MarP is widely conserved across mycobacterial species, which have been reported to survive (and even be enriched) in environments as hostile as volcanic rock at pH 1 (Walker et al., 2005) (Figure S2.6). Thus, acid tolerance likely evolved as a survival mechanism well before mycobacteria encountered macrophages or free-living amebae, and joins the catalog of determinants for environmental survival that have been repurposed for host survival by the pathogenic mycobacteria (Cambier et al., 2014a).

Experimental Procedures

Bacterial Strains and Methods

Wildtype *M. marinum* (strain M - ATCC #BAA-535) expressing tdTomato or mWasabi under the constitutive promoter *msp12* was used for measurement of bacterial burden (Mm Fluorescence) and was used for quantification of intracellular bacterial burdens (Takaki et al., 2013). Wildtype *M. marinum* expressing EBFP2 under the *msp12* promoter was used as noted. All *M. marinum* strains were grown under hygromycin (Mediatech), streptomycin (Mediatech), or kanamycin (Mediatech) selection in Middlebrook's 7H9 medium (Difco) supplemented with glycerol, oleic acid, albumin, dextrose and Tween-80 (Takaki et al., 2013). Single-cell stocks were prepared as described for injection, and inocula were determined by injection onto selective 7H10 plates (Takaki et al., 2013). Heat-killed bacteria were prepared by incubating at 80°C for 20 minutes (Cambier et al., 2014b). *M. marinum pks15* mutant was used as described (Cambier et al., 2014b). *mmar_5159* and *mmar_3309* mutants were isolated from a library of transposon mutants generated in *M. marinum* (CC, unpublished results). Briefly, a transposon was created that contains an excisable hygromycin-resistance cassette to allow capture of transposon proximal sequences and this transposon was used to mutagenize wildtype *M. marinum*. The location of the transposon insertion in each gene was confirmed by sequencing prior to use.

Mouse husbandry and *M. tuberculosis* infection

Mouse husbandry and experiments were conducted in accordance with an animal study proposal approved by the Center for Infectious Disease Research Animal Care and Use Committee. C57BL/6 mice were purchased from Jackson Laboratories or maintained in house. Mice were infected with ~200 CFU of aerosolized *Mycobacterium tuberculosis* (Mtb) strain

H37Rv expressing mCherry in a Glas-Col infection chamber (Glas-Col, Terre Haute, IN). Two mice from each infection were sacrificed and lung homogenates were plated to determine the deposition of Mtb.

For ex vivo imaging studies, single cell lung preparations were made as previously described (Moguche et al., 2015). Infected (mCherry expressing) cells were isolated by FACS sorting with a FACSAria II (BD Biosciences, Franklin Lakes, NJ). Infected cells were then seeded onto 24-well glass-bottom plates coated with Cell-Tak adhesive (Corning) and incubated with 75nM LysoTracker Green DND-26 (Molecular Probes) for 30 minutes. Cells were washed and immediately imaged using an inverted Nikon microscope fitted with 20x and 40x objectives.

Zebrafish husbandry and *M. marinum* infections in zebrafish

Zebrafish husbandry and experiments were in compliance with guidelines from the UK Home Office and the US National Institutes of Health and approved by the University of Washington Institutional Animal Care and Use Committee. The Tg(*mpeg1:YFP*)^{w200} line was used as previously described (Pagan et al., 2015). Transgenic lines were maintained as outcrosses to AB. Larvae were maintained in fish water supplemented with *N*-phenylthiourea (PTU) from 1 day post-fertilization. Larvae were infected at 48-72 hours post-fertilization via caudal vein (CV) or hindbrain ventricle (HBV) injection using thawed single-cell suspensions. Larvae were randomly assigned to different experimental conditions, and were assigned after infection for all drug treatment studies. For the infectivity assays, larvae were infected in the HBV at 2.5dpf with 0.4 bacteria per injection. Fish containing single bacteria were identified 3 hours post-infection (hpi) by confocal microscopy and were again scored at 12hpi for pHrodo sorting using cutoff parameters as in Figure S2A. Intramacrophage burdens were enumerated as described (Takaki et

al., 2013). Heterozygous *rag1* mutant zebrafish were obtained from Artemis Pharmaceuticals (Köln, Germany) (Wienholds et al., 2002) and maintained as heterozygotes via outcrosses to the AB line. Carriers were incrossed to generate *rag1*-/- individuals. Genotype was determined at 3 to 6 months of age using DNA obtained from a tail clip procedure as described previously (Swaim et al., 2006) using a Taqman genotyping mix containing the following primers and probes:

rag1_Forward 5'-CTCAGAGTCAGCAGACGAACTG-3' , rag1_Reverse 5'-GGTTTCCATGAAAGGCTTAGCAAAA-3', rag1_WT Reporter 5'-CCTTTGACTCGGTCACG-3', rag1_ Mutant Reporter 5'-CCTTTGACTCAGTCACG-3'. Adult intraperitoneal injections were conducted as previously described (Cosma et al., 2006). Appropriate dilutions of single cell *M. marinum* stocks were used for infection so that 5µl would contain approximately 500 CFU (acute infection) or 20 CFU (chronic infection). Inoculum was confirmed with plate counts (Cosma et al., 2006).

Poly (I:C) - Polyinosinic-polycytidylic acid (poly I:C) (Sigma-Aldrich P1530) was dissolved in PBS buffer to a concentration of 5mg/mL and sterile filtered. For adult injections, 5µL of this solution vs 5µL PBS was injected intraperitoneally. For larval injections, 2dpf larvae were injected with approximately 10nL of poly (I:C) 5mg/mL solution in the caudal vein.

Crfb17 IFNγ receptor mutants (sa1747 Sanger Zebrafish Resource) was confirmed with sequencing and then High Resolution Melt Analysis using the same primers: crfb17_HRMF: 5'-TGTCTCGAGCAGCGTATAATG-3', crfb17_HRMR: 5'- GCTGCTTCCATGTTGATTGA –3'

Microscopy

Fluorescence microscopy was performed as described (Pagan et al., 2015; Takaki et al., 2013). Quantification of bacterial burdens was performed using an inverted Nikon TiE microscope fitted with 4x and 10x objectives. For confocal microscopy, larvae were anesthetized in fish water with 0.025% Tricaine and embedded either in 1.5% low melting-point agarose or 2% hydroxymethylcellulose on optical bottom plates (MatTek). Confocal microscopy was done using a Nikon TiE microscope with 20x Plan Apo 0.75NA objective with A1 confocal system using a galvano scanner to generate 20-60µm stacks with 1-1.5µm vertical spacing. Photobleaching was performed using the 488nm laser on the confocal microscope with the minimal power and dwell time required to eliminate detection of bacterial fluorescence in the green channel. Larvae were incubated at 28°C for 12 hours prior to assessing for fluorescence recovery. Data were acquired using NIS Elements version 4.4. Microscope scoring of staining, and bacterial enumeration, were performed in a blinded manner whenever possible.

Staining

LysoTracker Red DND-99 dye (DMSO solution) (Molecular Probes) was diluted 1:25 in PBS prior to injection of 5nL into the HBV or CV of larvae, which were then incubated for 1hr prior to imaging. MagicRed-Cathepsin (Immunochemistry Technologies) was resuspended at the concentration suggested by the manufacturer in DMSO, diluted 1:4 in 1xPBS prior to injection into the HBV or CV of larvae which were incubated for 1.5hr prior to imaging. pHrodo Green STP Ester and pHrodo Red succinimidyl ester (Molecular Probes) https://www.thermofisher.com/uk/en/home/references/molecular-probes-the-handbook/ph-indicators/probes-useful-at-acidic-ph.html#head4 were resuspended in DMSO according to manufacturer instructions and stored in the dark at -20°C until use. Thawed single cell

preparations of *M. marinum* were resuspended in 200µL 1xPBS and incubated with 1µL pHrodo Green or Red for 30 min at 30°C. The bacteria were washed once with 1xPBS and resuspended in PBS pH 7.4 prior to injection into the zebrafish, or resuspended in phosphate-citrate buffer of appropriate pH for in vitro studies. For single-cell infections, the bacteria were confirmed to be pHrodo-negative at the time of dose confirmation.

Morpholinos

Morpholino oligonucleotides (mo) were designed and synthesized by Gene Tools (Philomath, OR). Morpholinos were diluted in 1x Buffer Tango (ThermoFisher) 2% phenol red sodium salt solution (Sigma) and injected 1nL into the yolk of 1 cell-stage embryos. *atp6v1a* translation blocking morpholino sequence: ATCCATCTTGTGTGTTAGAAAACTG as described (Horng et al., 2007). *tnfr1* morpholino was used as described (Roca and Ramakrishnan, 2013). *tnfr1* morpholino targeting the exon 5 / intron 6 boundary: CTGCATTGTGACTTACTTATCGCAC. *crfb17* splice blocking morpholino (GQ901865) TTAAACTAAATCGCCTTACCTTGTG, *ifng1* (NM_001020793) AAAAGAATACTGACCAGCATAGATG and *ifng2* (NM_212864) TGAAGGCGTTCGCTAAAGTTAGAGT were used as described (Aggad et al., 2010).

Drug treatments

A stock of Bafilomycin A1 (Cambridge Bioscience) was dissolved in DMSO prior to use. Larvae were treated with Baf at 50nM in 0.5% DMSO via soaking at 2dpf following infection and were assessed at 24-40 hpi.

RNA isolation and quantitative real-time PCR (qRT-PCR)

Adult fish were euthanized according to approved Animal Use Protocols. Fish were then flash-frozen with liquid nitrogen and homogenized using a mortar and pestle in 5ml Trizol reagent (Life Technologies). A 1mL aliquot was then further processed according to the manufacturer's protocol. Larval zebrafish were euthanized according to approved Animal Use Protocols. Total RNA from batches of ~30 embryos per biological replicate was isolated with TRIzol Reagent (Life Technologies) and used to synthesize cDNA with Superscript II reverse transcriptase and oligo-dT primers (Invitrogen). Quantitative RT-PCR was performed as previously described (Clay et al., 2007a) with SYBR green PCR Master Mix (Applied Biosystems) on an ABI Prism 7300 Real Time PCR System (Applied Biosystems). Each biological replicate was run in triplicate, and average values were plotted. Data were normalized to *b-actin* for ΔΔCt analysis. The primers used in this study were: ifng1-1 Forward = 5'-ATTCCTGCCTCAAAATGGTG-3', ifng1-1 Reverse 5' – TTTTCCAACCCAATCCTTTG-3', ifng1-2 Forward 5'- CTATGGGCGATCAAGGAAAA-3', ifng1-2 Reverse 5'= CTTTAGCCTGCCGTCTCTTG-3', bactin Forward 5'-ACCTCATGAAGATCCTGACC-3',
bactin Reverse 5'-TGCTAATCCACATCTGCTGG-3', tnf Forward 5'-AGGCAATTTCACTTCCAAGG-3', tnf Reverse 5'-CAAGCCACCTGAAGAAAAGG-3'

MIC assays

MICs for each strain were determined in 7H9 broth. A suspension of single bacteria was inoculated into 7H9 ($2x10^4$ ml^{-1}) containing antibiotics at different concentration and cultured for

6 days before scoring for turbidity with each concentration tested in triplicate. The MIC was defined as the minimal concentration at which turbidity was not observed.

Statistical analyses and image analysis

Images were analyzed using Imaris 7.7-8.2 (Bitplane). The Venn diagram was generated using the Pan-Omics Research Venn Diagram Plotter (http://omics.pnl.gov). Statistical analyses were performed using Prism 6 (GraphPad). Not significant (ns) $p \geq 0.05$; * $p < 0.05$; ** $p < 0.01$; *** $p < 0.001$; **** $p < 0.0001$.

Chapter 2 Figures and Tables

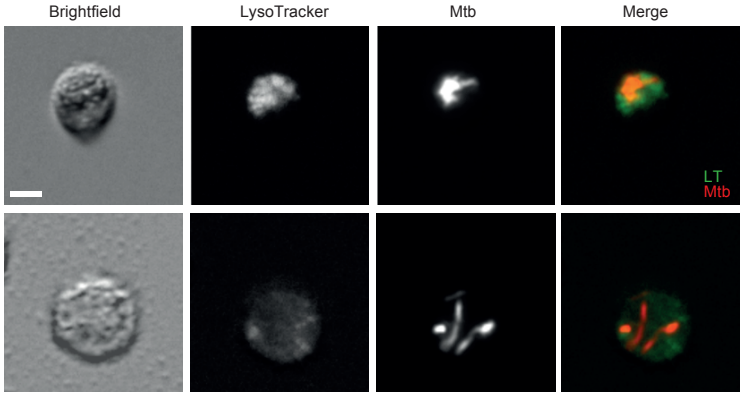

Figure 2.1: Direct ex vivo phagolysosomal localization of *M. tuberculosis*. Fluorescent images of mCherry expressing *M. tuberculosis* (Mtb) H37Rv from infected lung. Infected cells were sorted from lung tissue at 13 days post-infection and stained with LysoTracker (LT) Green dye. The top images show an infected macrophage in which the Mtb co-localizes with LysoTracker, while the bottom images show an infected macrophage in which the Mtb does not colocalize with dye. Representative of two mice. Scale bar, 5μm. See also Figure S2.1.

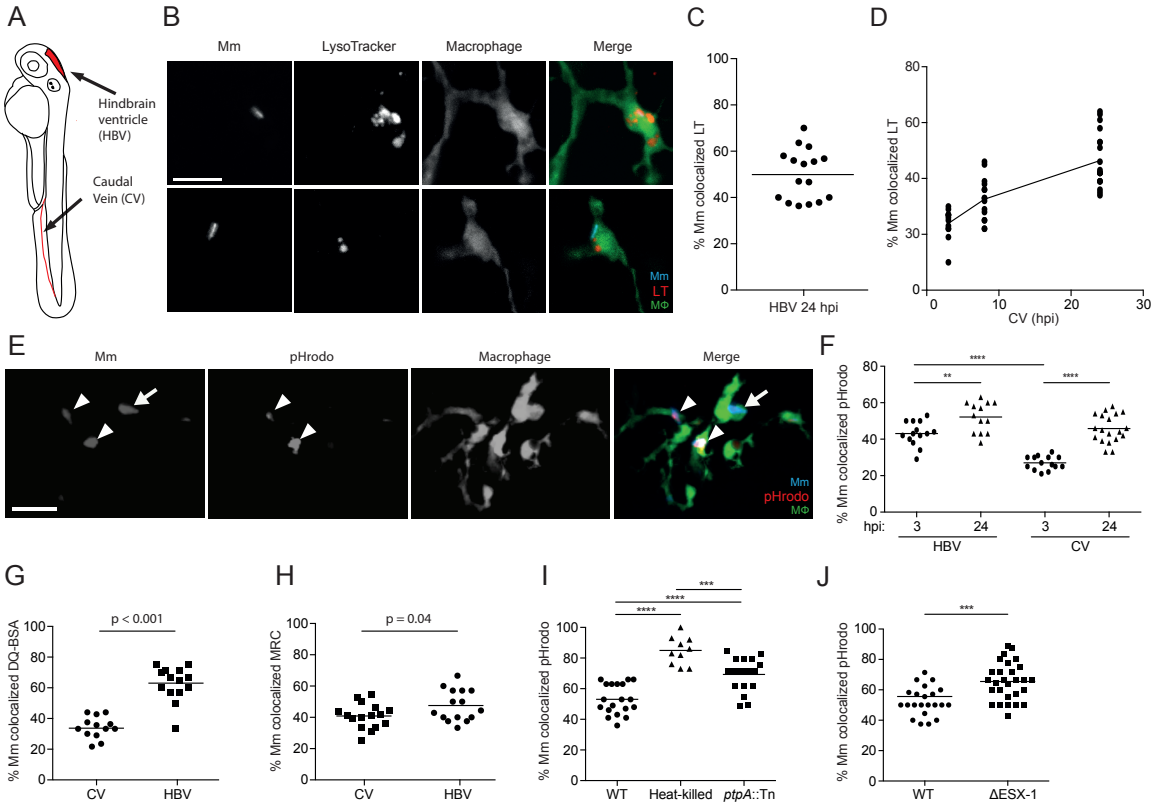

Figure 2.2: In vivo phagolysosomal trafficking of *M. marinum*. (A) Schematic illustration of zebrafish larvae with injection sites outlined in red. The hindbrain ventricle (HBV) is accessible to resident macrophages while the caudal vein (CV) traverses the caudal hematopoietic tissue where blood monocytes develop. (B) Confocal images of blue fluorescent *M. marinum* (Mm) that have been phagocytosed by green fluorescent macrophages in the brain of a 2 day post-fertilization (dpf) larva stained with LysoTracker; one bacterium shown colocalizes with LysoTracker and the other does not. Scale bar, 10μm. (C) Quantification of the percent of *M. marinum* colocalizing with LysoTracker dye 24 hours after infection into the HBV with 75 bacteria, representative of three experiments. (D) Quantification of the percent of *M. marinum* colocalizing with LysoTracker dye at 3, 8, and 24 hours post-infection (hpi) in the CV with 75 bacteria, representative of three experiments. (E) Confocal images of blue fluorescent *M.*

marinum that were pre-labeled with red fluorescent pHrodo prior to infection into the HBV of 2dpf larvae with green fluorescent macrophages; bacteria that colocalize with pHrodo (arrowheads) and one that does not (arrow). Scale bar, 10μm. (F) Quantification of the percent of Δ*pks15 M. marinum* (PGL-deficient) colocalizing with pHrodo at 3 and 24 hpi in the HBV or CV of a 3dpf larva with 80 bacteria, representative of two experiments. Δ*pks15* was used because it recruits only resident macrophages following HBV infection (C.J. Cambier and L.R., unpublished result). (G) Quantification of the percent of *M. marinum* colocalizing with MR-Cathepsin (MRC) 24 hpi in the HBV or CV of a 3dpf larva with 85 bacteria, representative of two experiments. (H) Quantification of the percent of live, heat-killed, or *ptpA*::Tn *M. marinum* pre-labeled with pHrodo prior to infection into the HBV of a 2dpf larva and scored 24 hpi with 80 bacteria, representative of three experiments. Significance tested using one-way ANOVA with Tukey's post-test (F,I) or two-tailed unpaired *t* test (G, H). Each point in C, D, F, G, H, and I represents one larva, with mean depicted as a horizontal line. See also Figure S2.2 and Figure S2.3.

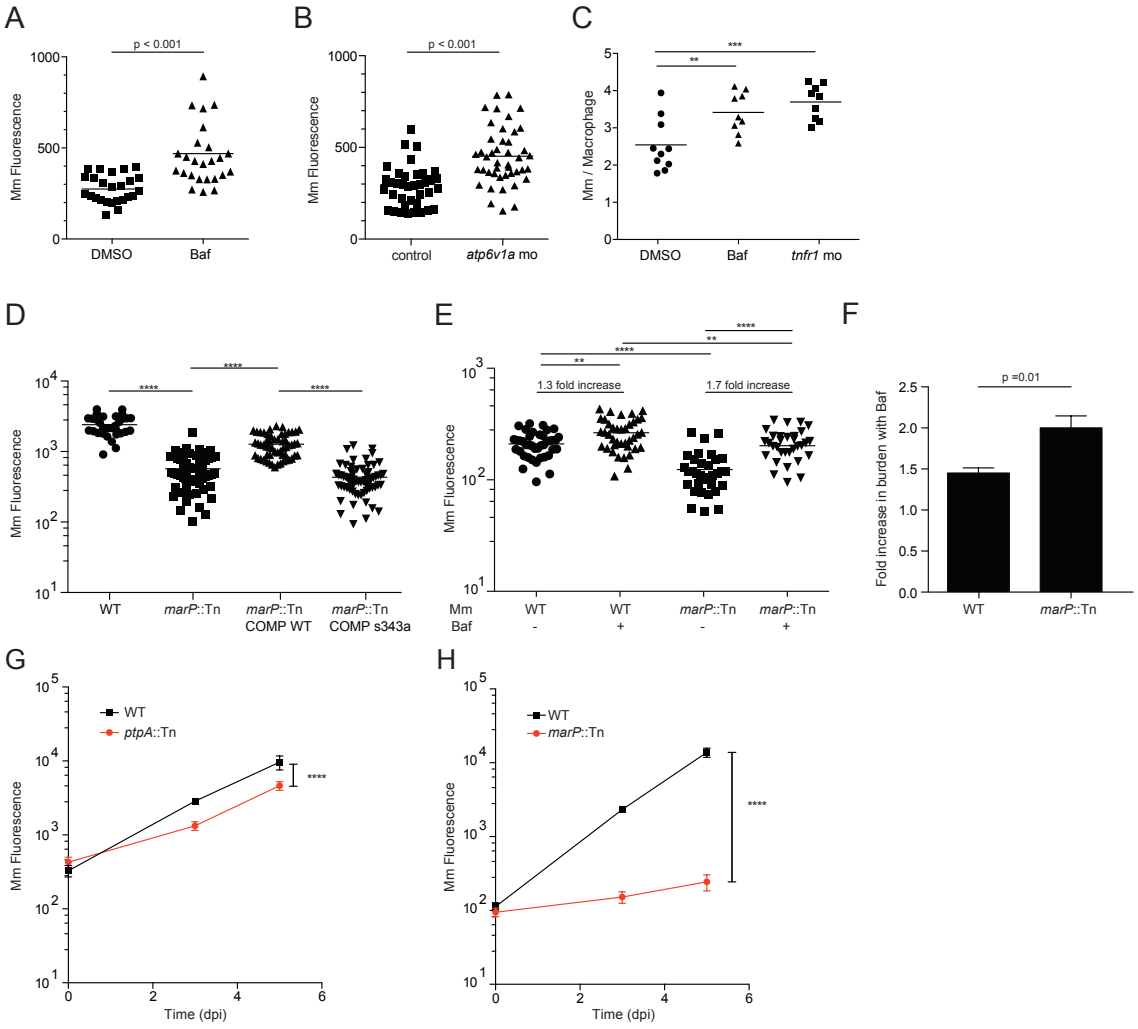

Figure 2.3. Lysosomal trafficking is a host-beneficial process, which is counteracted by *M. marinum* MarP. (A) Bacterial burden (FPC) measured 24 hpi with 300 *M. marinum* followed by splitting infected fish randomly into DMSO or 50nM Bafilomycin A1 (Baf) treatment, representative of three experiments. (B) Bacterial burden measured 24 hpi with 300 *M. marinum* into larvae injected at 0dpf with a morpholino targeting *atp6v1a* or control, representative of two experiments. (C) Average intramacrophage burden 40 hpi with 60 *M. marinum* into the CV comparing larvae treated with DMSO or 50nM Baf following infection, or injected with a

morpholino targeting *tnfr1* at 0dpf, which was used as a positive control, representative of three experiments. (D) Bacterial burden measured at 3 days post-infection (dpi) following infection with 200 wild-type *M. marinum*, *marP*::Tn, *marP*::Tn transformed with a plasmid containing *M. tuberculosis marP*, or *marP*::Tn transformed with a plasmid containing *M. tuberculosis marP* with a mutation in the active site serine (S343A), representative of two experiments. (E) Bacterial burden at 1dpi following infection with 200 wild-type or *marP*::Tn *M. marinum* and treatment with either DMSO or 50nM Baf, representative of three experiments. The fold increase in burden following treatment with Bafilomycin is shown for wildtype and *marP*::Tn. (F) Fold increase in bacterial burden during infection with wildtype or *marP*::Tn *M. marinum* following treatment with 50nM Bafilomycin. Shown is the average of four experiments as in (E) ±SEM. (G) Bacterial burden measured at 0, 3, and 5dpi following infection with 250 wild-type or *ptpA*::Tn *M. marinum* with mean and 95% CI shown, representative of three experiments. (H) Bacterial burden at 0, 3, and 5dpi following infection with 150 wild-type or *marP*::Tn *M. marinum* with mean and 95% CI shown, representative of three experiments. Significance tested using two-tailed unpaired *t* test (A, B, F, G, H) or one-way ANOVA with Tukey's post-test (C, D, E). Each point in A-E represents one larva. See also Figure S2.4 and Figure S2.5.

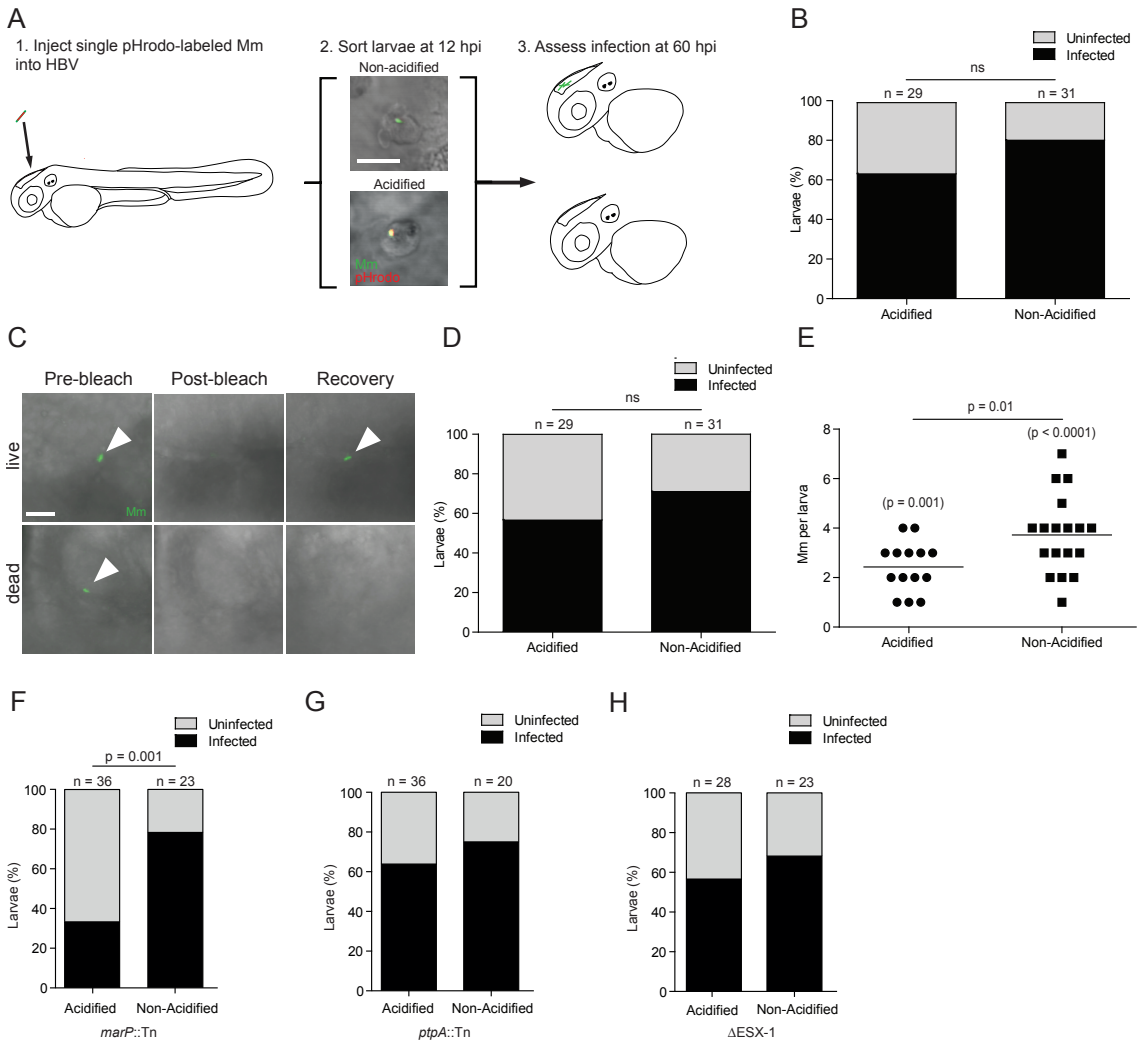

Figure 2.4. Lysosomal trafficking fails to eradicate *M. marinum* infection. (A) Cartoon diagram of infectivity experiment. Scale bar, 10μm. (B) Quantification of percentage of zebrafish larvae still infected at 60hpi following infection in the HBV with single pHrodo-labeled *M. marinum* and sorting into acidified/non-acidified groups, representative of three experiments. (C) Photobleaching assay to discern live from killed bacteria at the end of the infectivity assay showing a live bacterium that recovers fluorescence and a dead one that does

not. Scale bar, 5μm. (D) Data in (B) amended such that larvae containing only non-recovering bacteria are placed into the uninfected category, representative of three experiments. (E) Enumeration of bacterial numbers at the end of the infectivity experiment, showing only bacteria that recovered following photobleaching, representative of three experiments. P values in parentheses reflect the statistical significance of comparing each larva in that group to the starting bacterial number (1 in each fish) in a Wilcoxon matched-pair signed rank test. (F, G, H) Quantification of percentage of zebrafish larvae still infected at 60hpi which contained pHrodo-labeled *marP*::Tn (F), *ptpA*::Tn (G), and ΔESX-1 (H) *M. marinum* separated by whether the bacteria were pHrodo-positive (lysosomal) or pHrodo-negative (phagosomal) at sorting, representative of two (ΔESX-1) or three (*marP*::Tn, *ptpA*::Tn) experiments. Significance tested using two-tailed unpaired *t* test (E) or Fisher's exact test (B, D, F, G, H). Each point in (E) represents one larva. See also Figure S2.6.

Table S2.1. Prevalence of phagolysosomal trafficking of mycobacteria in vitro and in vivo

In vitro			
Bacterium	**Cell type**	**% phagosomes acidified (time)**	**Reference**
M. tuberculosis	Mouse peritoneal macrophages	36 (1 day) 23 (4 days)	Armstrong and Hart, 1971[7]
M. tuberculosis	Mouse peritoneal macrophages	23 (2 hours)	Hart *et al*., 1972[8]
M. tuberculosis (immune rabbit serum treated)	Mouse peritoneal macrophages	79 (1 day) 68 (7 days)	Armstrong and Hart, 1975[9]
M. tuberculosis	Human primary mononuclear cells	25 (3 hours) 15 (22 hours)	Clemens and Horwitz 1995[10]
M. tuberculosis	Mouse bone marrow macrophages	10 (2 hours)	Pethe *et al*, 2004[11]
M. tuberculosis	Human macrophage cell line (THP-1) THP-1 stimulated with IFNγ	10 (2 hours) 25 (2 hours)	Harris *et al*, 2008[12]
M. marinum	Mouse macrophage cell line (RAW)	21 (4 hours) 21 (8 hours) 27 (24 hours)	Barker *et al*, 1997[13]

In vivo			
Bacterium	**Host**	**% phagosomes acidified (time)**	**Reference**
M. tuberculosis	Mouse	30 (3 days)	Jayachandran *et al*., 2007[14]
M. tuberculosis	Human	30* (indeterminate)¢	Mwandumba *et al*., 2004[15]

Note that in cases where bar graphs were shown for acidification instead of exact numbers, the extent was estimated to the nearest 5%.

*Estimated from Figure 6 of the paper

¢Patients presented with suspected pulmonary tuberculosis.

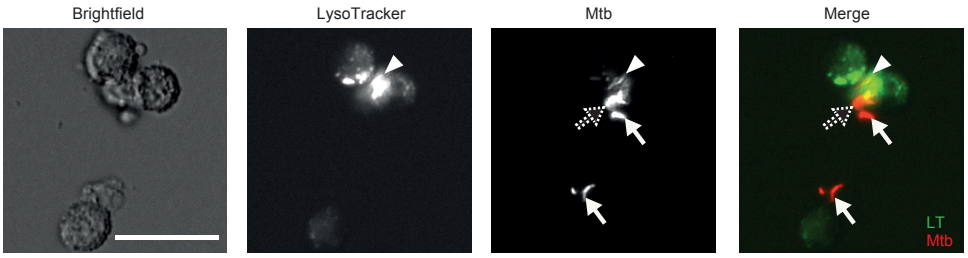

Figure S2.1: Direct ex vivo phagolysosomal localization of *M. tuberculosis* at 19 days post-infection, related to Figure 2.1. Fluorescence images of mCherry expressing *M. tuberculosis* (Mtb) H37Rv from infected lung. Infected cells were sorted from lung tissue at 19 days post-infection and stained with LysoTracker (LT) Green dye. Arrows depict bacteria that do not colocalize with LysoTracker while arrowheads depict bacteria colocalized with dye. The dotted arrow marks partially colocalized bacteria. Representative of three mice. Scale bar, 25μm.

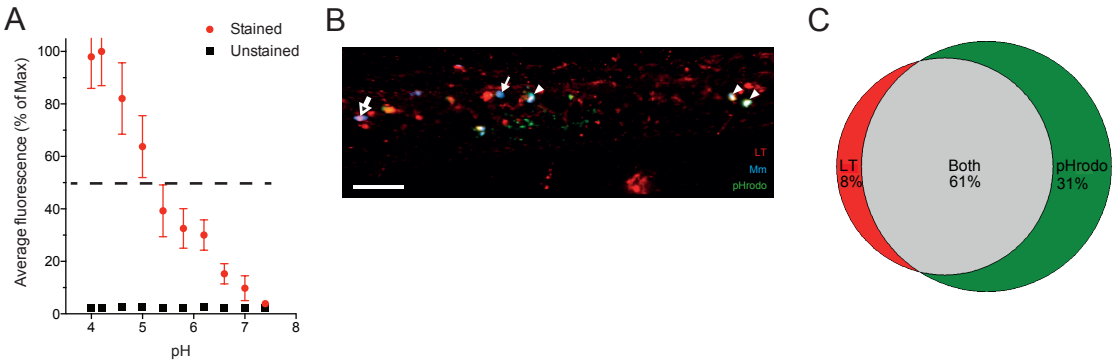

Figure S2.2. pHrodo efficiently labels acidified *M. marinum*, related to Figure 2.2. (A) Intensity of pHrodo fluorescence in stained *M. marinum* at various pH levels. Bacteria were pre-labeled with pHrodo, and then incubated in phosphate-citrate buffer at the indicated pH. The stained bacteria and unstained controls were imaged using the same confocal parameters as those used in zebrafish larvae. 3D surfaces were created from these images and pHrodo intensity was measured within each bacterium and intensity was plotted as a percentage of the maximum average value (pH 4.2). Shown is the average of at least 300 individual bacteria +/- one standard deviation. The dotted line represents the intensity cutoff used to assess pHrodo in vivo. (B) Confocal image of larva infected in the CV with pHrodo-labeled *M. marinum* (Mm), then stained with LysoTracker at 24hpi. White arrowheads denote bacteria that label with both LysoTracker and pHrodo, white arrow denotes a bacterium that does not label with either marker, and black arrow denotes a bacterium that labels with LysoTracker but not with pHrodo. Scale bar, 50μm. (C) Quantitative Venn diagram showing the distribution of *M. marinum* that were positive for either LysoTracker (LT), pHrodo or both in larvae infected in the CV with pHrodo-labeled *M. marinum* and then stained with LysoTracker at 24hpi with percentages noted, representative of two experiments.

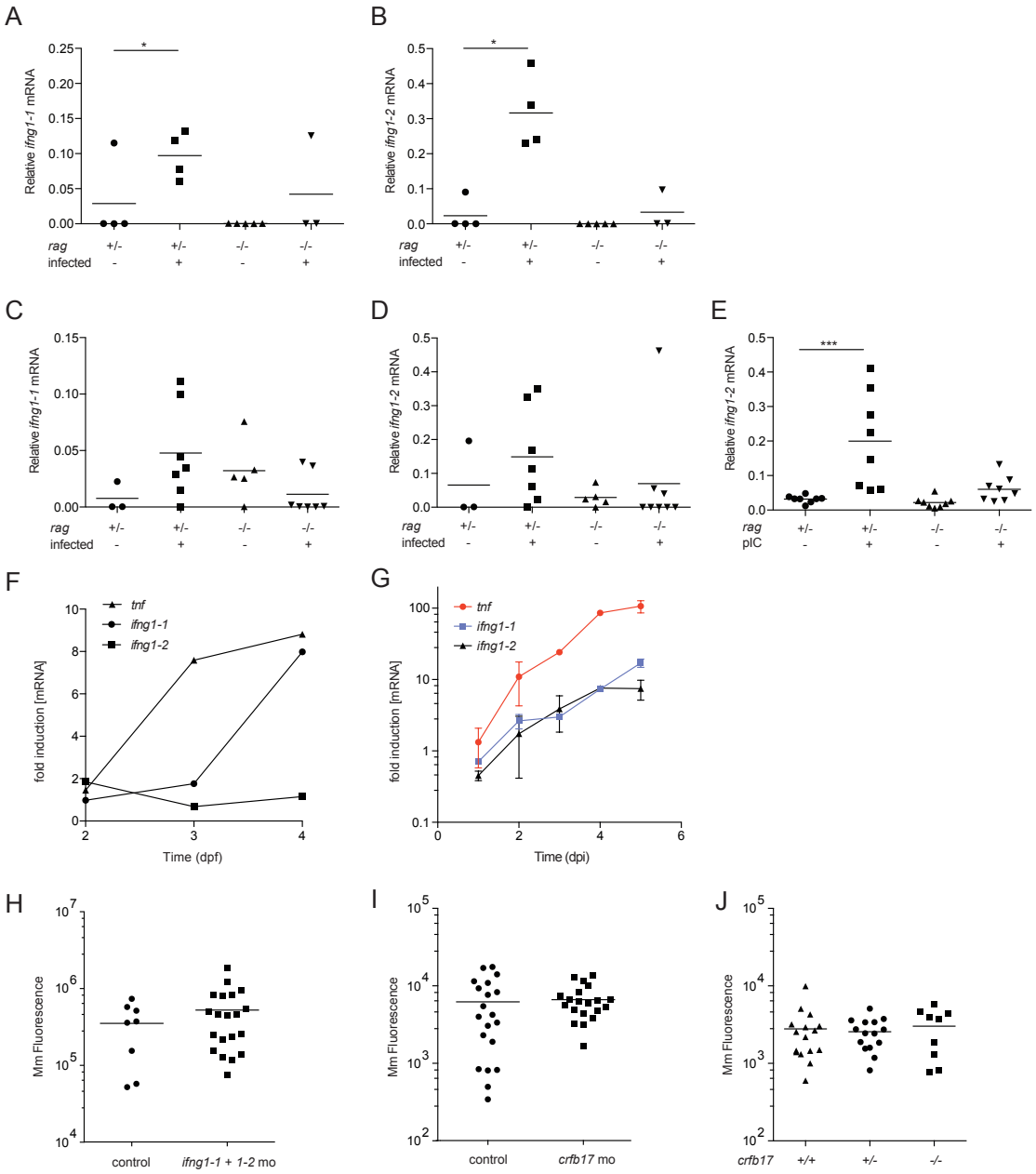

Figure S2.3. IFNγ induction does not occur in zebrafish larvae younger than 4dpf, related to Figure 2.2. (A, B) Real-time qPCR of *ifng1-1* (A) and *ifng1-2* (B) mRNA expression relative to *b-actin* in adult zebrafish at 6 weeks post-intraperitoneal infection with 20 CFU *M. marinum* in *rag* heterozygote and mutant adults. (C, D) Real-time qPCR of *ifng1-1* (C) and *ifng1-2* (D)

mRNA expression relative to *b-actin* in adult zebrafish at 2 weeks post-intraperitoneal infection with 500 CFU *M. marinum* in *rag* heterozygote and mutant adults. (E) Real-time qPCR of *ifng1-2* mRNA expression relative to *b-actin* in adult zebrafish four hours after intraperitoneal injection with poly(I:C). (F) Real-time qPCR of *ifng1-1*, *ifng1-2* and *tnf* mRNA expression relative to *b-actin* in larval zebrafish four hours after intravenous injection with poly(I:C). (G) Real-time qPCR of selected gene products following CV infection of 2dpf larvae with 275 CFU *M. marinum*. Shown for each point is an average of three experiments +/- SEM. (H) Bacterial burden measured at 4dpi following infection with 200 *M. marinum* in larvae treated at 0dpi with combined morpholinos targeting *ifng1-1* and *ifng1-2* or control. (I) Bacterial burden measured at 6dpi following infection with 200 *M. marinum* in larvae treated at 0dpi with a morpholino targeting *crfb17* or control. (J) Bacterial burden measured at 5dpi following infection with 250 *M. marinum* larvae from an incross of *crfb17* heterozygous (+/-) parents. Significance tested using ANOVA with Kruskal-Wallis multiple comparisons test. TNF induction was used as an independent indicator that adults and larvae were successfully infected. Each point in A-E represents one adult with the same adults tested in A-B and C-D. Each point in H-J represents one larva. Values in (F) and (G) represent pooled RNA from 30 larvae at each time point.

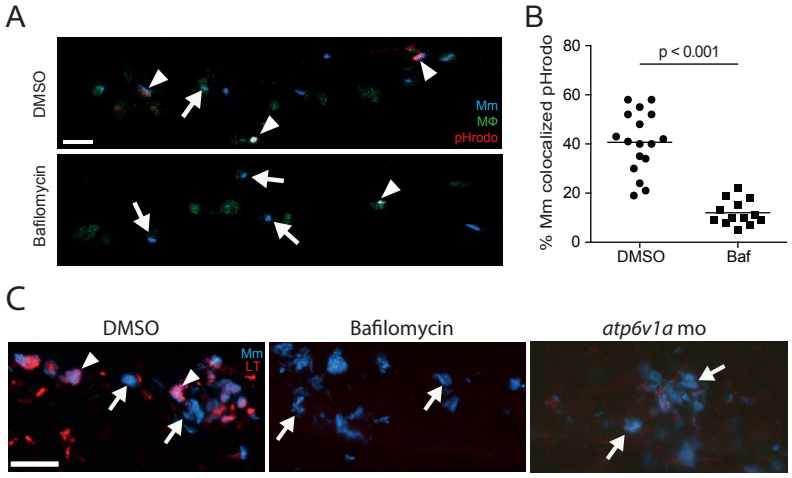

Figure S2.4. Pharmacological or genetic disruption of vATPase ablates pHrodo and LysoTracker staining during infection, related to Figure 2.3. (A) Confocal images of 3dpf larvae that were infected in the CV with 150 pHrodo-labeled *M. marinum* at 2dpf following treatment with 50nM Bafilomycin or DMSO control. Arrowheads denote bacteria labeled with pHrodo, while arrows show pHrodo-negative bacteria. (B) Quantification of the percent of *M. marinum* colocalizing with pHrodo at 24hpi (CV) with 75 bacteria after treatment with DMSO or 50nM Bafilomycin starting immediately after infection, representative of two experiments. (C) Confocal images of 3dpf larvae that were infected in the CV with 150 blue fluorescent *M. marinum* at 2dpf and stained with LysoTracker at 3dpf following treatment with DMSO, 50nM Bafilomycin, or morpholino targeting *atp6v1a* at 0dpf. Arrowheads denote bacteria that colocalize with LysoTracker, while arrows denote LysoTracker-negative bacteria. Significance tested using two-tailed unpaired *t* test (B).

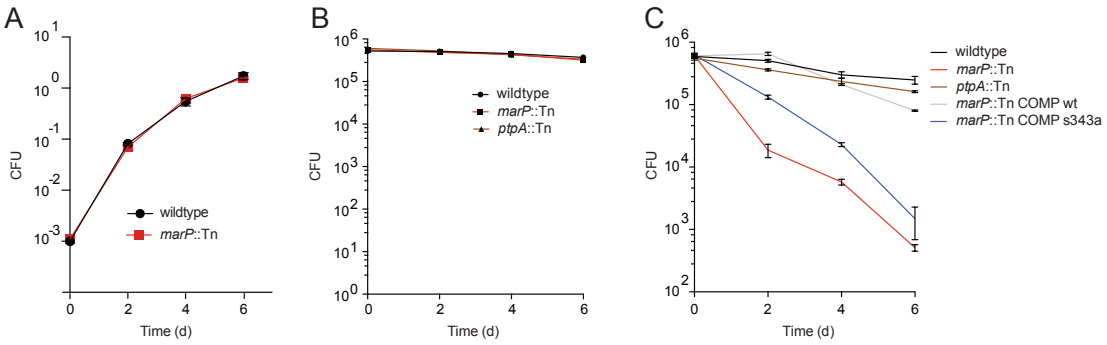

D

Strain	MIC (μg/mL)	
	Rif	Ery
wildtype	0.16	64
ΔESX-1	0.16	64
Δ*erp*	0.04	2
marP::Tn	0.02	2
ptpA::Tn	0.16	64

Figure S2.5. *marP*::Tn is unable to tolerate acidic environments and lipophilic antibiotics, related to Figure 2.3. (A) OD600 measurements of wild-type and *marP*::Tn in 7H9 media at neutral pH over 6 days of growth. (B) Wild-type, *marP*::Tn and *ptpA*::Tn bacteria were incubated for 6 days in phosphate-citrate buffer at pH 7 with CFU measurements taken every 2 days. (C) Wild-type, *marP*::Tn, *ptpA*::Tn, *marP*::Tn complemented with *marP* from *M. tuberculosis* and *marP*::Tn complemented with the *marP* S343A mutant were incubated in phosphate-citrate buffer at pH 4.5 for 6 days with CFU measurements taken every 2 days. (D) MIC measurements of hydrophobic antibiotics in wild-type, ΔESX-1, Δ*erp*, *marP*::Tn and *ptpA*::Tn. MICs were measured as described in Experimental Procedures and was determined as the minimum concentration that prevented the appearance of turbidity in culture. Rif, rifampin; Ery, erythromycin.

Values in A, B, and C represent the mean +/- SD.

```
M. tuberculosis              PVTRDVYTIRADVEQGDSGGPLIDLNGQVLGVVFGAAID----DAETGFVLTA
M. bovis (99% identity)      PVTRDVYTIRADVEQGDSGGPLIDLNGQVLGVVFGAAVD----DAETGFVLTA
M. avium (86% identity)      PVTRDVYTIRASVEQGNSGGPLIDLNGQVLGVVFGAAVD----DPDTGFVLTA
M. elephantis (67% identity) TVEREVYTIRGTVRQGNSGGPMIDRDGNVLGVVFGAAVD----DADTGFVLTA
M. smegmatis (66% identity)  TVTREVYTVRGTVRQGNSGGPMINRAGKVLGVVFGAAVD----DVDTGFVLTA
M. marinum (86% identity)    TLNGLIQV-DAAIAPGDSGGPIVNNMGQVVGMNTAASDNFQMSGGGTGFAIPI
```

Figure S2.6. The serine protease encoded by MarP is highly conserved across mycobacterial species, related to Figure 2.4. Alignment of a section of MarP from *M. tuberculosis* (with active site serine S343 shown in red) with other species of mycobacteria. The overall identity between a given species and the entire gene from *M. tuberculosis* is reported in parentheses (alignments performed using LALIGN from NCBI database sequences).

Chapter 3: Lysosomal Disorders Drive Susceptibility to Tuberculosis by Compromising Macrophage Migration

Summary

A zebrafish genetic screen for determinants of susceptibility to *Mycobacterium marinum* identified a hypersusceptible mutant deficient in lysosomal cysteine cathepsins that manifests hallmarks of human lysosomal storage diseases. Under homeostatic conditions, mutant macrophages accumulate undigested lysosomal material, which disrupts endocytic recycling and impairs their migration to, and thus engulfment of, dying cells. This causes a buildup of unengulfed cell debris. During mycobacterial infection, macrophages with lysosomal storage cannot migrate towards infected macrophages undergoing apoptosis in the tuberculous granuloma. The unengulfed apoptotic macrophages undergo secondary necrosis causing granuloma breakdown and increased mycobacterial growth. Macrophage lysosomal storage similarly impairs migration to newly infecting mycobacteria. This phenotype is recapitulated in human smokers, who are at increased risk for tuberculosis. A majority of their alveolar macrophages exhibit lysosomal accumulations of tobacco smoke particulates and do not migrate to *Mycobacterium tuberculosis*. The incapacitation of highly microbicidal first-responding macrophages may contribute to smokers' susceptibility to tuberculosis.

Introduction

Tuberculosis (TB) involves a series of interactions between macrophages and the infecting mycobacterium with this proposed sequence of events (Cambier et al., 2014a; Srivastava et al., 2014): Inhaled mycobacteria are engulfed by lung alveolar macrophages and, if not cleared during this initial interaction, are transported deeper into the lung. Here, newly-recruited myeloid and other immune cells aggregate around the infected cells to form organized granulomas.

The study of zebrafish infected with *M. marinum* has enabled the dissection of these steps of TB pathogenesis, aided by the genetic tractability of this model organism and its optical transparency during its first few weeks of life (Cambier et al., 2014a). Newly infecting bacteria can be transported across epithelial barriers by permissive macrophages (Cambier et al., 2014b). Additional macrophages are recruited to the initial infected macrophage to form the tuberculous granuloma (Cambier et al., 2014a). Cellular expansion of the granuloma, and intracellular bacterial growth within it, proceed through apoptosis of the infected macrophages and their phagocytosis by newly arriving uninfected macrophages (Davis and Ramakrishnan, 2009). On the one hand, bacterially-mediated granuloma expansion can promote infection through bacterial spread into newly recruited macrophages (Davis and Ramakrishnan, 2009). On the other hand, if the supply of uninfected macrophages is limiting, apoptotic infected cells in the granuloma undergo secondary necrosis, causing granuloma breakdown and the release of bacteria into the extracellular space which enables their accelerated growth (Pagan et al., 2015).

In this work, we characterize a zebrafish mutant identified in a forward genetic screen (Tobin et al., 2010) to reveal how during genetic lysosomal storage disorders, the accumulation of undegraded products in the macrophage lysosome impairs the migration of these phagocytic

cells. The disruption of macrophage migration contributes to the pathogenesis of the lysosomal storage disease in the uninfected state, and causes granuloma breakdown during tuberculous infection, which underlies hypersusceptibility. The mutation maps to *snapc1b,* a transcriptional co-regulator that causes lysosomal storage through reduced expression of lysosomal cysteine cathepsins B and L. Using zebrafish models of human lysosomal storage diseases, we generalize our findings to show that the accumulation of diverse biological substrates, as well as inert particles, compromises macrophage migration through the derangement of endocytic recycling. We then show that lysosomal storage in macrophages inhibits their migration to engulf newly-infecting bacteria. Because the resident alveolar macrophages of human cigarette smokers have been reported to accumulate particulate material, we asked if smokers' macrophages are similarly compromised in their response to mycobacterial infection. We find that the majority of smokers' alveolar macrophages have enlarged lysosomes filled with opaque material, and are impaired in their migration to *M. tuberculosis*. The compromised migration of these highly-microbicidal first responding macrophages suggest a mechanistic explanation for the reported association between smoking and TB (Lin et al., 2007).

Results

snapc1b Zebrafish Mutant Hypersusceptibility to *M. marinum* Infection is Characterized by Granuloma Breakdown

The zebrafish mutant *fh111*, identified in a forward genetic screen (Tobin et al., 2010), was hypersusceptible to *M. marinum*, displaying increased bacterial growth relative to wildtype siblings after intravenous infection (Figure 3.1A and 3.1B). *fh111* infection was characterized by the breakdown of forming granulomas accompanied by bacterial cording, a characteristic morphology acquired by rapidly growing extracellular bacteria after release from necrotic macrophages (Pagan et al., 2015; Tobin et al., 2010) (Figure 3.1C). We used bacterial cording as a sensitive and specific phenotype to map *fh111* (Figure 3.1D)(Tobin et al., 2010). *fh111* maps to a splice acceptor site mutation in the exon 1-2 junction of the zebrafish *snapc1b* gene on chromosome 13 (Figure S3.1A), one of two orthologs of human *SNAPC1* (Small Nuclear RNA Activating Complex Polypeptide 1) that encodes a component of the basal transcriptional machinery for RNA Pol II and III dependent transcription (Henry et al., 1998). Zebrafish *snapc1b* has higher amino acid identity to human *SNAPC1* than its paralog *snapc1a*, located on chromosome 20 (39% versus 35%, respectively)(Flicek et al., 2014). RNA sequencing (RNAseq) analysis of WT animals at 6 days post-fertilization (dpf) showed that *snapc1b* RNAs were ~35-fold more abundant than *snapc1a* RNAs (GEO GSE74196). We confirmed the location and transcriptional consequence of *fh111* by RNAseq and quantitative reverse transcriptase PCR (Figure S3.1A and S3.1B). Causality of the *fh111* mutation was confirmed by a splice-blocking antisense oligonucleotide (morpholino) that targeted the same exon 1-2 splice junction of *snapc1b* (Table S3.1) that phenocopied *fh111* susceptibility (Figure S3.1C and S3.1D) and by

non-complementation with an independent retroviral insertion allele that disrupts exon1 of *snapc1b* (*la010158*) (Figure S3.1E and S3.1F)(Varshney et al., 2013).

In sum, our findings suggest that Snapc1b deficiency causes hypersusceptibility to mycobacterial infection through early granuloma breakdown, which releases mycobacteria into the extracellular milieu that is more growth-permissive than the intracellular environment, culminating in bacterial cording morphology (Pagan et al., 2015).

Macrophages of *snapc1b* Mutants Are Increased in Number and Have Enlarged Lysosomes

Granuloma breakdown can result from a global reduction in macrophage numbers available to replenish the granuloma (Pagan et al., 2015). We were surprised to find that even in uninfected *snapc1b* mutants, macrophage numbers were increased as revealed by increased numbers of fluorescent macrophages in transgenic animals (Ellett et al., 2011), and by staining with neutral red, a vital dye which accumulates in macrophages (Davis and Ramakrishnan, 2009)(Figure 3.1E-G). The increased abundance of microglia, tissue resident macrophages of the brain derived from a primitive hematopoietic lineage (Clements and Traver, 2013), suggested a derangement in multiple waves of myelopoiesis (Figure 3.1H and 3.1I).

Most of the macrophages in mutants were enlarged and discoid in shape (Figure 3.1J, 3.1K, and S3.2A-C). The enlarged macrophages contained prominent vacuoles, which were revealed to be fused lysosomes by staining with LysoTracker (Figure 3.1L) (Peri and Nüsslein-Volhard, 2008). The mutant lysosomes were larger than wildtype and occupied a greater proportion of total macrophage volume (Figure 3.1M). This aberrant macrophage morphology is similar to what has been observed in human lysosomal storage disorders (Kieseier et al., 1997). Our observation of an increased abundance of tissue resident macrophages (histiocytosis)

accompanied by increased expression of myeloid growth factors (Table S3.2), also mirrors findings in several human lysosomal storage disorders (Allen, 2008; Hsu et al., 2012). Neutrophils, the other myeloid cells present at this developmental stage, were not increased in *snapc1b* mutants and displayed normal morphology, consistent with their lack of involvement in homeostatic scavenger functions (Figure S3.2D and data not shown).

snapc1b Mutant Macrophages Become Vacuolated and Immotile as a Result of Lysosomal Accumulation of Undigested Cell Debris

To understand the development of vacuolated morphology, we compared microglial morphology and dynamics in uninfected animals during physiological efferocytosis of apoptotic neurons. In wildtype animals, macrophages assumed a vacuolated morphology upon phagocytosis of particulate material (presumably cell debris) but reverted to normal within four hours (Figure 3.2A and Movie S3.1). Vacuolated morphology was accompanied by a transient reduction in speed of homeostatic migration; movement resumed upon reversion to normal morphology (Figure 3.2A and 3.2B and Movie S1). In *snapc1b* mutants, macrophages became irreversibly vacuolated after only a few phagocytic events, accompanied by sustained immotility and consequently reduced displacement - 36μm versus 131μm for wildtype - over a 13-hour observation period (Figure 3.2A and 3.2B, and Movie S1). These vacuolated macrophages did not have obvious phagocytic defects and continued to extend pseudopods in apparent phagocytic events (Figure 3.2A and Movie S1). Vacuolated macrophages were also unable to migrate in response to the chemotactic molecule CCL2 injected into the hindbrain ventricle (HBV) (Cambier et al., 2014b), indicating a broad migratory defect towards both cell debris and chemotactic factors (Figure 3.2C). These findings are consistent with observations that

macrophages from patients with Gaucher's disease, the most common human lysosomal storage disorder, are defective for migration but competent for phagocytosis (Aflaki et al., 2014).

Acridine orange staining confirmed that the lysosomal accumulations in mutant macrophages were phagocytosed apoptotic bodies (Abrams et al., 1993; Peri and Nüsslein-Volhard, 2008)(Figure 3.2D). Together, these findings suggested that lysosomal accumulation of undigested cell debris in mutant macrophages impairs migration irreversibly and leads to progressive macrophage incapacitation. If so, then we hypothesized that mutants would have an accumulation of extracellular apoptotic bodies in the brain as seen in several human lysosomal storage disorders (Huang et al., 1997). They did (Figure 3.2E and 3.2F). Furthermore, a global reduction in apoptosis induced by the pancaspase inhibitor Q-VD-OPh reduced extracellular cell debris (Figure S3.3A) and decreased the number of macrophages with lysosomal accumulations of the debris and with enlarged lysosomes (Figure S3.3B and S3.3C).

Together, these findings show that *snapc1b* mutant macrophages become irreversibly vacuolated due to their inability to degrade phagocytosed cell debris. As more and more macrophages lose their migratory capability, a deficit of functioning macrophages may develop.

Macrophage Migration Deficit Underlies Granuloma Breakdown in *snapc1b* Mutants

We recently showed that reduction in the macrophage supply reduces granuloma macrophage replenishment to the point at which apoptotic infected macrophages, failing to be engulfed, undergo secondary necrosis (Pagan et al., 2015). Having observed that the vacuolated macrophages of *snapc1b* mutants failed to migrate to dying cells in the uninfected state and failed to migrate to newly infecting bacteria, we wondered if they were also unable to migrate to dying cells in the tuberculous granuloma. If so, a functional macrophage deficiency could

develop in the context of global macrophage excess, providing an explanation for our observation of early granuloma breakdown.

We performed detailed time-lapse confocal imaging of forming granulomas in wildtype and *snapc1b* mutant larvae over ~18 hours. Wildtype granulomas retained cellularity over this period through continuous influx of macrophages (Movie S2 and Figure 3.3A and 3.3B). In contrast, Snapc1b-deficient granulomas broke down soon after formation (Movie S2). Mutant granulomas were surrounded by mostly vacuolated macrophages that failed to migrate into the granuloma (Figure 3.3A and 3.3B and Movie S2). The migration deficit in *snapc1b* mutants was specific to the vacuolated macrophages; the morphologically normal macrophages in the mutants maintained displacements and speeds similar to those of wildtype animals (Figure 3.3C and 3.3D and Movie S2). Thus, macrophage lysosomal storage leads to granuloma breakdown by preventing migration to the forming structure, and is functionally equivalent to a global macrophage deficiency. Our findings suggest that once the *snapc1b* mutants have exhausted their migration-competent macrophages, the tuberculous granuloma breaks down resulting in bacterial cording.

Lysosomal Cathepsin Deficiency Underlies *snapc1b* Mutant Macrophage Abnormalities and Hypersusceptibility to *M. marinum*

Human SNAPC1 is involved in global RNA polymerase II dependent transcription (Baillat et al., 2012). RNAseq analysis of *snapc1b* mutants and wildtype siblings revealed more than 1000 differentially expressed genes in the mutant (Table S3.3), suggesting zebrafish Snapc1b functions in a similar manner. How might a broadly-acting transcriptional regulator produce such specific phenotypes? Guided by the *snapc1b* mutant phenotype, we analyzed the

RNAseq dataset for lysosomal genes including those associated with human lysosomal storage disorders (Table S3.2)(Platt et al., 2012). Only two, the myeloid cell-specific lysosomal cysteine cathepsins B and L1 *(ctsbb* and *ctsl1)* (Heng et al., 2008), were underrepresented in the mutant, at 9% and 13% of wildtype levels, respectively (Table S3.2), and we confirmed their commensurate reduction by quantitative reverse transcriptase PCR analysis (85% and 83% respectively) (Figure 3.4A and data not shown). We were able to test lysosomal cathepsin activity in situ using MagicRed (MR)-Cathepsin L, a modified cathepsin L target sequence which fluoresces only when cleaved (Peri and Nüsslein-Volhard, 2008). In wildtype animals, brain macrophages quickly cleaved injected MR-cathepsin L; this number was reduced as expected by administration of the irreversible pan-cysteine cathepsin inhibitor, E64d (42.7% of macrophages in control vs. 3.63% in E64d-treated larvae, $p<0.0001$) (Murray et al., 1997) (Figure 3.4B). *snapc1b* mutants displayed reduced MR-cathepsin-L cleavage compared to wildtype siblings, indicative of reduced lysosomal cathepsin L activity (47.2% of macrophages in WT animals vs. 5.3% in mutants, $p<0.0001$) (Figure 3.4C).

We next tested whether cysteine cathepsin deficiency underlies all of the *snapc1b* mutant phenotypes. Inhibition of cysteine cathepsins by E64d recapitulated both baseline and infected *snapc1b* mutant phenotypes - macrophage lysosomal storage with accompanying migratory defects at baseline, and hypersusceptibility to infection with bacterial cording (Figure 3.4D-F). We attempted morpholino knockdown of *ctsbb* and *ctsl1* to probe their individual culpabilities in the *snapc1b* mutant phenotypes (Table S3.1). As the *ctsbb* morpholino was highly toxic, we could only pursue *ctsl1* further. *ctsl1* morphants recapitulated the *snapc1b* phenotypes (Figure 3.4G-3.4I). Transient overexpression of *ctsl1* mRNA in *snapc1b* mutant larvae restored normal macrophage morphology in uninfected *snapc1b* mutants and rescued cording (Figure 3.4J and

Figure 3.4K). Together these experiments implicate cysteine cathepsins in *snapc1b* hypersusceptibility resulting from macrophage incapacitation. Our data ascribe a substantial portion of *snapc1b* phenotypes to cathepsin L1 deficiency though we cannot rule out a minor role for cathepsin B deficiency. Prior findings that cathepsin L knockout mice are not hypersusceptible to *M. tuberculosis* (Nepal et al., 2008) may reflect functional redundancies present in the mouse but not the zebrafish.

Our finding that cathepsin L1 deficiency mediated hypersusceptibility prompted us to ask if this lysosomal hydrolase might play a role in macrophage microbicidal activity for two reasons. First, a deficit in macrophage microbicidal activity (e.g. through TNF deficiency) has been shown to result in granuloma breakdown with bacterial cording (Tobin et al., 2010). Second, in vitro, cathepsin L has been reported to indirectly facilitate mycobacterial killing by cleaving ubiquitin into microbicidal peptides (Alonso et al., 2007). However, we found that macrophages of both *snapc1b* mutants and *ctsl1* morphants restricted bacterial growth normally (Figure S3.4). These findings suggest that cathepsin L-mediated macrophage microbicidal capacity is dispensable in vivo and confirms that its deficiency induces susceptibility by compromising macrophage migration.

Zebrafish Models of Human Lysosomal Storage Disorders Display Accelerated Tuberculous Granuloma Breakdown

While cathepsin deficiency causes protein accumulation in lysosomes, many human genetic lysosomal storage disorders result from the accumulation of diverse lipid species (Platt et al., 2012). Patients with Gaucher's disease, the most common lysosomal storage disease, have macrophages with migration defects in vitro (Aflaki et al., 2014; Liel et al., 1994) and are

susceptible to a variety of pathogens including mycobacteria, though this may be due to concomitant immune defects including pancytopenias (Aker et al., 1993; Jain and Yelwatkar, 2011; Machaczka et al., 2014; Zimran, 2011). We asked if the mechanism of susceptibility uncovered for *ctsl1* deficiency extended to lysosomal storage disorders characterized by lipid accumulation. Knockdown of the zebrafish orthologs of the genes responsible for Gaucher's disease, Tay-Sachs disease, and metachromatic leukodystrophy produced increased numbers of vacuolated macrophages with enlarged lysosomes and migratory defects (Tables S3.1 and S3.2 and Figure 3.5A-3.5C). Upon infection, all three exhibited early granuloma breakdown and bacterial cording (Figure 3.5D-3.5F). Thus, etiologically diverse lysosomal storage disorders can increase susceptibility to tuberculous infection, regardless of the nature of the accumulated material.

Macrophage Lysosomal Storage Disrupts Endocytic Recycling

Our work so far had linked macrophage lysosomal storage to impaired migration to increased susceptibility to mycobacteria. Having understood the cellular basis of the link between impaired macrophage migration and susceptibility, we sought to understand how macrophage lysosomal storage might impair migration. Recycling between the endosomal and plasma membranes is known to be required for cell migration. This recycling delivers membrane lipids and proteins required for movement to the plasma membrane and facilitates adjustments in cell surface area that are critical for cell motility (Bretscher and Aguado-Velasco, 1998; Traynor and Kay, 2007; Veale et al., 2010). Lysosomes share contents with endosomes and recent evidence suggests that, like endosomes, they participate in recycling to the plasma membrane (Bright et al., 2005; Bright et al., 2015). Accordingly, embryonic fibroblasts isolated from two

mouse models of severe lysosomal storage disorders display broad dysregulation of the entire endocytic pathway (Fraldi et al., 2010).

We asked whether endocytic recycling was disrupted in the zebrafish macrophages with lysosomal storage by monitoring the fate of fluorescently labeled high molecular weight dextran (10,000MW) in normal animals and those with macrophage lysosomal storage. Following endocytosis, high molecular weight dextran is trafficked to lysosomes but not readily degraded and its loss from lysosomes strictly reflects trafficking from them. In pulse-chase experiments, dextran-labeled lysosomes have been shown to fuse rapidly with endosomes, and several hours later the dextran is released into the extracellular medium suggesting subsequent fusion events that involve trafficking to the plasma membrane (Bright et al., 2015).

We injected fluorescent dextran into the brains of 3 dpf zebrafish larvae - wildtype, cathepsin-deficient by E64d treatment and *gba*-deficient morphants. In all groups, 74-82% of the macrophages had taken up the dye within 5 hours (Figure 3.6). After 30 hours, only 33% and 39% of the macrophages in the wildtype fish retained the dextran whereas 77% and 79% did in the cathepsin and *gba*-deficient animals, respectively (Figure 3.6), suggesting that stalling of the entire endocytic system is a common feature of lysosomal storage diseases and underlies the defective migration displayed by vacuolated macrophages.

Our finding that the lysosomal accumulation of diverse biomolecules compromises endocytic recycling and thus cell motility suggested a common mechanism independent of the specific lysosomal substrate. If so, then lysosomal storage induced by non-biological particles should produce the same phenotypes. We injected beads into the HBV, which were phagocytosed by brain resident macrophages (Figure S3.5A). Bead-laden macrophages were

compromised for homeostatic migration and exhibited disruption of endocytic recycling (Figure S3.5B-S3.5E).

Lysosomal Accumulation Compromises Macrophage Migration to Newly-Infecting Mycobacteria

In addition to their role in forming and maintaining the granuloma, resident macrophages are the first cells to migrate to mycobacteria at the initial site of infection (Cambier et al., 2014a; Philips and Ernst, 2012). This first macrophage-mycobacterium interaction can be visualized in the zebrafish hindbrain ventricle (HBV), a cavity into which phagocytes migrate in response to mycobacteria (Cambier et al., 2014b). In the *snapc1b* mutant, only the subset of brain-resident macrophages that still had normal morphology migrated to the bacteria and phagocytosed them, while the vacuolated macrophages, failing to migrate from the adjacent brain parenchyma, remained uninfected (data not shown). We could not directly test the migration of bead-laden brain resident macrophages, as only a minority of them engulfed sufficient numbers of beads injected into the HBV. So we injected either beads or the nuclear stain Hoechst 33342 into the caudal vein followed by bacteria into the HBV (Figure S3.5F). As observed previously, the Hoechst-stained macrophages could be discerned by their blue nuclei and were morphologically normal (Figure S3.5G) (Davis and Ramakrishnan, 2009). After confirming that similar numbers of circulating macrophages were labeled blue by either dye or beads, we injected bacteria into the HBV (Figure S3.5F). Multiple Hoechst-positive macrophages migrated to the HBV in response to the bacteria, as expected (Davis and Ramakrishnan, 2009), but hardly any bead-filled ones did (Figure S3.5G-S3.5I). Thus, the accumulation of indigestible inert particles in

macrophage lysosomes compromises their migration so as to preclude their ability to phagocytose infecting mycobacteria.

Lysosomal Accumulation of Tobacco Smoke Particulates Compromises Macrophage Migration to *M. tuberculosis* in Humans

Human TB is thought to begin when mycobacteria are phagocytosed by pulmonary alveolar macrophages, the resident macrophages at the air-lung interface (Bates et al., 1965; Hocking and Golde, 1979b; Ratcliffe and Wells, 1948; Verrall et al., 2014). Consistent with their role in primary defense against diverse inhaled bacteria (Green and Kass, 1964; Hocking and Golde, 1979b), the ability of a substantial number of individuals to clear *M. tuberculosis* early after infection has been ascribed to the microbicidal activity of the alveolar macrophage(Verrall et al., 2014). Despite their central defensive role, many alveoli are normally devoid of macrophages because their numbers are limiting (Betz et al., 1993; Ferin, 1982). Therefore, efficient and complete phagocytosis of inhaled particulates is predicated on the rapid migration of alveolar macrophages from nearby alveoli (Lehnert, 1992; Peao et al., 1993). This migration should be particularly relevant to TB, the outcome of which depends upon the fate of the 1-3 bacteria deposited in a distal alveolus, which might not contain a macrophage (Bates et al., 1965; Ratcliffe and Wells, 1948). In light of our findings that bead-laden macrophages were compromised for migration to newly-infecting in the zebrafish, we wondered if the accumulation of tobacco smoke particulates in the alveolar macrophages of cigarette smokers (Harris et al., 1970; Martin, 1973) might be similarly compromised, accounting for the poorly understood association between smoking and the acquisition of new TB infection (Anderson et al., 1997; den Boon et al., 2005). If an infecting mycobacterium were to be deposited in a macrophage-

deficient alveolus and not rapidly phagocytosed by nearby alveolar macrophages rendered immotile secondary to lysosomal engorgement, it would have an extended period of extracellular growth before engulfment by alveolar macrophages or other myeloid cells recruited from afar.

We examined alveolar macrophages obtained from smokers, nonsmokers and ex-smokers by bronchoalveolar lavage (O'Leary et al., 2014) (Table S3.4 and Supplemental Experimental Procedures). The majority of smokers' alveolar macrophages exhibited vacuolated morphology and had accumulated opaque material in large lysosomal inclusions as evidenced by staining with neutral red, a vital dye that concentrates in lysosomes (Figure 3.7A and 3.7B). These cells were present at a lower frequency in ex-smokers and virtually absent in non-smokers (Figure 3.7A and 3.7B). The abnormal cells were readily identified by their autofluorescence, consistent with previous findings (Martin, 1973).

Using a transwell assay, we confirmed prior reports that alveolar macrophages from nonsmokers and ex-smokers migrate to zymosan-activated serum, a rich source of the chemoattractant C5a (Figure S3.6A) (Barlow et al., 2008; Sweeney et al., 2015). In this assay, nonsmokers' and ex-smokers' alveolar macrophages also migrated to *M. tuberculosis* within two hours (Figure 3.7C and S3.6B). Migration of smokers' macrophages to *M. tuberculosis* was impaired (Figure 3.7D). Our hypothesis predicts that this overall migration impairment is due to a selective inability of the vacuolated subset to migrate. Indeed, by calculating the fraction of the smokers' normal versus vacuolated macrophages that migrated, we found that the migration impairment was specific to the vacuolated subset (Figure 3.7E). In sum, we show that the majority of smokers' macrophages fail to migrate towards *M. tuberculosis* due to lysosomal accumulation of particulates, and their non-participation may contribute to the susceptibility of these individuals to TB.

Discussion

We have described a zebrafish mutant in the *snapc1b* basal transcription factor component that displays the hallmark characteristics of human lysosomal storage disorders and is hypersusceptible to *M. marinum* infection. RNA-seq of *snapc1b* mutants revealed reduced expression of the lysosomal degradative cathepsins L and B, and pharmacological inhibition of cathepsin activity or knockdown of cathepsin L recapitulates the key mutant phenotypes of vacuolated macrophage morphology and susceptibility to infection.

Though cathepsin L is involved in the lysosomal degradation of phagocytosed material, its deficiency here mediates susceptibility to mycobacteria not by reducing macrophage microbicidal capacity but rather by causing lysosomal accumulation of undigested cell debris. This disrupts endocytic membrane recycling and thereby compromises macrophage migration in a variety of contexts. By modeling human lysosomal storage diseases in the zebrafish, we find that the accumulation of diverse substrates causes susceptibility to infection through this same mechanism. Our studies provide insights into the fundamental and common role played by macrophages as scavengers of dying cells during homeostasis and during tuberculous granuloma maintenance. These insights shed light on the protective role of tissue macrophages in early tuberculous infection and how lysosomal accumulation of tobacco smoke products may compromise this role.

Macrophage Migration Defects Due to Lysosomal Accumulation of Undigested Cell Debris Contribute to the Pathogenesis of Lysosomal Storage Disorders

Sequential live visualization of the developing *snapc1b* mutant highlights the continuous scavenging role of macrophages under homeostatic conditions. Our work suggests that the

accumulation of undigested cell debris in macrophage lysosomes may itself contribute substantially to the pathogenesis of human lysosomal storage diseases. We find that defects in macrophage degradative function render the cell vacuolated, immotile, and unable to further perform a critical scavenging function, which depends on directed migration to the dying cell (Hochreiter-Hufford and Ravichandran, 2013). This may contribute to the accumulation of unphagocytosed debris from cells undergoing apoptosis in the course of homeostatic tissue remodeling and repair, and the pathological consequences of their secondary necrosis.

The increased number of apoptotic bodies observed in human lysosomal storage disorders has been attributed to increased cell death triggered by the accumulation of lysosomal substrates (Huang et al., 1997). However, macrophages also accumulate lysosomal substrates in a variety of human lysosomal storage diseases (Kieseier et al., 1997); our findings suggest that the resultant immotility of an increasing proportion of macrophages may contribute to the accumulation of dead cells. Because tissue turnover is high in the developing brain, the macrophage scavenging deficit we propose may be particularly relevant for the pathogenesis of the neurological manifestations of lysosomal storage disorders hitherto attributed to neuronal dysfunction (Jeyakumar et al., 2005). Hematopoietic stem cell transplants in humans and mice improve clinical manifestations of lysosomal storage disorders, including neurological ones that are recalcitrant to enzyme replacement therapy (Biffi et al., 2004; Malatack et al., 2003; Norflus et al., 1998). In light of our findings, we speculate that hematopoietic stem cell transplantation alleviates disease pathology by restoring macrophage degradative function and consequently migration to engulf cell debris.

Macrophage Migration Defects Caused by Lysosomal Accumulation Promote Tuberculous Granuloma Breakdown

Our studies of the *snapc1b* mutant, in which vacuolated macrophages fail to migrate into the tuberculous granuloma, reveal the inextricable link between macrophage homeostatic and immune function. Like the brain, the forming tuberculous granuloma is an environment with high cell turnover and the maintenance of its cellularity depends on the continuous migration of new macrophages that engulf dying infected macrophages (Davis and Ramakrishnan, 2009; Pagan et al., 2015). In the context of tissue remodeling, the clearance of dying cells prevents their secondary necrosis and release of inflammatory material into the extracellular space (Hochreiter-Hufford and Ravichandran, 2013). Likewise, in the TB granuloma, timely engulfment of dying infected macrophages prevents their secondary necrosis and release of bacteria into the extracellular milieu (Pagan et al., 2015). Granuloma breakdown is clinically significant because it increases both disease severity and risk of transmission (Cambier et al., 2014a).

Human lysosomal storage disorders are rare and often lethal within the first year of life, and thus unlikely to be significant contributors to the global burden of TB. Likewise, *snapc1b* mutant zebrafish fail to reach adulthood, and *SNAPC1* null mutations in humans are likely embryonic lethal. However, even relatively small reductions in the macrophage supply to the granuloma can accelerate its breakdown (Pagan et al., 2015). It is possible that subtle alterations in macrophage degradative function, caused by altered expression of SNAPC1, or lysosomal cathepsins or other hydrolases, could create local macrophage deficits and increased susceptibility to TB. Thus, macrophage lysosomal accumulation from diverse genetic etiologies may together be not insignificant contributors to the global TB burden.

Lysosomal Accumulation in Alveolar Macrophages of Smokers May Contribute to TB Susceptibility

Finally, our findings that lysosomal storage also compromises the migration of lung resident alveolar macrophages to mycobacteria suggests a mechanism for the observed susceptibility of smokers to new TB infection. There is accumulating evidence for a role for alveolar macrophages being first-responding protective cells in TB. In mice, aerosolized *M. tuberculosis* is found almost exclusively in alveolar macrophages for the first 7 days, after which infection moves into other myeloid cells such as monocytes and dendritic cells recruited from the lung interstitium or circulation (Srivastava et al., 2014; Urdahl, 2014). Their greater microbicidal capacity is mirrored in humans whose alveolar macrophages inhibit *M. tuberculosis* growth in contrast to peripheral blood monocytes, which are growth-permissive (Aston et al., 1998). Our findings suggest that migration defects resulting from macrophage lysosomal engorgement impede the rapid engulfment (and therefore eradication) of infecting microbes at points of entry, and may therefore facilitate bacterial entry into growth-permissive cells.

Cigarette smoking increases not only the risk of progression to active pulmonary TB disease, but also the risk of new TB infection, suggesting defective early-response mechanisms in smokers (Anderson et al., 1997; den Boon et al., 2005; Gyawali et al., 2012). Smokers' alveolar macrophages phagocytose bacteria and yeast normally, and have normal bactericidal activity against *M. tuberculosis* (Cohen and Cline, 1971; Harris et al., 1970; O'Leary et al., 2014). The incapacitation of alveolar macrophages by tobacco smoke particulates may contribute to increased risk of infection in two ways: i) delayed time to phagocytosis by the alveolar

macrophage, allowing for a longer extracellular growth period by the bacteria, and ii) increased chance of initial phagocytosis by a recruited, growth-permissive macrophage.

In addition to providing an explanation for the increased susceptibility of individuals with genetic lysosomal storage disorders to respiratory, skin and mucosal infections (Jain and Yelwatkar, 2011; Machaczka et al., 2014), our findings may constitute a basis for the susceptibility of smokers to other respiratory infections (Bagaitkar et al., 2008; Lin et al., 2007), Finally, this mechanism may also contribute to the poorly understood association between indoor air pollution and TB (Sumpter and Chandramohan, 2013).

Smokers' increased susceptibility to infection may be reversible. A longitudinal study of alveolar macrophages after transplant of a smoker's lung into a nonsmoker revealed a progressive decrease in "smokers alveolar macrophages" from >90% to 3% in three years (Marques et al., 1997). In our cohort, ex-smokers not only had significantly fewer alveolar macrophages with lysosomal storage than smokers, but overall migration to *M. tuberculosis* was restored. These findings provide an additional rationale for smoking cessation as a prescription for TB prevention.

Experimental Procedures

Zebrafish husbandry and larval injections

Zebrafish husbandry and experiments were conducted according to guidelines from the UK Home Office, and the US National Institutes of Health (approved by the University of Washington Institutional Animal Care and Use Committee). The wildtype AB strain was used for experiments except those in which the *snapc1b(fh111)* line or transgenic lines were used. Unless noted, crosses using *snapc1b(fh111)* were performed as heterozygote incrosses which were genotyped at the completion of the experiment, to ensure blinded scoring of phenotypes. Except where noted, "WT" refers to *snapc1b*$^{fh111/+}$ and *snapc1b*$^{+/+}$. Bacteria, beads and dye were injected into the caudal vein and/or hindbrain ventricle. The Tg(*mpeg1:YFP)*^{w200}, Tg(*mpeg1:Brainbow)*^{w201} (expressing tdTomato) and Tg(*lysC:eGFP)*^{nz117} lines were used as previously described (Hall et al., 2007; Pagan et al., 2015; Roca and Ramakrishnan, 2013). All transgenic and *snapc1b(fh111)* lines were maintained as outcrosses to AB.

Bead injections

As a chemoattractant, heat killed bacteria were prepared by incubating a 2x10^4/uL culture of Mm in 7H9.OADS at 80°C for 30min. Sterile blue fluorescent 1 micron beads (Life Technologies F-8814) were mixed with heat killed Mm at a 1:9 ratio of beads:heat-killed Mm and then diluted to $3.64x10^3$ beads/nL. Approximately 5 nL of the resulting bead:heat-killed Mm mixture was injected into the hindbrain ventricle of 2 dpf larvae for a total of $1.8\ x10^4$ beads per larva. Images were captured using confocal laser microscopy 24 hours following injection.

Dye and protein injections

LysoTracker Red DND-99 dye (DMSO solution, Life Technologies) was diluted 1:25 in PBS prior to injection of 5 nl into the HBV of 3 dpf larvae. MagicRed-Cathepsin (Immunochemistry Technologies, LLC) was resuspended at the concentration suggested by the manufacturer in DMSO, diluted 1:1 in 1xPBS and injected into the brain of 3 dpf larvae. Dextran-Alexa488 (10,000MW, Molecular Probes) was resuspended in 1xPBS to a concentration of 1 mg/mL, then diluted 1:100 prior to injection into the brain of 3 dpf larvae. CCL2 was injected into the HBV as previously described (Cambier et al., 2014b).

Construction of Venus-V2A-*ctsl1* plasmid and *in vitro* transcription

The zebrafish *ctsl1* gene was amplified from cDNA and used to replace *csf1a* in a vector containing pCMV:nlsVenus-V2A (a gift from D. Parichy) by Gibson Assembly (Life Technologies). In vitro transcription was performed with mMessage mMachine SP6 kit (Life Technologies).

Morpholino and RNA injections

All morpholinos used in this work (Table S3.1) and *in vitro* transcribed *ctsl1* mRNA were diluted in a 1x Tango Buffer (Thermo Scientific), 2% phenol red sodium salt solution (Sigma) and injected 1 nL into the yolk of 1-2 cell stage embryos (Tobin et al., 2012).

Zebrafish mutagenesis, screening and positional cloning

fh111 carriers were identified by infection of gynodiploid larvae (Johnson et al., 1995) with 150-200 CFU of green fluorescent Mm. Putative *fh111* carriers were outcrossed to the wildtype WIK strain and mutants and carriers identified by random crosses between siblings. Bulk segregant

analysis (BSA) was performed on pools of mutant progeny and phenotypically wildtype as described (Bahary et al., 2004). Intermediate and fine mapping were conducted using published markers and new markers generated by resequencing of mutant and wild-type progeny within the linked region. Fine mapping determined the causative locus lay between a WIK AseI site at 37.97 mb and a SNP at 38 mb on Chromosome 13. This region contained a single gene, *snapc1b*. Sequencing of all exons and splice junctions within the critical region in mutant embryos and their siblings identified a single splice acceptor site mutation immediately upstream of exon 2, in which the canonical A of the highly conserved AG immediately upstream of the splice acceptor site was converted to GG at position chr13:37996163 (A to G transition). We detected no recombination events at this locus in 854 total meioses from mapping crosses.

Staining

Neutral red staining of 6 dpf larvae was performed as described (Herbomel et al., 2001). Acridine Orange staining was performed by soaking larvae in fish water containing 2 µg/mL acridine orange (ImmunoChemistry, Bloomington, MN) for 30 minutes at 29°C in the dark. Larvae were washed for 5 minutes in fish water at room temperature and then mounted for microscopy as previously described (Yang et al., 2012).TUNEL assay assay staining of larvae was performed by incubationfor 24 hr in 50 µM of Q-VD-OPh (R&D Systems, Inc.) dissolved in DMSO, after which TUNEL staining was performed as described (Volkman et al., 2004).

Drug treatments

E64d. E64d (Sigma) was dissolved in DMSO and added to fish water to a final concentration of 2-3 μg/mL in 0.5% DMSO. Larvae at 2 dpf were treated with the resulting E64d solution for 24 hours and then transferred to clean fish water for the duration of the experiment.

Q-VD-OPh: Larvae were treated with 50 μM Q-VD-OPh in 0.5% DMSO commencing at 2 dpf with daily water changes.

Genotyping

HRM genotyping: High resolution melt genotyping was conducted using the CFX Connect Real- Time PCR Detection System (BioRad) and the EvaGreen iTag Precision melt supermix. HRM primers were used at final concentration of 0.2 mM with ~10 ng of gDNA in 10 ul reaction. PCR was conducted using Biorad HRM standard cycling parameters.

***snapc1b*$^{\mathbf{Tg(}la010158\mathbf{)}}$**: The retroviral insertion mutant *snapc1b*$^{Tg(la010158)}$ (ZIRC) (GenBank ID JM495858.1) was genotyped using agarose gel electrophoresis using primers flanking the insertion site and a primer specific for the retroviral insertion (GT186). Wildtype Forward: 5' - GCTGAAATCCATGTCCTTCCA - 3'. GT186 Forward: 5' - GAGTGATTGACTACCCGTCAGCGG - 3'. Common Reverse: 5' - TGCTTTTCTCATGAGCTTCTCT - 3'

***snapc1b*^{fh111}:** *snapc1b*^{fh111} mutants were genotyped using High Resolution Melt (Tucker and Huynh, 2014). An insertion-deletion polymorphism is present in intron 1-2 in the wildtype AB population. The genomic sequences are

*

Reference 5'- ATTTTTTTCCCTG---C**A**GTGGTAAAC -3'

Fh111 5’- ATTTTTTTCCCTG---C**G**GTGGTAAAC -3’

WT INDEL 5’- ATT----------AAAC**A**GTGGTAAAC -3’

All genotypes are distinguishable with HRM sequencing primers, which bind outside of the polymorphic region: snapc1b_HRM Forward: 5’ - CCACAAATTCCAAATGACATTGA -3’. snapc1b_HRM Reverse: 5’ - CCTTTTCTCTCTTGGCTCTTGTTT -3’.

Quantitative RT-PCR

Quantitative RT-PCR was performed as previously described (Clay et al., 2007b). Total RNA from batches of ~30 embryos per biological replicate was isolated with TRIzol Reagent (Life Technologies) and used to synthesize cDNA with Superscript II reverse transcriptase and oligo dT primers (Invitrogen). Quantitative RT-PCR assays were performed with SYBR green PCR Master Mix (Applied Biosystems) on an ABI Prism 7300 Real Time PCR System (Applied Biosystems). Each biological replicate was run in triplicate, and average values were plotted. Data were normalized to *b-actin* for ΔCt analysis. Primers used for RT-qPCR in this study were: Spliced *snapc1b* Forward: 5’- TGA AAC ACT GCT TGG TCG TC -3’; Spliced *snapc1b* Reverse: 5’- CCC GAC TCT GAT CTG GAA AG -3’; *ctsbb* Forward: 5’- GAG GAA CAG AGG AAC AGA CTT TA-3’; *ctsbb* Reverse: 5’- TGA TCA TCT CAT CAT GTG TGT GA-3’; *ctsl1* Forward: 5’- AGG AAG AGT CAC ACC GTC AG -3’; *ctsl1* Reverse: 5’- GTC ACA TAG CCC TTG TCC CT -3’*; b-actin* Forward 5’- ACC TGA CAG ACT ACC TGA TG -3’; *b-actin* Reverse 5’- TGA AGG TGG TCT CAT GGA TAC -3’; *tnf* Forward 5’- AGG CAA TTT CAC TTC CAA GG -3’; *tnf* Reverse 5’- CAA GCC ACC TGA AGA AAA GG -3’.

RNA-sequencing and analysis

Individual larvae were euthanized at 6 dpf and a small piece of tissue from the head of each animal removed with forceps. The head was placed in HotShot DNA extraction bufferand the torso was placed in 50 μL Trizol for RNA isolation (Invitrogen). gDNA was genotyped by HRM and mutant RNA pooled. Trizol extraction followed as per manufacturer's protocol. RNA was purified with LiCl extraction. Library construction was conducted by the Fred Hutchinson Cancer Research Center Genomics Core and proceeded as described (Miller et al., 2013). Approximately 1 μg RNA was poly-A selected, chemically fragmented and cDNA reverse transcribed using random hexamers. Libraries were prepared using the TruSeq Illumina protocol. Sequencing was performed on an Illumina HiSeq 2000 using 50 bp paired-end reads. RNA sequencing reads were aligned to the zebrafish reference genome (Zv9.69) using the TopHat/Bowtie aligner (Trapnell et al., 2013). Transcriptome expression analysis was then conducted using the Cufflinks software pipeline (Trapnell et al., 2013). Validation of splicing perturbations in *snapc1b* mutants was assessed using IGV (Thorvaldsdóttir et al., 2013).

Microscopy

Zebrafish: Fluorescence microscopy was performed as previously described (Takaki et al., 2013; Yang et al., 2012). Quantification of bacterial burdens, enumeration of macrophage numbers, and assessments of mycobacterial cording were performed with a Nikon Eclipse Ti-E inverted microscope fitted with 2x, 4x and 10x objectives. Cording was visually assessed as previously described (Clay et al., 2008). For confocal microscopy, larvae were anesthetized in fish water containing 0.025% Tricaine and embedded in 1.5% low melting point agarose on optical bottom plates (MatTek Corporation). A Nikon A1 confocal microscope with a 20x Plan

Apo 0.75 NA objective was used to generate 40-120 μm z-stacks with 1–2 μm step size. The galvano scanner was used for all static imaging, and the resonant scanner was used for time-lapse imaging. Time-lapse images were taken at 3-15 minute intervals for 5-20 hours. Data were acquired with NIS Elements Version 4.3 (Nikon). Macrophage tracks were generated and volume rendering performed using Imaris 7.7-8.0 (Bitplane Scientific Software). Movies were exported from Imaris to iMovie (Apple Corporation) for addition of labels and stitching. All microscope scoring of staining, bacterial morphology and macrophage morphology was performed blinded.

Human: Adherence purified AM were fixed with 2% paraformaldehyde, stained with Hoechst 33342 (10 μg/ml) and analyzed using a Zeiss LSM 510 laser confocal microscope (Carl Zeiss Microscopy GmbH, Oberkochen, Germany) to detect autofluorescence. Phase contrast images were collected with a transmitted light detector. Images were generated and viewed using Zen software (Carl Zeiss Microscopy).

Human alveolar macrophage experiments

Alveolar macrophages (AM) were retrieved at bronchoscopy after informed consent and as approved by the Research Ethics Committee of St. James' Hospital, using a protocol that preserves viability of macrophages from both smokers and nonsmokers (O'Leary et al, 2014). Macrophage migration and microscopical visualization procedures are detailed in the Supplemental Experimental Procedures.

Human alveolar macrophage migration assay

Human alveolar macrophages: Non-smokers were defined as those subjects reporting no smoking history, ex-smokers were defined as those having ceased smoking more than 6 months prior to sampling and smokers were defined as those currently smoking. Bronchial washing fluid was filtered through a 100 μm nylon strainer (BD Falcon, BD Bioscience, Belgium) and centrifuged at 390 g for 10 min. AM were resuspended in RPMI 1640 culture media supplemented with 0.1% heat inactivated fetal bovine serum (FBS, Gibco), 50 U/ml amphotericin B and 50 μg/ml cefotaxime. For characterization of initial cell population, 0.5 x 10^5 cells were seeded on an 8 chamber Lab-teks® (Thermo Fisher Scientific), fixed with ice cold methanol containing 10 μg/ml of Hoechst 33258 (Sigma Aldrich) for 4 minutes.

Mycobacteria: *M. tuberculosis* H37Ra was obtained from the American Type Culture Collection (ATCC 25177, Manassas, VA) and prepared as previously described (Ryan et al, 2011) and resuspended at 1 x 10^8 CFU/ml in RPMI 1640 with 0.1% heat inactivated fetal bovine serum (RPMI/0.1% hiFBS).

Migration assay: The migration assay was carried out in transwell chambers consisting of 8 μm pore polycarbonate cell culture inserts in a 24-well companion plate (Corning Costar™ , Nijmegen, Netherlands) (Opalek et al., 2007). Experiments were performed in triplicate unless otherwise stated. Mtb, Tuberculin PPD (30μg/ml) (Statens Serum Institut, Denmark) diluted in RPMI/0.1% hiFBS, or RPMI/0.1% hiFBS alone or RPMI/10% zymosan-activated serum (ZAS) were placed in the lower chambers. AM (0.5 x 10^5 cells) were added to the upper chambers and plates were incubated at 37°C, 5% CO_2 for 2 hrs unless otherwise stated. Migrated cells were fixed in ice-cold methanol containing 10 μg/ml of Hoechst 33258 (Sigma Aldrich) for 4 minutes. AM were counted by fluorescent microscopy (Olympus IX51, Olympus Europa GmbH,

Germany) to establish the number of migrating cells and the percentage vacuolated AM in the initial and migrating cell populations.

Neutral red staining of lysosomes: Adherence-purified AM cultured in 24 well plates were stained by adding neutral red (Sigma) (40 μg/ml) and incubating for 30 min at 37°C, 5% CO_2 (Repetto et al., 2008). Images were obtained using an Olympus IX51 microscope with a DP71 CCD camera and cellSens software.

Bacterial strains

Wildtype *M. marinum* (Mm) (strain M - ATCC #BAA-535) expressing tdTomato under the constitutive promoter *msp12* was used for fluorescence microscopy and quantification of intracellular bacterial burdens (Takaki et al., 2013). The attenuated Δ*erp* mutant Mm was used to enumerate intracellular bacteria (Cosma et al., 2006; Takaki et al., 2013) and WT Mm was used for all other assays. Bacterial were cultures and prepared for injection as described (Takaki et al., 2013).

M. tuberculosis H37Ra (ATCC 25177, Manassas, VA) was used for the human alveolar macrophage studies and prepared as described in Supplemental Experimental Procedures. All Mm strains were grown under hygromycin (Mediatech) selection in Middlebrook's 7H9 medium (Difco) supplemented with glycerol, oleic acid, albumin, dextrose, and Tween-80 (Sigma) (Takaki et al., 2013). Single-cell stocks of Mm were prepared as previously described prior to injection (Takaki et al., 2013). Inocula were determined by microinjection onto 7H10 plates.

Statistical analyses

Statistical analyses were performed using Prism 6 (GraphPad). Not significant, $p \geq 0.05$, * $p < 0.05$; ** $p < 0.01$; *** $p < 0.001$; **** $p < 0.0001$.

Chapter 3 Figures and Tables

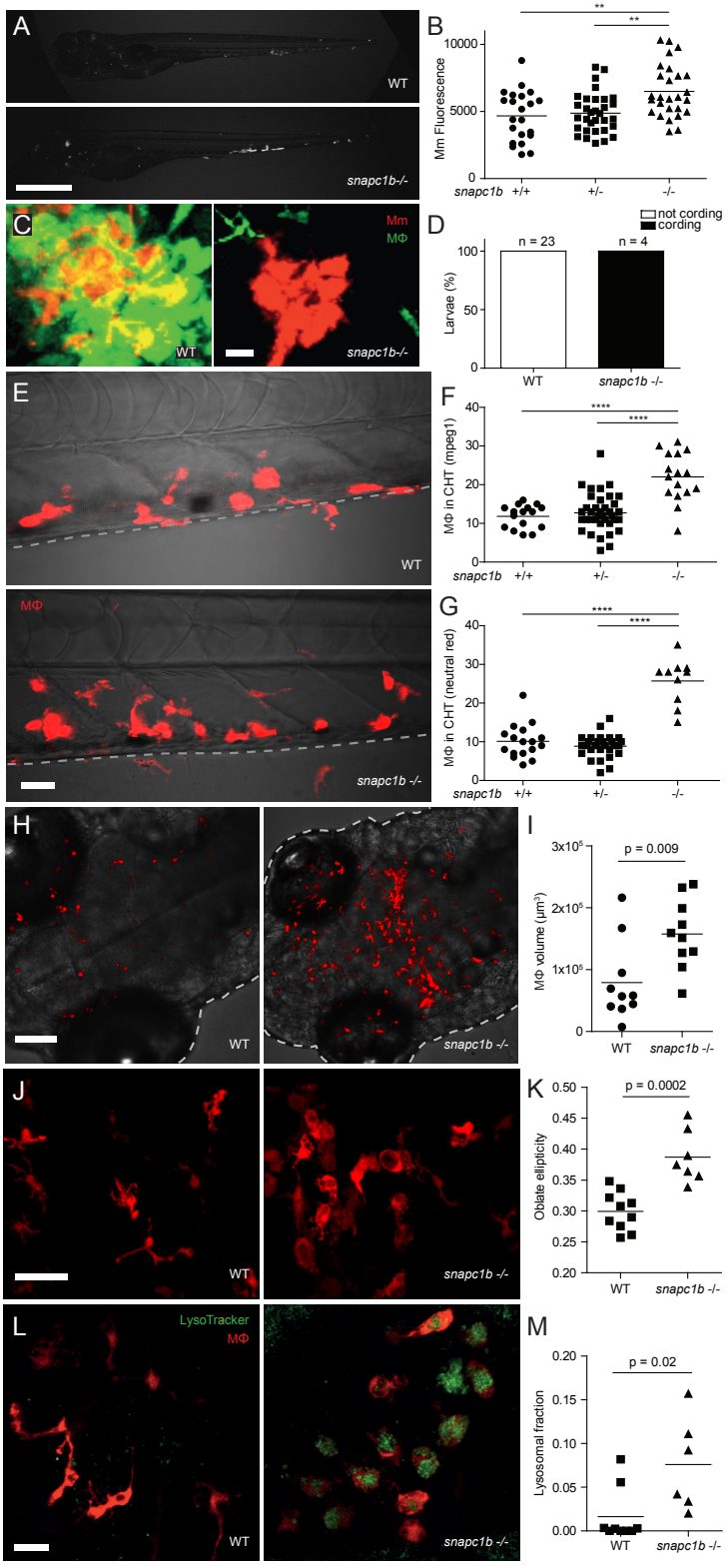

Figure 3.1. *snapc1b* mutants are hypersusceptible to *M. marinum* and have increased numbers of macrophages that display vacuolated morphology (A) Representative images of wildtype (WT) and *snapc1b*$^{fh111/fh111}$ mutant larvae 4 days post-infection (dpi) with 150 *M. marinum* (Mm) Scale bar, 300 μm. (B) Quantification of Mm burden measured by fluorescence in *snapc1b*$^{fh111/+}$ incross larvae at 5 dpi with 240 Mm. (C) Confocal images of green fluorescent macrophages and red fluorescent bacteria in intact granulomas of WT larvae and extracellular corded bacteria following complete granuloma breakdown in *snapc1b* mutant larva at 2 dpi with 200 Mm. Scale bar, 15μm. (D) Quantification of bacterial cording in larvae from an incross of *snapc1b*$^{fh111/+}$ parents at 5 dpi with 200 Mm. (E) Confocal images of the caudal hematopoietic tissue (CHT) of representative WT and *snapc1b* mutant larvae with red fluorescent macrophages at 6 days post-fertilization (dpf). Scale bar, 20μm. (F,G) Quantification of fluorescent macrophages (F) and neutral red stained cells (G) in the CHT of *snapc1b*$^{fh111/+}$ incross larvae at 6 dpf. (H) Confocal images of fluorescent macrophages in the head of representative WT and *snapc1b* mutant larvae at 3 dpf. Dotted lines indicate the outline of larvae. Scale bar, 100μm. (I) Total macrophage volume in the brains of WT and *snapc1b* mutant larvae at 5 dpf. Volumetric analysis performed from 3D confocal images on red fluorescence signal. (J) Confocal images of fluorescent macrophages in the brain of WT and *snapc1b* mutant larvae at 3 dpf. Scale bar, 60μm. (K) Measurement of oblate ellipticity of macrophages in the brains of WT and *snapc1b* mutant larvae at 3 dpf. (L) Confocal images red fluorescent macrophages stained with LysoTracker green in the brains of 3 dpf WT and *snapc1b* mutant larvae. Scale bar, 30μm. (M) Average lysosomal volume per animal normalized to total macrophage volume. Macrophage and lysosomal volumes were determined by volumetric analysis of red fluorescence (macrophages)

and green fluorescence (lysosomes) in 3D confocal images. Statistical significance was assessed by one-way ANOVA with Sidak's post-test (B,F,G) or Student's *t* test (I,K, and M). See also Figures S3.1 and S3.2, and Tables S3.2 and S3.3.

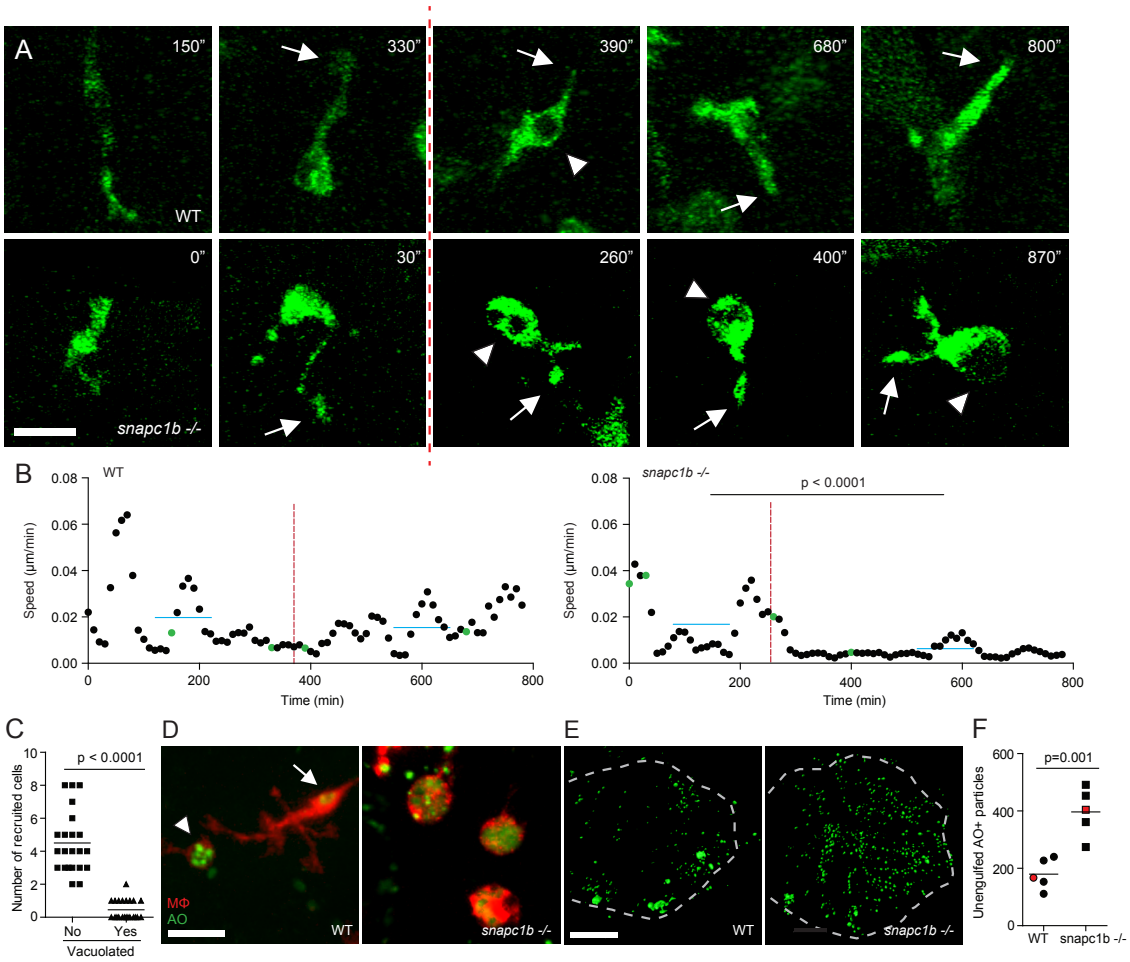

Figure 3.2. Lysosomal storage in *snapc1b* mutants compromises physiological efferocytosis

(A) Still images from confocal video of green fluorescent macrophages in *snapc1b* mutant larval and WT sibling brains. Time of image indicated in minutes. Arrows mark pseudopodia, arrowheads mark vacuoles. Vertical dotted red line indicates the time point immediately following phagocytic event. Scale bar, 15 μm. (B) Speed of WT and *snapc1b* mutant macrophages from the confocal video in (A). Average speed before and after the phagocytic events are indicated by a horizontal blue line. Green dots correspond to time points in the images shown in (A). (C) Migration of normal and vacuolated macrophages from the same animal to

CCL2 injected into the HBV. (D) Representative confocal image of red fluorescent macrophages stained with acridine orange (AO) in brains of *snapc1b* mutant larvae and WT siblings at 3 dpf. Arrow marks a wildtype macrophage with very little AO staining. Arrowhead marks a rare AO positive macrophages seen in WT brains. Scale bar, 30 μm. (E,F) Confocal images (E) and quantification (F) of green fluorescent acridine orange stained unengulfed cell debris in the brains of *snapc1b* mutant larvae and WT siblings at 5 dpf. Scale bar, 150 μm. Images in (E) denoted as red data points in (F). Statistical significance was assessed by Student's *t* test (B, F) and paired *t* test (C). See also Figure S3.3.

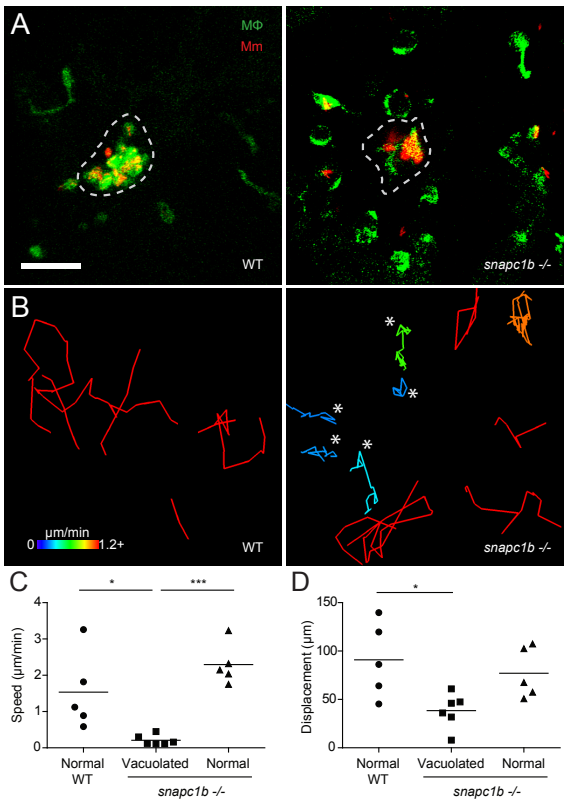

Figure 3.3. *snapc1b* mutant macrophages fail to participate in granuloma formation (A) Confocal images of granulomas in the hindbrain ventricle of *snapc1b* mutant larvae and WT siblings with green fluorescent macrophages at 2 dpi with 100 red fluorescent Mm. Scale bar, 60 µm. (B) Tracks of macrophage movement following granuloma formation in *snapc1b* mutant larvae and WT siblings shown in (A). Tracks are coded for speed. Tracks created by vacuolated macrophages are indicated with an asterisk. (C,D) Speed (C) and displacement (D) of *snapc1b* mutant and WT sibling macrophages in (A and B). Statistical significance was assessed using one-way ANOVA with Sidak's post-test.

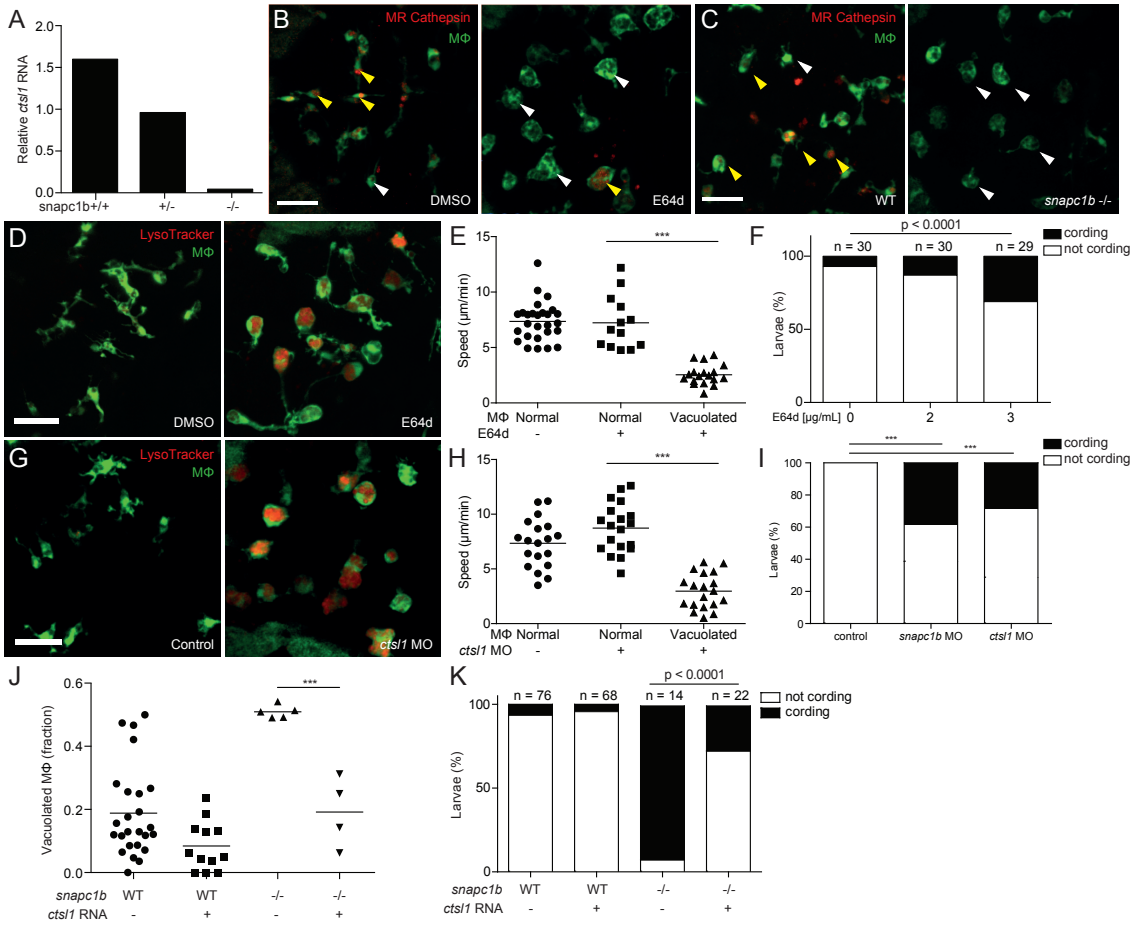

Figure 3.4. Cathepsin L deficiency causes *snapc1b* mutant vacuolated macrophage morphology and susceptibility to *M. marinum* (A) Quantitative real-time PCR of relative *ctsl1* transcript in *snapc1b*$^{+/-}$ incross larvae at 6 dpf. Values normalized to transcript level of the heterozygous larvae, representative of two experiments. (B, C) Confocal images of green fluorescent macrophages in larvae injected with red fluorescent MR-Cathepsin L at 3 dpf, either following treatment with E64d or DMSO control at 2dpf (B) or in *snapc1b* mutants and WT siblings (C). Yellow or white arrowheads denote macrophages that are positive or negative for MR-Cathepsin, respectively. Scale bar, 50μm. (D) Confocal images of green fluorescent macrophages stained with LysoTracker red in the brains of 3 dpf E64d-treated and DMSO

control larvae. Scale bar, 50μm. (E) Average macrophage speeds during a 5-hour movie in the brains of 3 dpf E64d-treated and DMSO control larvae. (F) Quantification of bacterial cording in DMSO control and E64d-treated larvae at 5 dpi with 150 Mm. (G) Confocal images of green fluorescent macrophages stained with LysoTracker red in the brains of 3 dpf *ctsl1* morphants and control larvae. Scale bar, 50μm. (H) Average macrophage speeds during a 5-hour movie in the brains of 3 dpf *ctsl1* morphants and control larvae. (I) Quantification of bacterial cording in control, *snapc1b* and *ctsl1* morphants at 5 dpi with 200 Mm. (J) Quantification of vacuolated macrophages in the brains of 3 dpf WT or *snapc1b* mutant larvae following injection of *ctsl1* RNA or control at 0 dpf. (K) Quantification of bacterial cording at 2 dpi with 215 Mm in the HBV of *snapc1b* mutants and WT siblings following injection of *ctsl1* RNA or control. Statistical significance was assessed by ANOVA with Sidak's post test (E, H, and J) or Fisher's exact test (F, I, and K). See also Figure S3.4.

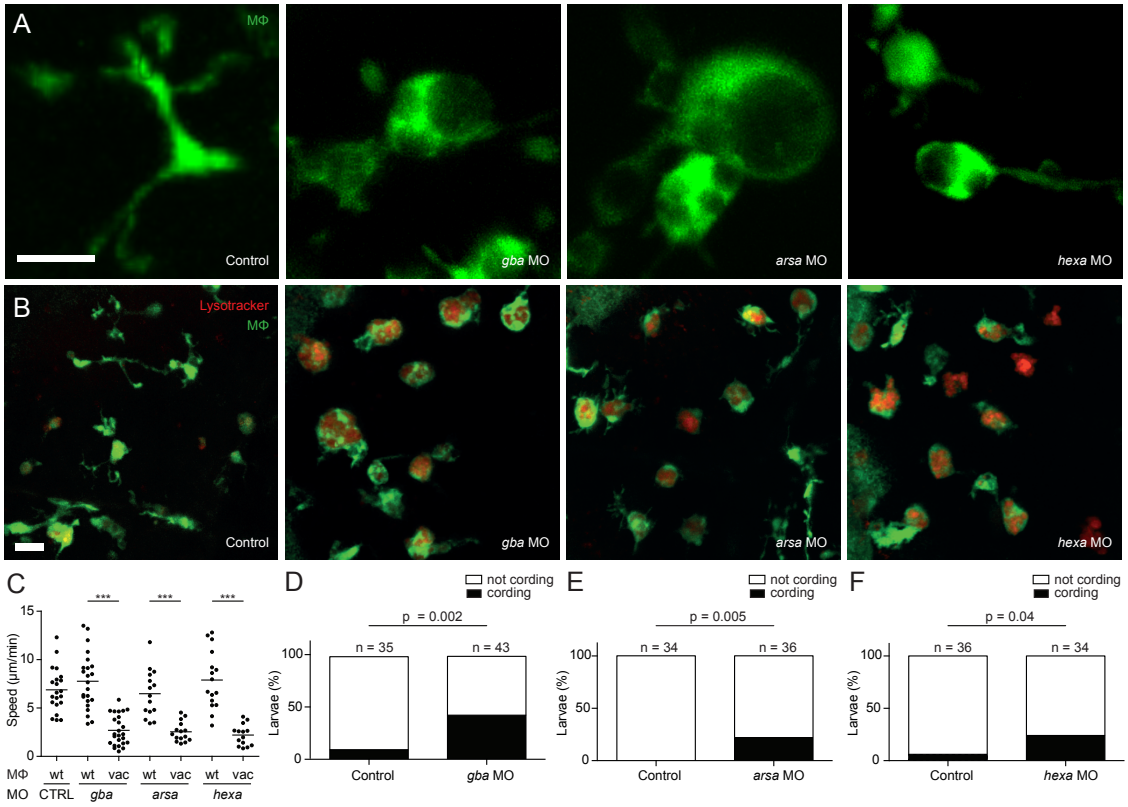

Figure 3.5. Lysosomal storage disorders disrupt macrophage migration and cause granuloma breakdown. (A,B) Confocal images of green fluorescent macrophages in the brain of 3 dpf control and morphant larvae, unstained (A) or following staining with LysoTracker Red (B). Scale bars, 10µm. (C) Quantification of average macrophage speed in control and morphant larvae by macrophage morphology (wt for wildtype and vac for vacuolated). (D-F) Quantification of bacterial cording in control and morphant larvae at 3 dpi with 200 Mm. Statistical significance determined using paired *t* tests with Bonferroni correction (C) and Fisher's exact test (D-F).

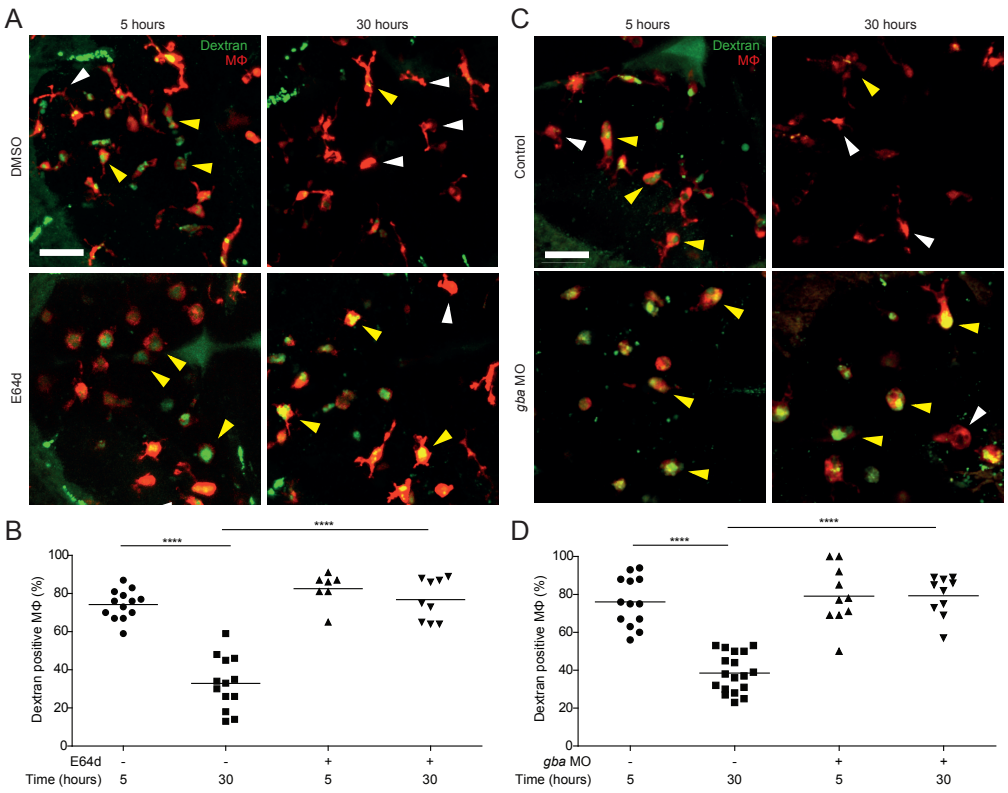

Figure 3.6. Macrophage lysosomal storage disrupts endocytic recycling (A) Confocal images of red fluorescent macrophages following injection of green fluorescent dextran in E64d-treated and DMSO control larvae (3 dpf) at 5 and 30 hours post-injection. Yellow and white arrowheads denote macrophages with and without dextran, respectively. Scale bar, 50μm. (B) Quantification of the percentage of macrophages which are positive for dextran in E64d-treated and DMSO control larvae (3 dpf) at 5 and 30 hours post-injection. (C) Confocal images of red fluorescent macrophages following injection of green fluorescent dextran in *gba* morphants and control larvae (3 dpf) at 5 and 30 hours post-injection. Yellow and white arrowheads denote macrophages with and without dextran, respectively. Scale bar, 50μm. (D) Quantification of the percentage of macrophages which are positive for dextran in *gba* morphants and control larvae (3 dpf) at 5 and 30 hours post-injection. See also Figure S3.5.

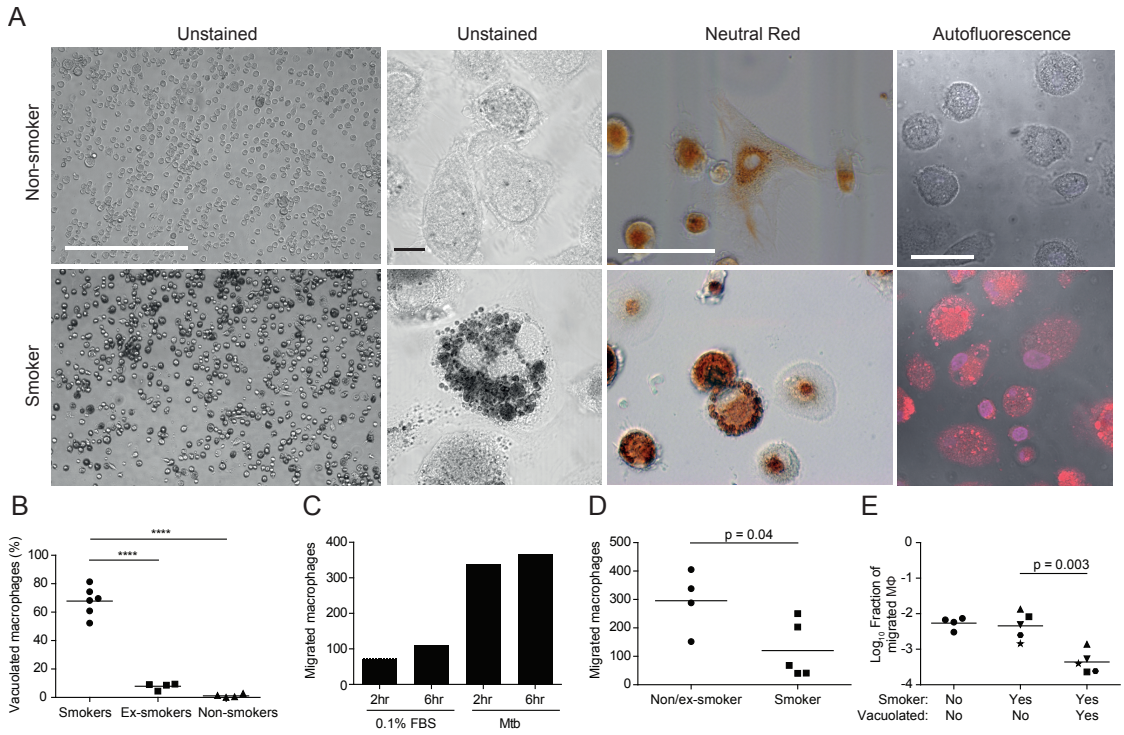

Figure 3.7. Lysosomal accumulation of tobacco smoke products in alveolar macrophages compromises migration to *M. tuberculosis* (A) Representative images showing the characteristics of macrophages isolated by bronchoalveolar lavage from smokers and non-smokers. Scale bars (left to right): 400µm, 10µm, 20µm, 10µm. (B) Percentage of vacuolated macrophages was assessed in smokers, ex-smokers and non-smokers. Vacuolated macrophages were scored based on their autofluorescence and morphology. (C) Number of macrophages that migrated through a transwell was assessed at 2 and 6 hours of incubation with either 0.1% FBS or Mtb H37Ra using macrophages from an ex-smoker. Values represent averages of a single experiment performed in triplicate. (D) Number of macrophages from non/ex-smokers that migrated through a transwell towards Mtb H37Ra (assessed following 2-hour incubation). (E) Fraction of macrophages that migrated in the transwell assay calculated from initial vs. migrated macrophages of each morphology. Samples from smokers are split into vacuolated and normal

with unique symbols for each patient. Statistical significance was assessed by one-way ANOVA with Sidak's post-test (B), Student's *t* test (D), paired *t* test (E). See also Figure S3.6 and Table S3.4.

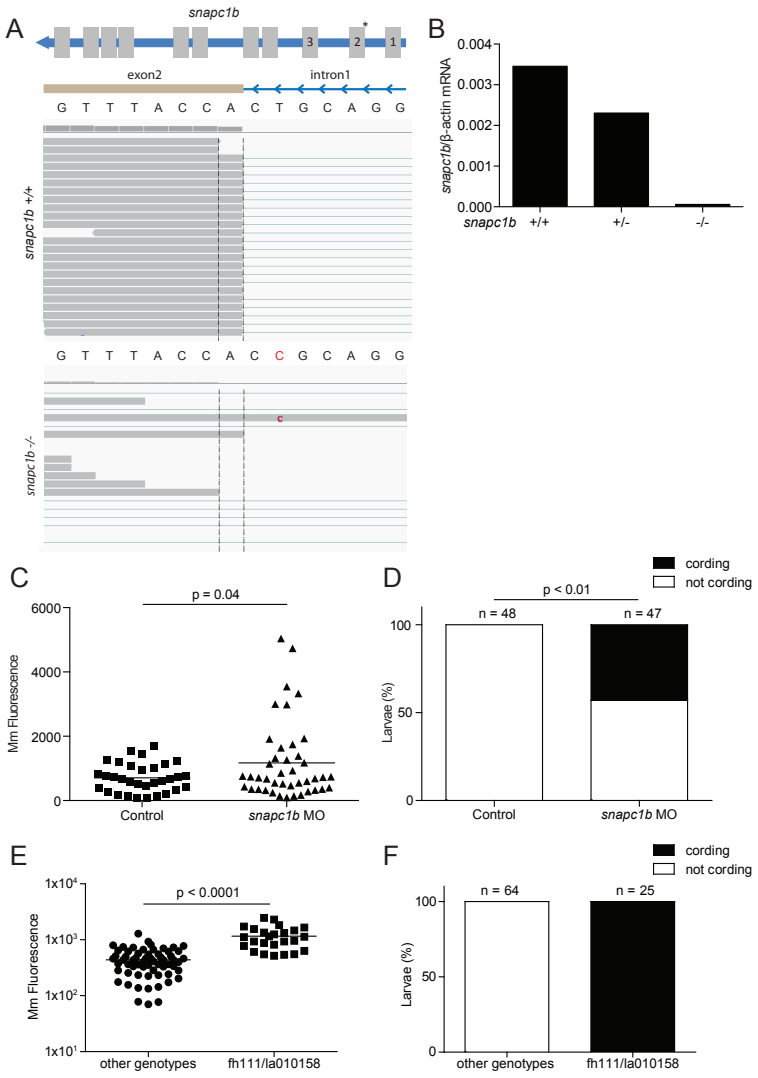

Figure S3.1. Genetic disruption of the *snapc1b* locus confers susceptibility to *M. marinum* infection, related to Figure 3.1. (A) Top: Diagram of *snapc1b* gene showing introns (blue), exons (gray), and location of the *fh111* splice acceptor mutation denoted by an asterisk above the relevant exon-intron boundary. Bottom: RNA-sequencing reads aligned to the exon 2 splice acceptor site from WT and *snapc1b*$^{fh111/fh111}$ mutant larvae with wildtype and mutant sequence. The *snapc1b(fh111)* mutation is denoted in red. (B) Quantitative real-time PCR of properly spliced *snapc1b* transcript in *snapc1b*$^{+/-}$ incross larvae at 6 dpf. Values normalized to transcript level of β-*actin*, representative of two experiments. (C,D) Quantification of bacterial burden (C)

and cording (D) in control and morphant larvae at 4 dpi with 250 Mm. (E,F) Quantification of bacterial burden and cording in *snapc1b*$^{Tg(la010158)/+}$ *x snapc1b*$^{fh111/+}$ cross larvae at 5 dpi with 150 Mm. Statistical significance was assessed by Student's t test (C,E) and Fisher's exact test (D).

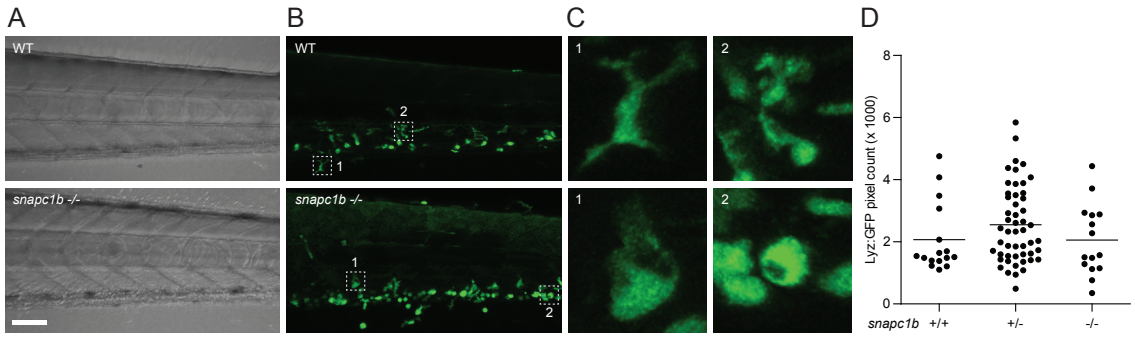

Figure S3.2. *snapc1b* mutants have numerous vacuolated macrophages and normal neutrophil numbers in the caudal hematopoietic tissue (CHT), related to Figure 3.1. (A) Brightfield and (B) confocal images of the CHT of representative WT and *snapc1b*$^{-/-}$ mutant larvae at 5 dpf. Scale bar 50μm. (C) 8X magnification of outlined regions in (B) showing normal (top) and vacuolated (bottom) morphology.

(D) Quantification of Lyz:eGFP positive, green fluorescent neutrophils in *snapc1b*$^{+/-}$ incross larvae at 6 dpf.

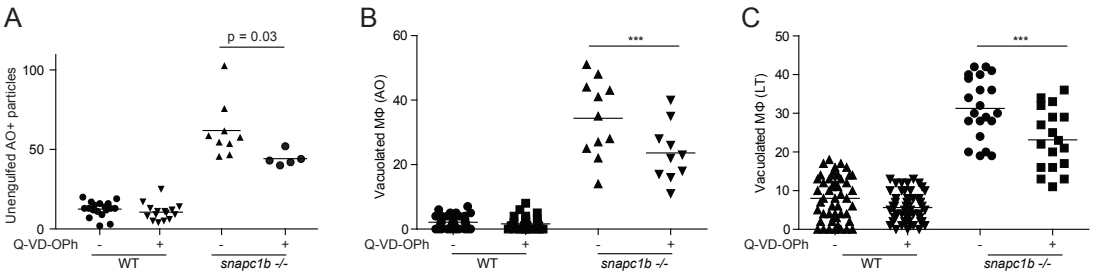

Figure S3.3. Global inhibition of apoptosis reduces the abundance of vacuolated macrophages in the *snapc1b* mutant, related to Figure 3.2. (A) Quantification of extracellular AO positive particles in WT and *snapc1b* mutant larvae at 3 dpf following treatment with 10μM Q-VD-OPh or DMSO control. (B) Quantification of AO-positive vacuolated macrophages in *snapc1b* mutant larvae and WT siblings at 3dpf following treatment with 10μM Q-VD-OPh or DMSO control. (C) Quantification of LysoTracker-positive macrophages in *snapc1b* mutant larvae and WT siblings at 3dpf following treatment with 50μM Q-VD-OPh or DMSO.

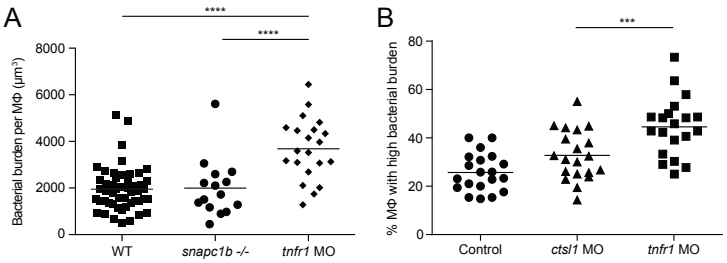

Figure S3.4. Macrophages of *snapc1b* mutant and cathepsin L deficient animals restrict mycobacterial growth normally, related to Figure 3.4. (A) Macrophage intracellular bacterial burdens of *snapc1b*$^{+/-}$ incross larvae and *tnfr1* morphants infected with 100 red fluorescent Mm at 2 dpf in the caudal vein. Bacterial volume (μm^3) was quantified per animal from 3D confocal images captured in the tail region at 40 hpi. The intramacrophage replication of Mm is unrestricted in *tnfr1* morphants as expected (Clay et al., 2008; Pagan et al., 2015; Tobin et al., 2010). (B) Percentage of macrophages with high intracellular bacterial burdens in control, *ctsl1* and *tnfr1* morphants infected with ~75 red fluorescent Mm at 2 dpf in the caudal vein. Bacterial burden was quantified per animal by counting the average number of bacteria per macrophage and categorizing as low (1-5 bacteria) or high (>5 bacteria). Statistical significance was assessed by one-way ANOVA with Sidak's post test (A, B).

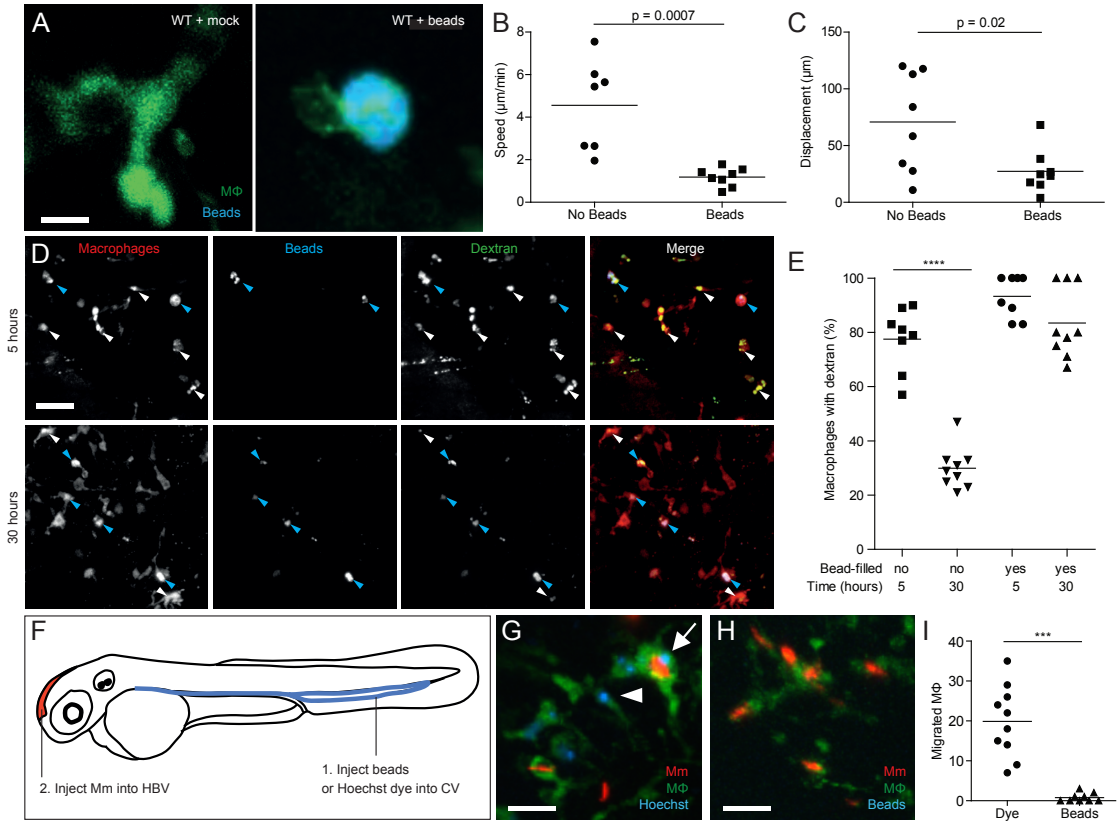

Figure S3.5. Lysosomal accumulation of inert particles compromises endocytic recycling and migration to the initial site of mycobacterial infection, related to Figure 3.6. (A) Confocal images of green fluorescent macrophages in larvae mock-injected or injected with $5x10^5$ blue fluorescent 1μm polystyrene beads. Scale bar, 12μm. (B,C) Speed (B) and displacement (C) of macrophages with and without beads (D) Confocal images of red fluorescent macrophages in 3dpf larvae pre-loaded with blue fluorescent polystyrene beads as in (A), injected 12 hours later with green fluorescent dextran and imaged at 5 and 30 hours post-dextran injection. Blue and white arrowheads denote macrophages containing dextran, with and without blue beads, respectively. Scale bar, 50μm. (E) Quantification of macrophages that retained dextran at 5 and 30 hours post injection. (F) Diagram showing the experimental outline in which 2 dpf larvae were injected with Hoechst dye or beads in the CV followed by infection in the

HBV with 200 Mm. (G,H) Confocal images of larval HBV containing green-fluorescent macrophages following CV injections with Hoechst (G) or blue fluorescent beads (H). Arrow and arrowhead denote Hoechst-positive macrophages that have migrated from the CHT, with and without phagocytosed red fluorescent Mm, respectively. Scale bar, 10μm. (I) Number of macrophages in the HBV after injection of dye or beads in the CV followed by Mm infection in the HBV. Statistical significance was assessed using Student's t test (B, C, and I), and one-way ANOVA with Sidak's post test (E).

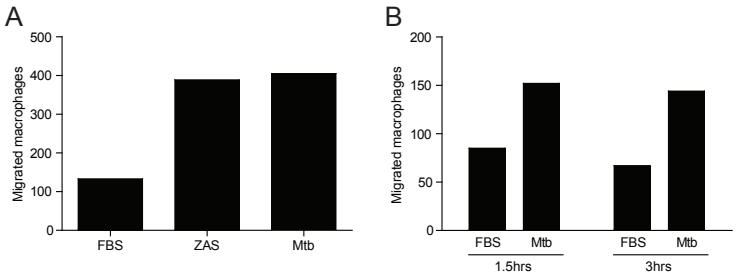

Figure S3.6. Alveolar macrophage migration to ZAS and Mtb, related to Figure 3.7.

(A) Migration of macrophages from nonsmoker SJH209 to 0.1% FBS, ZAS or Mtb at 2 hours.

(B) Migration of macrophages from ex-smoker to Mtb at 1.5 and 3 hours in transwell assay.

Table S3.1. Morpholinos used in this study, related to Experimental Procedures.

Gene[a]	Used name[b]	Morpholino sequence	MO target	MO concentration (mM)	Reference
snapc1b	snapc1b	CTTGTTTACCACTGCAGGGAAAAAA	i1/e2	0.05	This work
snapc1b	snapc1b	ACCACTTCCCTGAAATGCTCCATCC	atg/5'UTR	0.5	This work
ctsl.1	ctsl1	GTTTGTTTTAATTTCCTACCATGTC	e3i3	1.3	This work
ctsbb	ctsbb	ACACTGCAGATGGAGAAAACACACA	i3e4	0.05	This work
ctsbb	ctsbb atg	GCGAACACACACACACGCCACATCC	atg/5'UTR	0.05	This work
tnfr1	tnfr1	CTGCATTGTGACTTACTTATCGCAC	E5/i6	0.32	(Roca & Ramakrishnan, 2013)
hexa	hexa	ACATTGCCAGGAAGTACTCACAGCT	e2/i2	1	This work
gba	gba	CGTCTGATTATTGTTACACACCTCT	e1/i1	0.5	This work
arsa	arsa	TATGTTTGACCTGGCTTTACCTGGA	e1/i1	1	This work

[a]Gene abbreviations follow the "Zebrafish Nomenclature Guidelines"

(https://wiki.zfin.org/display/general/ZFIN+Zebrafish+Nomenclature+Guidelines)

[b]Name, often simplified, that was used in this paper

Table S3.2. Selected differentially expressed genes in *snapc1b* mutants, related to Figure 3.1.

Category	Gene	*snapc1b* +/+ FPKM	*snapc1b* -/- FPKM	Fold change (mutant/wt)	Associated LSD
Myelopoeisis	csf1rb	1.07	0.32	0.29	
	csf3r	0.85	0.71	0.84	
	csf1a	1.78	1.85	1.04	
	csf1ra	5.24	5.86	1.12	
	csf2rb	0.34	0.46	1.37	
	csf1b	2.60	3.75	1.44	
	spi1b	2.57	2.47	0.96	
	spi1a	1.63	2.46	1.51	
	irf8	0.89	1.99	2.23	
	mpeg1 (2 of 3)	11.05	32.07	2.90	
	mpeg1	3.12	4.82	1.54	
	gata1a	1.78	1.24	0.69	
	gata1b	0.09	0.03	0.35	
	gata2a	4.31	3.49	0.81	
	gata2b	0.49	0.40	0.80	
	gata3	20.87	15.79	0.76	
	gata4	3.26	2.70	0.83	
	gata5	5.73	7.57	1.32	
	gata6	9.49	10.00	1.05	
	cebp1	0.41	0.29	0.71	
	cebpa	16.82	17.12	1.02	
	cebpb	24.19	44.02	1.82	
	cebpd	116.14	137.37	1.18	
	cebpg	31.68	29.80	0.94	
Inflammation	atf3	8.93	15.99	1.79	
	cebpb	24.19	44.02	1.82	
	elf3	15.67	28.85	1.84	
	junbb	16.86	38.72	2.30	
	junba	11.23	36.13	3.22	
	ptgs2a	6.72	10.64	1.58	
	rgs4	22.31	45.92	2.06	
	ptgs2b	2.62	5.71	2.18	
	ncf1	2.48	5.44	2.20	
	plek	1.23	118.44	96.27	
	m17	0.04	0.21	5.10	
	il1b	0.89	9.07	10.24	

	mmp13a	2.23	10.09	4.52	
	mmp9	3.89	23.70	6.09	
	irg1	0.46	3.62	7.93	
	irg1l	9.42	91.73	9.74	
	tnfa	0.034	0.18	2.44	
Lysosomal	npc1	15.07	20.63	1.37	
	npc2	59.17	63.20	1.07	
	smpd1	7.82	9.84	1.26	
	hexb	26.29	25.22	0.96	
	hexa	8.24	6.58	0.80	Tay-Sachs
	arsa	3.48	2.59	0.75	Metachromatic leukodystrophy
	arsb	6.71	7.20	1.07	
	gba	4.82	5.00	1.04	Gaucher's
	gla	0.52	0.42	0.80	
	ctsa	23.99	24.66	1.03	
	ctsba	72.88	96.18	1.32	
	ctsbb	**57.38**	**5.18**	**0.09**	
	ctsc	25.25	24.17	0.96	
	ctsd	98.61	134.24	1.36	
	ctsf	66.41	60.22	0.91	
	ctsh	44.06	22.82	0.52	
	ctsk	14.80	19.61	1.33	
	ctskl	5.20	3.85	0.74	
	ctsl.1	**378.02**	**47.93**	**0.13**	
	ctsl1a	305.85	655.09	2.14	
	galns	2.57	2.56	0.99	
	gnsa	10.79	10.74	1.00	
	gnsb	13.39	10.69	0.80	
	naglu	1.03	1.16	1.13	
	neu1	15.07	20.63	1.37	
	psap	59.17	63.20	1.07	
	scpep1	7.82	9.84	1.26	
	sgsh	26.29	25.22	0.96	
	idua	8.24	6.58	0.80	
	tpp1	3.48	2.59	0.75	
	tmem55a	6.71	7.20	1.07	
	tmem55b(1 of 2)	4.82	5.00	1.04	
	tmem55b (2 of 2)	0.52	0.42	0.80	
	lamp1	23.99	24.66	1.03	
	lamp2	71.91	86.35	1.20	

	atp6v1h	29.75	30.88	1.04	
	clcn7	5.19	6.04	1.16	
	FPKM = Fragments per kilobase mapped				

Table S3.4. Characteristics and migration of alveolar macrophages retrieved by bronchoalveolar lavage from non-smokers, ex-smokers and smokers, related to Figure 3.7.

				Initial AM population		Migrated AM to Mtb H37Ra	
Sample	**Age years (mean ± SEM)**	**Smoking status**	**Pack years (years ceased)**	**# cells counted**	**% vacuolar cells (mean ± SEM)**	**# cells counted**	**% vacuolar cells (mean ± SEM)**
SJH209		non-smoker	-	320	2.81	405[a]	non-detectable
SJH222		non-smoker	-	441	1.36	-	-
SJH223		non-smoker	-	580	0.00	-	-
SJH226		non-smoker	-	479	0.42	-	-
	52.75 ± 4.27				**1.15 ± 0.62**		
SJH210		ex-smoker	40 (6)	107	9.35	288[ab] (284[c])	non-detectable
SJH211		ex-smoker	27 (16)	201	4.48	152[ab] (144[c])	non-detectable
SJH212		ex-smoker	(0.5)	418	8.61	338	non-detectable
SJH219		ex-smoker	54 (34)	439	9.57	-	-
	55.25 ± 9.74				**8.00 ± 1.19**		
SJH214		smoker	56	441	52.15	203	2.96
SJH215		smoker	100	398	60.80	40	30.00
SJH216		smoker	20	429	74.36	41	21.95
SJH220		smoker	5.7	412	69.66	250	19.20
SJH227		smoker	52.5	424	81.37	68	32.35
SJH218		smoker	47	531	68.17	-	-
	65 ± 3.04				**67.75 ± 4.18**		**21.29 ± 5.19**

[a] Experiments not performed in triplicate [b] migrated cells at 1.5hr timepoint [c] migrated cells at 3hr timepoint

Chapter 4: Multifaceted roles of the macrophage lysosome during early tuberculous infection

The earliest macrophage-mycobacterium interaction sets the course of infection

Between the 17th and 19th centuries, tuberculosis (TB) was estimated to be responsible for 1 in 5 deaths in Europe and North America, killing more than a billion people (Holmberg, 1990). While the mortality rate in untreated patients (50%) and its mode of spread (aerosol) are more consistent with a "crowd" disease, TB is also characteristic of older infections which progress slowly and reactivate after extended periods of latency, features that reflect adaptation to low-density populations (Blaser and Kirschner, 2007; Cambier et al., 2014a; Comas et al., 2013; Wolfe et al., 2007). TB is one of the oldest human infections and has afflicted humanity for roughly 70,000 years, predating the increased population density that accompanied animal domestication and agriculture (Comas et al., 2013). Despite evidence of co-adaptation between humans and *M. tuberculosis*, the bacterium responsible for TB, and despite the fact that humans are the only known host of *M. tuberculosis,* it is estimated that 30-50% of humans clear infection quickly after exposure and this clearance is mediated by the innate immune system as evidenced by a lack of T-cell-mediated responsiveness to the tuberculin skin antigen test (PPD) (Comas et al., 2013; Morrison et al., 2008; Verrall et al., 2014).

TB begins with the deposition of only 1-3 bacteria into the lung alveolus (Ratcliffe and Wells, 1948). The bacterium is phagocytosed by tissue-resident alveolar macrophages, which are broadly microbicidal first-responders that clear a variety of invading pathogens (Green and Kass, 1964). If the bacterium survives this first encounter, it mediates its own transfer into more permissive macrophages recruited from deeper tissues, and uses these macrophages to cross the alveolar epithelial barrier (Cambier et al., 2014a)(CJ Cambier, unpublished results). Intracellular

replication of the mycobacteria proceeds within the macrophage, which then dies through apoptosis or necrosis (Pagan et al., 2015; Roca and Ramakrishnan, 2013) presenting the host with a lose-lose scenario. Apoptotic infected macrophages are phagocytosed by newly arriving uninfected macrophages and contribute to granuloma formation and expansion of the intracellular growth niche (Davis and Ramakrishnan, 2009). Necrotic death (or post-apoptotic secondary necrosis) is associated with extracellular release of bacteria where they grow unimpeded (Pagan et al., 2015) and occurs if the apoptotic infected macrophage is not phagocytosed by uninfected cells.

The central roles of the macrophage in the establishment and early expansion of tuberculous infection have been appreciated for some time, but isolating their functions during these distinct steps of pathogenesis has been difficult using previously available tools. Whether the host clears the initial infection is thought to be determined by the outcome of the first interaction between infecting mycobacteria and the first-responding tissue-resident macrophage (CJ Cambier, unpublished data). If the establishment of infection is successful, its extent and progression are dictated by the early stages of intramacrophage replication and granuloma formation as more macrophages are recruited to and take part in the expanding infection. Host immune deficits can impact either or both of these stages.

Macrophages are traditionally thought of in the context of single activities, either as responders to infection or phagocytes that maintain tissue homeostasis through the clearance of apoptotic cells. Here we reflect on the intersections of four central functions of the macrophage that are relevant to homeostasis and infection: 1) Degradation of apoptotic cells; 2) Migration to phagocytose newly arriving bacteria; 3) Restriction of intracellular bacterial replication; and 4) Migration to dying infected cells in the granuloma.

Lysosomal defects prevent phagocytosis by disrupting macrophage migration

Tissue-resident macrophages are tasked with clearing cells that die by apoptosis during normal tissue turnover (Hochreiter-Hufford and Ravichandran, 2013). They first recognize "find me" signals produced by dying cells, then migrate towards those cells and phagocytose them with the assistance of "eat me" signals that are exposed on the target cell's plasma membrane (Poon et al., 2014). The phagocytosed material is subsequently trafficked to the macrophage lysosome for degradation. Defects in macrophage degradative function disrupt this process by preventing the proper breakdown of phagocytosed apoptotic cells, whose components accumulate in the macrophage lysosome. The accumulation of material in the macrophage lysosome disrupts endocytic recycling, which is required to deliver lipids and proteins required for cell movement to the plasma membrane. This in turn renders the macrophage immotile and unable to migrate to other dying cells in the vicinity. The central mechanism of migration defects resulting from endocytic stalling holds for the lysosomal accumulation of any substrate that cannot be degraded, even synthetic material. In cases of genetic lysosomal hydrolase deficiency, this presents as a progressive macrophage incapacitation at the tissue level as phenotypically normal (but hydrolase-deficient) macrophages migrate to and phagocytose apoptotic cells, but then are rendered vacuolated and immotile when they fail to degrade their cargo. The progressive incapacitation may contribute to the observed excess of unphagocytosed apoptotic cell debris in the tissues of patients with lysosomal storage diseases (Huang et al., 1997; Kieseier et al., 1997). This theory is consistent with studies showing that hematopoietic stem cell transplantation in humans and mice improves neurological effects of lysosomal storage disorders, which do not

respond to enzyme replacement therapy (Biffi et al., 2004; Malatack et al., 2003; Norflus et al., 1998).

Disrupting macrophage migration impairs early responses to tuberculous infection

The inability of macrophages with accumulated lysosomal material to migrate is not specific to their phagocytosis and clearance of dead cells, but also impacts the macrophage's ability to perform its parallel function, which is to phagocytose and destroy invading pathogens. In humans, genetic defects that disrupt phagocyte or leukocyte migration are associated with a variety of immunodeficiencies including WHIM (warts, hypogammaglobulinemia, infections, myelokathexis) syndrome, LAD (leukocyte adhesion deficiency), and Wiskott-Aldrich syndrome (Badolato, 2013). A remarkable case of macrophage lysosomal storage is that of smokers, whose alveolar macrophages are filled with tobacco smoke particulates (Harris et al., 1970; Martin, 1973). In human smokers, the macrophages that exhibit lysosomal storage constitute a majority of those observed on bronchoalveolar lavage and these cells fail to migrate to extracellular *M. tuberculosis* while the few normal macrophages in smokers are competent for migration. The delayed phagocytosis of *M. tuberculosis* could result in susceptibility either by providing an extended growth period in the alveolus, or by increasing the chances of initial phagocytosis by a less-microbicidal macrophage recruited from deeper tissues (CJ Cambier, unpublished data). This mechanism could explain the susceptibility of smokers to a variety of respiratory infections including TB (Anderson et al., 1997; Bagaitkar et al., 2008; den Boon et al., 2005; Lin et al., 2007) and the association between indoor air pollution and TB (Sumpter and Chandramohan, 2013).

The idea that "clogged up" macrophages fail to respond to invading pathogens because they cannot migrate demonstrates that not all macrophage-pathogen interactions are created equal. Lysosomal storage defects resulting from genetic or environmental causes will not impact all tissues equally, and would lead to more incapacitation in high cell turnover tissues in genetic disorders (such as the brain) versus more incapacitation in highly exposed tissues in acquired lysosomal storage (such as the lungs of smokers). Thus the phagocytic history of the macrophages in a given tissue informs the vulnerability of that tissue to invasion by pathogens. In turn, this would impact the anatomical locations in which infections occur, and thus the types of infections to which patients with genetic or acquired lysosomal defects would be hypersusceptible.

The macrophage lysosome can slow replication of *M. tuberculosis* but is not responsible for clearance of infection

The macrophage clears pathogens using much the same machinery that is used to clear dead cells; following phagocytosis, phagosomes containing engulfed cargo undergo a stepwise maturation consisting of compartment acidification and a series of fission and fusion events that leads to fusion with lysosomes, or the creation of phagolysosomes (Desjardins, 1995). The resident macrophages of the lung frequently succeed in clearing tuberculous infection without the assistance of adaptive immune cells (Verrall et al., 2014). Given the lysosome's role as the primary degradative compartment of the cell and the primary location of antimicrobial compounds like reactive nitrogen and oxygen intermediates, it is surprising that this compartment confers little benefit to the clearance of mycobacterial invaders. This raises an important question of how 30% of humans might quickly clear *M. tuberculosis*, which could

have broad implications for vaccine development and for prophylactic chemotherapeutic approaches to *M. tuberculosis* infection.

The lysosome does limit the intramacrophage replication of invading mycobacteria to some extent, which could be clinically significant during later stages of infection when a significant proportion of mycobacteria are reported to be in lysosomal compartments due presumably to the action of cytokines such as gamma-interferon (Bouley et al., 2001; MacMicking, 2008). There is some circumstantial evidence for the limited efficacy of enhanced lysosomal acidification in the control of tuberculosis. Imatinib, a small molecule inhibitor of Abl tyrosine kinase that is used for the treatment of chronic myelogenous leukemia (CML) enhances lysosomal acidification by upregulating v-ATPase expression and reduces survival of *M. tuberculosis* in vitro (Bruns et al., 2012). Imatinib treatment of infected mice resulted in a small but statistically significant reduction in overall bacterial burden (Napier et al., 2011). Thus, while enhancing the lysosomal trafficking of *M. tuberculosis* may serve as an adjunctive therapy to reduce the overall burden of infection, its effects are likely to be modest at best given *Mycobacterium*'s robust ability to tolerate phagosomal acidification in vivo.

Genetic lysosomal defects worsen infection by hastening extracellular release of bacteria

We are just beginning to appreciate the ways in which mycobacteria hijack tissue-resident macrophages to ensure their delivery in the more favourable growth environment of recruited permissive monocytes (Cambier et al., 2014a). Once in these cells, mycobacteria drive the development of infection through the apoptosis of infected macrophages with subsequent phagocytosis by newly-recruited uninfected macrophages, which expands the intracellular niche (Davis and Ramakrishnan, 2009). At this stage of infection, failure by the host to supply enough

macrophages to phagocytose the dying infected cells results in extracellular escape and subsequent extracellular multiplication of bacteria (Pagan et al., 2015). While a normal tissue likely contains sufficient numbers of macrophages to contend with both homeostatic and immune necessities, disruption of one function can have profound consequences on the other. For example, macrophage incapacitation by loading with plastic beads inhibits migration to newly infecting mycobacteria delivered to nutrient-rich tissues that are normally devoid of phagocytes in the zebrafish. At the same time, in genetically wildtype animals faced with overwhelming infection, macrophages migrate away from developing tissues towards the infection, resulting in an accumulation of extracellular dead cell debris (Davis et al., 2002).

In order for a newly arriving uninfected macrophage to successfully contain the bacteria from a dying cell, it must migrate to and phagocytose the infected macrophage. As in the case of macrophage migration to newly invading bacteria, the lysosome once again plays a critical role in cell motility. Disruption of macrophage endocytic recycling secondary to lysosomal storage prevents the migration to and subsequent efferocytosis of dying infected cells, leading to granuloma breakdown similar to that seen in more straightforward macrophage deficiency resulting from a deficiency of hematopoietic factors responsible for macrophage development (Pagan et al., 2015). Macrophage migration during tuberculous infection is absolutely critical; lysosomal storage-mediated macrophage incapacitation can cause hypersusceptibility even in the context of global macrophage excess.

Distinct and shared roles for the macrophage lysosome during tuberculous infection

The lysosome's functions in macrophage migration and in the control of intramacrophage replication are distinct roles, which can independently control infection to some extent.

Disruption of one of these two functions results in hypersusceptibility to bacterial infection, but does not necessarily impact the other. For example, macrophages deficient in cathepsins B and L fail to degrade dead cells that they have engulfed, which results in lysosomal storage and macrophage immotility, but leaves intact the macrophage's ability to control intracellular bacterial replication presumably because cathepsins B and L do not have anti-microbial functions (Figure 4.1). On the other hand, some microbicidal compounds within the lysosome are likely dispensible for the breakdown of dead cells (Figure 4.1). But a subset of lysosomal components is probably required for both antimicrobial function and dead cell breakdown. For instance, genetic defects in lysosomal acidification machinery (e.g. in the v-ATPase proton pump) could have effects on both processes. The enzymes responsible for degradation of dead cell material function only in low-pH environments, and phagosome maturation does limit the expansion of infection to some extent. While the migratory role of the lysosome appears to outweigh its microbicidal capacity during the establishment of infection, studying these types of deficiencies could provide insight into the relative importance of each lysosomal function during the expansion of infection.

Chapter 4 Figures

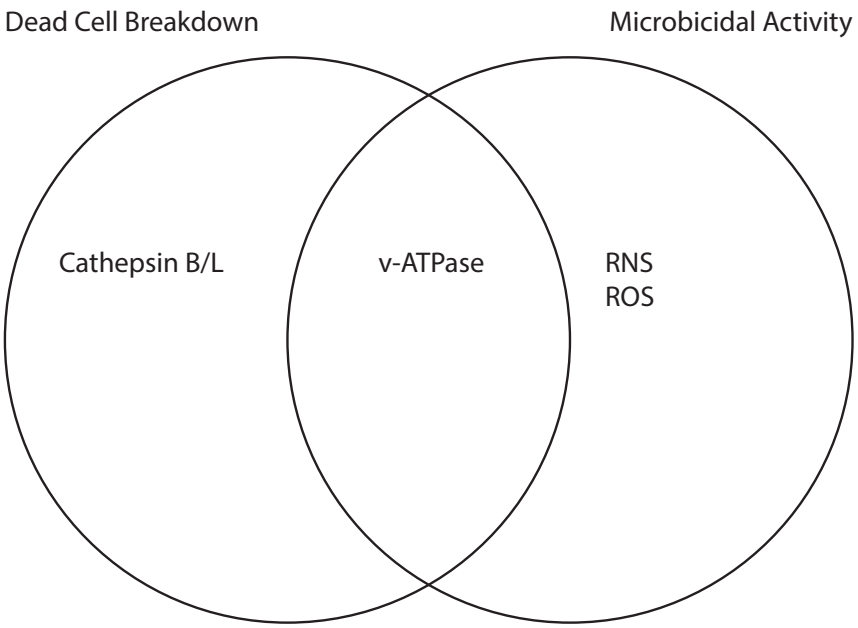

Figure 4.1. The intersection of lysosomal functions

Concluding Thoughts

The macrophage lysosome's central functions in the establishment and expansion of tuberculous infection have been studied for decades, but are only now becoming fully appreciated. This work expands our understanding of the critical role that the lysosome plays in infection, beginning prior to the initial arrival of invading pathogens and continuing through the formation of the tuberculous granuloma. It clarifies the relative importance of acid avoidance and tolerance strategies employed by mycobacteria immediately upon their arrival in host tissues, and challenges the widely held notion that first-responding macrophages clear infecting mycobacteria by relegating them to lysosomal compartments. Finally, this work underscores the inextricable link between the homeostatic and immune functions of the macrophage and highlights the importance of considering both functions in the context of infection.

References

Abrams, J.M., White, K., Fessler, L.I., and Steller, H. (1993). Programmed cell death during Drosophila embryogenesis. Development *117*, 29-43.

Aflaki, E., Stubblefield, B.K., Maniwang, E., Lopez, G., Moaven, N., Goldin, E., Marugan, J., Patnaik, S., Dutra, A., Southall, N.*, et al.* (2014). Macrophage models of Gaucher disease for evaluating disease pathogenesis and candidate drugs. Sci Transl Med *6*, 240ra273.

Aggad, D., Stein, C., Sieger, D., Mazel, M., Boudinot, P., Herbomel, P., Levraud, J.-P., Lutfalla, G., and Leptin, M. (2010). In Vivo Analysis of Ifn-g1 and Ifn-g2 Signalling in Zebrafish. Journal of Immunology *185*.

Aker, M., Zimran, A., Abrahamov, A., Horowitz, M., and Matzner, Y. (1993). Abnormal neutrophil chemotaxis in Gaucher disease. British journal of haematology *83*, 187-191.

Allen, T.C. (2008). Pulmonary Langerhans cell histiocytosis and other pulmonary histiocytic diseases: a review. Arch Pathol Lab Med *132*, 1171-1181.

Alonso, S., Pethe, K., Russell, D.G., and Purdy, G.E. (2007). Lysosomal killing of Mycobacterium mediated by ubiquitin-derived peptides is enhanced by autophagy. Proc Natl Acad Sci U S A *104*, 6031-6036.

Anderson, R.H., Sy, F.S., Thompson, S., and Addy, C. (1997). Cigarette smoking and tuberculin skin test conversion among incarcerated adults. American journal of preventive medicine *13*, 175-181.

Armstrong, J.A., and Hart, P.D. (1971). Response of cultured macrophages to Mycobacterium tuberculosis, with observations on fusion of lysosomes with phagosomes. The Journal of experimental medicine *134*, 713-740.

Armstrong, J.A., and Hart, P.D. (1975). Phagosome-lysosome interactions in cultured macrophages infected with virulent tubercle bacilli. Reversal of the usual nonfusion pattern and observations on bacterial survival. The Journal of experimental medicine *142*, 1-16.

Asrat, S., de Jesus, D.A., Hempstead, A.D., Ramabhadran, V., and Isberg, R.R. (2014). Bacterial pathogen manipulation of host membrane trafficking. Annu Rev Cell Dev Biol *30*, 79-109.

Aston, C., Rom, W.N., Talbot, A.T., and Reibman, J. (1998). Early inhibition of mycobacterial growth by human alveolar macrophages is not due to nitric oxide. Am J Respir Crit Care Med *157*, 1943-1950.

Bach, H., Papavinasasundaram, K.G., Wong, D., Hmama, Z., and Av-Gay, Y. (2008). Mycobacterium tuberculosis virulence is mediated by PtpA dephosphorylation of human vacuolar protein sorting 33B. Cell Host Microbe *3*, 316-322.

Badolato, R. (2013). Defects of leukocyte migration in primary immunodeficiencies. Eur J Immunol *43*, 1436-1440.

Bagaitkar, J., Demuth, D.R., and Scott, D.A. (2008). Tobacco use increases susceptibility to bacterial infection. Tobacco induced diseases *4*, 12.

Bahary, N., Davidson, A., Ransom, D., Shepard, J., Stern, H., Trede, N., Zhou, Y., Barut, B., and Zon, L.I. (2004). The Zon laboratory guide to positional cloning in zebrafish. Methods Cell Biol *77*, 305-329.

Baillat, D., Gardini, A., Cesaroni, M., and Shiekhattar, R. (2012). Requirement for SNAPC1 in transcriptional responsiveness to diverse extracellular signals. Mol Cell Biol *32*, 4642-4650.

Baldridge, M., King, K., Boles, N., Weksberg, D., and Goodell, M. (2010). Quiescent haematopoietic stem cells are activated by IFN-g in response to chronic infection. Nature *465*, 793-797.

Barker, L.P., George, K.M., Falkow, S., and Small, P.L. (1997). Differential trafficking of live and dead Mycobacterium marinum organisms in macrophages. Infect Immun *65*, 1497-1504.

Barlow, P.G., Brown, D.M., Donaldson, K., MacCallum, J., and Stone, V. (2008). Reduced alveolar macrophage migration induced by acute ambient particle (PM10) exposure. Cell biology and toxicology *24*, 243-252.

Bates, J.H., Potts, W.E., and Lewis, M. (1965). Epidemiology of Primary Tuberculosis in an Industrial School. The New England journal of medicine *272*, 714-717.

Behar, S.M., and Baehrecke, E.H. (2015). Tuberculosis: Autophagy is not the answer. Nature *528*, 482-483.

Betz, P., Nerlich, A., Penning, R., and Eisenmenger, W. (1993). Alveolar macrophages and the diagnosis of drowning. Forensic science international *62*, 217-224.

Biffi, A., De Palma, M., Quattrini, A., Del Carro, U., Amadio, S., Visigalli, I., Sessa, M., Fasano, S., Brambilla, R., Marchesini, S*., et al.* (2004). Correction of metachromatic leukodystrophy in the mouse model by transplantation of genetically modified hematopoietic stem cells. The Journal of clinical investigation *113*, 1118-1129.

Blaser, M.J., and Kirschner, D. (2007). The equilibria that allow bacterial persistence in human hosts. Nature *449*, 843-849.

Bouley, D.M., Ghori, N., Mercer, K.L., Falkow, S., and Ramakrishnan, L. (2001). Dynamic nature of host-pathogen interactions in Mycobacterium marinum granulomas. Infect Immun *69*, 7820-7831.

Bretscher, M.S., and Aguado-Velasco, C. (1998). EGF induces recycling membrane to form ruffles. Curr Biol *8*, 721-724.

Bright, N.A., Gratian, M.J., and Luzio, J.P. (2005). Endocytic delivery to lysosomes mediated by concurrent fusion and kissing events in living cells. Curr Biol *15*, 360-365.

Bright, N.A., Wartosch, L., and Luzio, J.P. (2015). Lysosome fusion in cultured mammalian cells. Methods Cell Biol *126*, 101-118.

Bruns, H., Stegelmann, F., Fabri, M., Dohner, K., van Zandbergen, G., Wagner, M., Skinner, M., Modlin, R.L., and Stenger, S. (2012). Abelson tyrosine kinase controls phagosomal acidification required for killing of Mycobacterium tuberculosis in human macrophages. J Immunol *189*, 4069-4078.

Cambier, C.J., Falkow, S., and Ramakrishnan, L. (2014a). Host evasion and exploitation schemes of Mycobacterium tuberculosis. Cell *159*, 1497-1509.

Cambier, C.J., Takaki, K.K., Larson, R.P., Hernandez, R.E., Tobin, D.M., Urdahl, K.B., Cosma, C.L., and Ramakrishnan, L. (2014b). Mycobacteria manipulate macrophage recruitment through coordinated use of membrane lipids. Nature *505*, 218-222.

Clay, H., Davis, J.M., Beery, D., Huttenlocher, A., Lyons, S.E., and Ramakrishnan, L. (2007a). Dichotomous role of the macrophage in early Mycobacterium marinum infection of the zebrafish. Cell Host and Microbe *2*, 29-39.

Clay, H., Davis, J.M., Beery, D., Huttenlocher, A., Lyons, S.E., and Ramakrishnan, L. (2007b). Dichotomous role of the macrophage in early Mycobacterium marinum infection of the zebrafish. Cell Host Microbe *2*, 29-39.

Clay, H., Volkman, H.E., and Ramakrishnan, L. (2008). Tumor necrosis factor signaling mediates resistance to mycobacteria by inhibiting bacterial growth and macrophage death. Immunity *29*, 283-294.

Clemens, D.L., and Horwitz, M.A. (1995). Characterization of the Mycobacterium tuberculosis phagosome and evidence that phagosomal maturation is inhibited. The Journal of experimental medicine *181*, 257-270.

Clements, W.K., and Traver, D. (2013). Signalling pathways that control vertebrate haematopoietic stem cell specification. Nat Rev Immunol *13*, 336-348.

Cohen, A.B., and Cline, M.J. (1971). The human alveolar macrophage: isolation, cultivation in vitro, and studies of morphologic and functional characteristics. The Journal of clinical investigation *50*, 1390-1398.

Comas, I., Coscolla, M., Luo, T., Borrell, S., Holt, K.E., Kato-Maeda, M., Parkhill, J., Malla, B., Berg, S., Thwaites, G., *et al.* (2013). Out-of-Africa migration and Neolithic coexpansion of Mycobacterium tuberculosis with modern humans. Nat Genet *45*, 1176-1182.

Cosma, C.L., Sherman, D.R., and Ramakrishnan, L. (2003). The secret lives of the pathogenic mycobacteria. Annu Rev Microbiol *57*, 641-676.

Cosma, C.L., Swaim, L.E., Volkman, H., Ramakrishnan, L., and Davis, J.M. (2006). Zebrafish and frog models of Mycobacterium marinum infection. Curr Protoc Microbiol *Chapter 10*, Unit 10B.12.

Cotter, P.D., and Hill, C. (2003). Surviving the acid test: responses of gram-positive bacteria to low pH. Microbiol Mol Biol Rev *67*, 429-453, table of contents.

Davis, J.M., Clay, H., Lewis, J.L., Ghori, N., Herbomel, P., and Ramakrishnan, L. (2002). Real-time visualization of Mycobacterium-macrophage interactions leading to initiation of granuloma formation in zebrafish embryos. Immunity *17*, 693-702.

Davis, J.M., and Ramakrishnan, L. (2009). The role of the granuloma in the expansion and dissemination of early tuberculous infection. Cell *136*, 37-49.

den Boon, S., van Lill, S.W., Borgdorff, M.W., Verver, S., Bateman, E.D., Lombard, C.J., Enarson, D.A., and Beyers, N. (2005). Association between smoking and tuberculosis infection: a population survey in a high tuberculosis incidence area. Thorax *60*, 555-557.

Desjardins, M. (1995). Biogenesis of phagolysosomes: the 'kiss and run' hypothesis. Trends Cell Biol *5*, 183-186.

Egen, J.G., Rothfuchs, A.G., Feng, C.G., Winter, N., Sher, A., and Germain, R.N. (2008). Macrophage and T cell dynamics during the development and disintegration of mycobacterial granulomas. Immunity *28*, 271-284.

Ehrt, S., Rhee, K., and Schnappinger, D. (2015). Mycobacterial genes essential for the pathogen's survival in the host. Immunol Rev *264*, 319-326.

Ellett, F., Pase, L., Hayman, J.W., Andrianopoulos, A., and Lieschke, G.J. (2011). mpeg1 promoter transgenes direct macrophage-lineage expression in zebrafish. Blood *117*, e49-56.

Ferin, J. (1982). Pulmonary alveolar pores and alveolar macrophage-mediated particle clearance. The Anatomical record *203*, 265-272.

Flicek, P., Amode, M.R., Barrell, D., Beal, K., Billis, K., Brent, S., Carvalho-Silva, D., Clapham, P., Coates, G., Fitzgerald, S.*, et al.* (2014). Ensembl 2014. Nucleic Acids Res *42*, D749-755.

Flynn, J., and Chan, J. (2001). Immunology of tuberculosis. Annu Rev Immunol *19*, 93-129.

Fraldi, A., Annunziata, F., Lombardi, A., Kaiser, H.J., Medina, D.L., Spampanato, C., Fedele, A.O., Polishchuk, R., Sorrentino, N.C., Simons, K.*, et al.* (2010). Lysosomal fusion and SNARE function are impaired by cholesterol accumulation in lysosomal storage disorders. The EMBO journal *29*, 3607-3620.

Gomes, M.S., Paul, S., Moreira, A.L., Appelberg, R., Rabinovitch, M., and Kaplan, G. (1999). Survival of Mycobacterium avium and Mycobacterium tuberculosis in acidified vacuoles of murine macrophages. Infect Immun *67*, 3199-3206.

Green, G.M., and Kass, E.H. (1964). The Role of the Alveolar Macrophage in the Clearance of Bacteria from the Lung. The Journal of experimental medicine *119*, 167-176.

Grundner, C., Cox, J.S., and Alber, T. (2008). Protein tyrosine phosphatase PtpA is not required for Mycobacterium tuberculosis growth in mice. FEMS microbiology letters *287*, 181-184.

Gyawali, N., Gurung, R., Poudyal, N., Amatya, R., Niraula, S.R., Jha, P., and Bhattacharya, S.K. (2012). Prevalence of tuberculosis in household contacts of sputum smears positive cases and associated demographic risk factors. Nepal Medical College journal : NMCJ *14*, 303-307.

Hall, C., Flores, M.V., Storm, T., Crosier, K., and Crosier, P. (2007). The zebrafish lysozyme C promoter drives myeloid-specific expression in transgenic fish. BMC Dev Biol *7*, 42.

Harris, J., Hope, J.C., and Keane, J. (2008). Tumor necrosis factor blockers influence macrophage responses to Mycobacterium tuberculosis. J Infect Dis *198*, 1842-1850.

Harris, J.O., Swenson, E.W., and Johnson, J.E., 3rd (1970). Human alveolar macrophages: comparison of phagocytic ability, glucose utilization, and ultrastructure in smokers and nonsmokers. The Journal of clinical investigation *49*, 2086-2096.

Hart, P.D., Armstrong, J.A., Brown, C.A., and Draper, P. (1972). Ultrastructural study of the behavior of macrophages toward parasitic mycobacteria. Infect Immun *5*, 803-807.

Heng, T.S., Painter, M.W., and Immunological Genome Project, C. (2008). The Immunological Genome Project: networks of gene expression in immune cells. Nat Immunol *9*, 1091-1094.

Henry, R.W., Mittal, V., Ma, B., Kobayashi, R., and Hernandez, N. (1998). SNAP19 mediates the assembly of a functional core promoter complex (SNAPc) shared by RNA polymerases II and III. Genes Dev *12*, 2664-2672.

Herbomel, P., Thisse, B., and Thisse, C. (2001). Zebrafish Early Macrophages Colonize Cephalic Mesenchyme and Developing Brain, Retina, and Epidermis through a M-CSF Receptor-Dependent Invasive Process. Developmental Biology *238*, 274-288.

Hinshaw, H.C., FELDMAN, W.H., and PFUETZE, K.H. (1946). Treatment of tuberculosis with streptomycin; a summary of observations on one hundred cases. J Am Med Assoc *132*, 778-782.

Hochreiter-Hufford, A., and Ravichandran, K.S. (2013). Clearing the dead: apoptotic cell sensing, recognition, engulfment, and digestion. Cold Spring Harbor perspectives in biology *5*, a008748.

Hocking, W.G., and Golde, D.W. (1979a). The pulmonary-alveolar macrophage (first of two parts). The New England journal of medicine *301*, 580-587.

Hocking, W.G., and Golde, D.W. (1979b). The pulmonary-alveolar macrophage (second of two parts). The New England journal of medicine *301*, 639-645.

Holmberg, S.D. (1990). The rise of tuberculosis in America before 1820. Am Rev Respir Dis *142*, 1228-1232.

Horng, J.L., Lin, L.Y., Huang, C.J., Katoh, F., Kaneko, T., and Hwang, P.P. (2007). Knockdown of V-ATPase subunit A (atp6v1a) impairs acid secretion and ion balance in zebrafish (Danio rerio). Am J Physiol Regul Integr Comp Physiol *292*, R2068-2076.

Houk, V.N. (1980). Spread of tuberculosis via recirculated air in a naval vessel: the Byrd study. Annals of the New York Academy of Sciences *353*, 10-24.

Houk, V.N., Baker, J.H., Sorensen, K., and Kent, D.C. (1968). The epidemiology of tuberculosis infection in a closed environment. Arch Environ Health *16*, 26-35.

Hsu, C.L., Lin, W., Seshasayee, D., Chen, Y.H., Ding, X., Lin, Z., Suto, E., Huang, Z., Lee, W.P., Park, H.*, et al.* (2012). Equilibrative nucleoside transporter 3 deficiency perturbs lysosome function and macrophage homeostasis. Science *335*, 89-92.

Huang, J.Q., Trasler, J.M., Igdoura, S., Michaud, J., Hanal, N., and Gravel, R.A. (1997). Apoptotic cell death in mouse models of GM2 gangliosidosis and observations on human Tay-Sachs and Sandhoff diseases. Hum Mol Genet *6*, 1879-1885.

Huynh, K.K., and Grinstein, S. (2007). Regulation of vacuolar pH and its modulation by some microbial species. Microbiol Mol Biol Rev *71*, 452-462.

Jain, V.V., and Yelwatkar, S. (2011). Unusual presentation of adult Gaucher's disease: A long and difficult road to diagnosis. Indian Journal of Endocrinology and Metabolism *15*, 224-226.

Jayachandran, R., Sundaramurthy, V., Combaluzier, B., Mueller, P., Korf, H., Huygen, K., Miyazaki, T., Albrecht, I., Massner, J., and Pieters, J. (2007). Survival of mycobacteria in macrophages is mediated by coronin 1-dependent activation of calcineurin. Cell *130*, 37-50.

Jeyakumar, M., Dwek, R.A., Butters, T.D., and Platt, F.M. (2005). Storage solutions: treating lysosomal disorders of the brain. Nature reviews Neuroscience *6*, 713-725.

Johnson, S.L., Africa, D., Horne, S., and Postlethwait, J.H. (1995). Half-tetrad analysis in zebrafish: mapping the ros mutation and the centromere of linkage group I. Genetics *139*, 1727-1735.

Kasper, D.L., Fauci, A.S., Hauser, S.L., Longo, D.L., Jameson, J.L., Loscalzo, J., Harrison, T.R., and McGraw-Hill Companies. (2015). Harrison's principles of internal medicine. In

McGraw-Hill's AccessMedicine (New York: McGraw Hill Education,), pp. 1 online resource (2000 p.

Khader, S.A., Bell, G.K., Pearl, J.E., Fountain, J.J., Rangel-Moreno, J., Cilley, G.E., Shen, F., Eaton, S.M., Gaffen, S.L., Swain, S.L.*, et al.* (2007). IL-23 and IL-17 in the establishment of protective pulmonary CD4+ T cell responses after vaccination and during Mycobacterium tuberculosis challenge. Nat Immunol *8*, 369-377.

Kieseier, B.C., Wisniewski, K.E., and Goebel, H.H. (1997). The monocyte-macrophage system is affected in lysosomal storage diseases: an immunoelectron microscopic study. Acta Neuropathol *94*, 359-362.

Lehnert, B.E. (1992). Pulmonary and thoracic macrophage subpopulations and clearance of particles from the lung. Environmental health perspectives *97*, 17-46.

Liel, Y., Rudich, A., Nagauker-Shriker, O., Yermiyahu, T., and Levy, R. (1994). Monocyte dysfunction in patients with Gaucher disease: evidence for interference of glucocerebroside with superoxide generation. Blood *83*, 2646-2653.

Lin, H.H., Ezzati, M., and Murray, M. (2007). Tobacco smoke, indoor air pollution and tuberculosis: a systematic review and meta-analysis. PLoS medicine *4*, e20.

MacGurn, J.A., and Cox, J.S. (2007). A genetic screen for Mycobacterium tuberculosis mutants defective for phagosome maturation arrest identifies components of the ESX-1 secretion system. Infect Immun *75*, 2668-2678.

Machaczka, M., Lorenz, F., Kleinotiene, G., Bulanda, A., Markuszewska-Kuczyńska, A., Raistenskis, J., and Klimkowska, M. (2014). Recurrent pulmonary aspergillosis and mycobacterial infection in an unsplenectomized patient with type 1 Gaucher disease. Ups J Med Sci *119*, 44-49.

MacMicking, J.D. (2008). M. tuberculosis passes the litmus test. Nat Med *14*, 809-810.

Malatack, J.J., Consolini, D.M., and Bayever, E. (2003). The status of hematopoietic stem cell transplantation in lysosomal storage disease. Pediatric neurology *29*, 391-403.

Marques, L.J., Teschler, H., Guzman, J., and Costabel, U. (1997). Smoker's lung transplanted to a nonsmoker. Long-term detection of smoker's macrophages. Am J Respir Crit Care Med *156*, 1700-1702.

Martin, R.R. (1973). Altered morphology and increased acid hydrolase content of pulmonary macrophages from cigarette smokers. Am Rev Respir Dis *107*, 596-601.

Miller, A.C., Obholzer, N.D., Shah, A.N., Megason, S.G., and Moens, C.B. (2013). RNA-seq-based mapping and candidate identification of mutations from forward genetic screens. Genome Res *23*, 679-686.

Mindell, J.A. (2012). Lysosomal acidification mechanisms. Annu Rev Physiol *74*, 69-86.

Moguche, A.O., Shafiani, S., Clemons, C., Larson, R.P., Dinh, C., Higdon, L.E., Cambier, C.J., Sissons, J.R., Gallegos, A.M., Fink, P.J.*, et al.* (2015). ICOS and Bcl6-dependent pathways maintain a CD4 T cell population with memory-like properties during tuberculosis. The Journal of experimental medicine *212*, 715-728.

Morrison, J., Pai, M., and Hopewell, P.C. (2008). Tuberculosis and latent tuberculosis infection in close contacts of people with pulmonary tuberculosis in low-income and middle-income countries: a systematic review and meta-analysis. Lancet Infect Dis *8*, 359-368.

Murray, E.J., Grisanti, M.S., Bentley, G.V., and Murray, S.S. (1997). E64d, a membrane-permeable cysteine protease inhibitor, attenuates the effects of parathyroid hormone on osteoblasts in vitro. Metabolism *46*, 1090-1094.

Mwandumba, H.C., Russell, D.G., Nyirenda, M.H., Anderson, J., White, S.A., Molyneux, M.E., and Squire, S.B. (2004). Mycobacterium tuberculosis resides in nonacidified vacuoles in endocytically competent alveolar macrophages from patients with tuberculosis and HIV infection. J Immunol *172*, 4592-4598.

Napier, R.J., Rafi, W., Cheruvu, M., Powell, K.R., Zaunbrecher, M.A., Bornmann, W., Salgame, P., Shinnick, T.M., and Kalman, D. (2011). Imatinib-sensitive tyrosine kinases regulate mycobacterial pathogenesis and represent therapeutic targets against tuberculosis. Cell Host Microbe *10*, 475-485.

Nepal, R.M., Vesosky, B., Turner, J., and Bryant, P. (2008). DM, but not cathepsin L, is required to control an aerosol infection with Mycobacterium tuberculosis. J Leukoc Biol *84*, 1011-1018.

Norflus, F., Tifft, C.J., McDonald, M.P., Goldstein, G., Crawley, J.N., Hoffmann, A., Sandhoff, K., Suzuki, K., and Proia, R.L. (1998). Bone marrow transplantation prolongs life span and ameliorates neurologic manifestations in Sandhoff disease mice. The Journal of clinical investigation *101*, 1881-1888.

Nunes-Alves, C., Booty, M.G., Carpenter, S.M., Jayaraman, P., Rothchild, A.C., and Behar, S.M. (2014). In search of a new paradigm for protective immunity to TB. Nat Rev Microbiol *12*, 289-299.

O'Leary, S., O'Sullivan, M.P., and Keane, J. (2011). IL-10 blocks phagosome maturation in mycobacterium tuberculosis-infected human macrophages. American journal of respiratory cell and molecular biology *45*, 172-180.

O'Leary, S.M., Coleman, M.M., Chew, W.M., Morrow, C., McLaughlin, A.M., Gleeson, L.E., O'Sullivan, M.P., and Keane, J. (2014). Cigarette smoking impairs human pulmonary immunity to Mycobacterium tuberculosis. Am J Respir Crit Care Med *190*, 1430-1436.

Opalek, J.M., Ali, N.A., Lobb, J.M., Hunter, M.G., and Marsh, C.B. (2007). Alveolar macrophages lack CCR2 expression and do not migrate to CCL2. Journal of inflammation *4*, 19.

Pagan, A.J., Yang, C.T., Cameron, J., Swaim, L.E., Ellett, F., Lieschke, G.J., and Ramakrishnan, L. (2015). Myeloid Growth Factors Promote Resistance to Mycobacterial Infection by Curtailing Granuloma Necrosis through Macrophage Replenishment. Cell Host Microbe *18*, 15-26.

Peao, M.N., Aguas, A.P., de Sa, C.M., and Grande, N.R. (1993). Morphological evidence for migration of particle-laden macrophages through the interalveolar pores of Kohn in the murine lung. Acta anatomica *147*, 227-232.

Peri, F., and Nüsslein-Volhard, C. (2008). Live imaging of neuronal degradation by microglia reveals a role for v0-ATPase a1 in phagosomal fusion in vivo. Cell *133*, 916-927.

Pethe, K., Swenson, D.L., Alonso, S., Anderson, J., Wang, C., and Russell, D.G. (2004). Isolation of Mycobacterium tuberculosis mutants defective in the arrest of phagosome maturation. Proc Natl Acad Sci U S A *101*, 13642-13647.

Philips, J.A., and Ernst, J.D. (2012). Tuberculosis pathogenesis and immunity. Annual review of pathology *7*, 353-384.

Platt, F.M., Boland, B., and van der Spoel, A.C. (2012). The cell biology of disease: lysosomal storage disorders: the cellular impact of lysosomal dysfunction. J Cell Biol *199*, 723-734.

Poon, I.K., Lucas, C.D., Rossi, A.G., and Ravichandran, K.S. (2014). Apoptotic cell clearance: basic biology and therapeutic potential. Nat Rev Immunol *14*, 166-180.

Ramakrishnan, L. (2013). The zebrafish guide to tuberculosis immunity and treatment. Cold Spring Harb Symp Quant Biol *78*, 179-192.

Ratcliffe, H.L., and Wells, W.F. (1948). Tuberculosis of rabbits induced by droplet nuclei infection; initial response to infection. The Journal of experimental medicine *87*, 575-584.

Renshaw, S.A., and Trede, N.S. (2012). A model 450 million years in the making: zebrafish and vertebrate immunity. Dis Model Mech *5*, 38-47.

Repetto, G., del Peso, A., and Zurita, J.L. (2008). Neutral red uptake assay for the estimation of cell viability/cytotoxicity. Nat Protoc *3*, 1125-1131.

Roca, F.J., and Ramakrishnan, L. (2013). TNF dually mediates resistance and susceptibility to mycobacteria via mitochondrial reactive oxygen species. Cell *153*, 521-534.

Schaible, U.E., Sturgill-Koszycki, S., Schlesinger, P.H., and Russell, D.G. (1998). Cytokine activation leads to acidification and increases maturation of Mycobacterium avium-containing phagosomes in murine macrophages. J Immunol *160*, 1290-1296.

Sieger, D., Stein, C., Neifer, D., van der Sar, A.M., and Leptin, M. (2009). The role of gamma interferon in innate immunity in the zebrafish embryo. Dis Model Mech *2*, 571-581.

Small, J.L., O'Donoghue, A.J., Boritsch, E.C., Tsodikov, O.V., Knudsen, G.M., Vandal, O., Craik, C.S., and Ehrt, S. (2013). Substrate specificity of MarP, a periplasmic protease required for resistance to acid and oxidative stress in Mycobacterium tuberculosis. J Biol Chem *288*, 12489-12499.

Srivastava, S., Ernst, J.D., and Desvignes, L. (2014). Beyond macrophages: the diversity of mononuclear cells in tuberculosis. Immunol Rev *262*, 179-192.

Stallings, C.L., and Glickman, M.S. (2010). Is Mycobacterium tuberculosis stressed out? A critical assessment of the genetic evidence. Microbes Infect *12*, 1091-1101.

Sumpter, C., and Chandramohan, D. (2013). Systematic review and meta-analysis of the associations between indoor air pollution and tuberculosis. Tropical medicine & international health : TM & IH *18*, 101-108.

Swaim, L.E., Connolly, L.E., Volkman, H.E., Humbert, O., Born, D.E., and Ramakrishnan, L. (2006). Mycobacterium marinum infection of adult zebrafish produces caseating granulomatous tuberculosis and is moderated by adaptive immunity. Infect Immun *74*, 6108-6117.

Sweeney, S., Grandolfo, D., Ruenraroengsak, P., and Tetley, T.D. (2015). Functional consequences for primary human alveolar macrophages following treatment with long, but not short, multiwalled carbon nanotubes. International journal of nanomedicine *10*, 3115-3129.

Takaki, K., Davis, J.M., Winglee, K., and Ramakrishnan, L. (2013). Evaluation of the pathogenesis and treatment of Mycobacterium marinum infection in zebrafish. Nat Protoc *8*, 1114-1124.

Tameris, M.D., Hatherill, M., Landry, B.S., Scriba, T.J., Snowden, M.A., Lockhart, S., Shea, J.E., McClain, J.B., Hussey, G.D., Hanekom, W.A.*, et al.* (2013). Safety and efficacy of MVA85A, a new tuberculosis vaccine, in infants previously vaccinated with BCG: a randomised, placebo-controlled phase 2b trial. Lancet *381*, 1021-1028.

Tan, S., and Russell, D.G. (2015). Trans-species communication in the Mycobacterium tuberculosis-infected macrophage. Immunol Rev *264*, 233-248.

Thorvaldsdóttir, H., Robinson, J.T., and Mesirov, J.P. (2013). Integrative Genomics Viewer (IGV): high-performance genomics data visualization and exploration. Brief Bioinform *14*, 178-192.

Tobin, D., Roca, F., Oh, S., McFarland, R., Vickery, T., Ray, J., Ko, D., Zou, Y., Bang, N., CHau, T.*, et al.* (2012). Host genotype-specific therapies can optimize the inflammatory response to mycobacterial infections. Cell *148*, 434-446.

Tobin, D.M., Vary, J.R., Ray, J.P., Walsh, G.S., Dunstan, S.J., Bang, N.D., Hagge, D.A., Khadge, S., King, M.-C., Hawn, T.R.*, et al.* (2010). The lta4h Locus Modulates Susceptibility to Mycobacterial Infection in Zebrafish and Humans. Cell *140*, 717-730.

Trapnell, C., Hendrickson, D.G., Sauvageau, M., Goff, L., Rinn, J.L., and Pachter, L. (2013). Differential analysis of gene regulation at transcript resolution with RNA-seq. Nat Biotechnol *31*, 46-53.

Traynor, D., and Kay, R.R. (2007). Possible roles of the endocytic cycle in cell motility. Journal of cell science *120*, 2318-2327.

Trede, N.S., Zapata, A., and Zon, L.I. (2001). Fishing for lymphoid genes. Trends Immunol *22*, 302-307.

Tucker, E.J., and Huynh, B.L. (2014). Genotyping by high-resolution melting analysis. Methods Mol Biol *1145*, 59-66.

Urdahl, K.B. (2014). Understanding and overcoming the barriers to T cell-mediated immunity against tuberculosis. Seminars in immunology *26*, 578-587.

Vandal, O.H., Nathan, C.F., and Ehrt, S. (2009). Acid resistance in Mycobacterium tuberculosis. J Bacteriol *191*, 4714-4721.

Vandal, O.H., Pierini, L.M., Schnappinger, D., Nathan, C.F., and Ehrt, S. (2008). A membrane protein preserves intrabacterial pH in intraphagosomal Mycobacterium tuberculosis. Nat Med *14*, 849-854.

Varshney, G.K., Lu, J., Gildea, D.E., Huang, H., Pei, W., Yang, Z., Huang, S.C., Schoenfeld, D., Pho, N.H., Casero, D.*, et al.* (2013). A large-scale zebrafish gene knockout resource for the genome-wide study of gene function. Genome Res *23*, 727-735.

Veale, K.J., Offenhauser, C., Whittaker, S.P., Estrella, R.P., and Murray, R.Z. (2010). Recycling endosome membrane incorporation into the leading edge regulates lamellipodia formation and macrophage migration. Traffic *11*, 1370-1379.

Verrall, A.J., Netea, M.G., Alisjahbana, B., Hill, P.C., and van Crevel, R. (2014). Early clearance of Mycobacterium tuberculosis: a new frontier in prevention. Immunology *141*, 506-513.

Via, L.E., Fratti, R.A., McFalone, M., Pagan-Ramos, E., Deretic, D., and Deretic, V. (1998). Effects of cytokines on mycobacterial phagosome maturation. Journal of cell science *111 (Pt 7)*, 897-905.

Volkman, H.E., Clay, H., Beery, D., Chang, J.C., Sherman, D.R., and Ramakrishnan, L. (2004). Tuberculous granuloma formation is enhanced by a mycobacterium virulence determinant. PLoS Biol *2*, e367.

Walker, J.J., Spear, J.R., and Pace, N.R. (2005). Geobiology of a microbial endolithic community in the Yellowstone geothermal environment. Nature *434*, 1011-1014.

Wienholds, E., Schulte-Merker, S., Walderich, B., and Plasterk, R.H. (2002). Target-selected inactivation of the zebrafish rag1 gene. Science *297*, 99-102.

Wolf, A.J., Linas, B., Trevejo-Nunez, G.J., Kincaid, E., Tamura, T., Takatsu, K., and Ernst, J.D. (2007). Mycobacterium tuberculosis infects dendritic cells with high frequency and impairs their function in vivo. J Immunol *179*, 2509-2519.

Wolfe, N.D., Dunavan, C.P., and Diamond, J. (2007). Origins of major human infectious diseases. Nature *447*, 279-283.

Yang, C.T., Cambier, C.J., Davis, J.M., Hall, C.J., Crosier, P.S., and Ramakrishnan, L. (2012). Neutrophils exert protection in the early tuberculous granuloma by oxidative killing of mycobacteria phagocytosed from infected macrophages. Cell Host Microbe *12*, 301-312.

Zimran, A. (2011). How I treat Gaucher disease. Blood *118*, 1463-1471.

Zumla, A., Raviglione, M., Hafner, R., and von Reyn, C.F. (2013). Tuberculosis. The New England journal of medicine *368*, 745-755.